"Predictive Optimal Control of Active and Passive Building Thermal Storage Inventory"

Final Report

Reporting Period Start Date: September 20, 2001

Reporting Period End Date: September 20, 2005

Principal Authors:

Principal Investigator:

Gregor P. Henze, Ph.D., P.E.
Associate Professor of Architectural Engineering
University of Nebraska – Lincoln
College of Engineering and Technology
Omaha, Nebraska 68182-0681

Co-Principal Investigator:

Moncef Krarti, Ph.D., P.E.
Professor of Architectural Engineering
University of Colorado at Boulder
College of Engineering
Boulder, Colorado 80309-0428

Date Report was Issued: October 2005

DOE Award Number:

DE-FC-26-01NT41255

Name and Address of Submitting Organization:

Primary Organization:

University of Nebraska – Lincoln
303 Canfield Administration Building
Lincoln, Nebraska 68588-0430

Subcontractor:

The Regents of the University of Colorado
University of Colorado at Boulder
Boulder, Colorado 80309-0428

Disclaimer

"This report was prepared as an account of work sponsored by an agency of the United States Government. Neither the United States Government nor any agency thereof, nor any of their employees, makes any warranty, express or implied, or assumes any legal liability or responsibility for the accuracy, completeness, or usefulness of any information, apparatus, product, or process disclosed, or represents that its use would not infringe on privately owned rights. Reference herein to any specific commercial product, process, or service by trade name, trademark, manufacturer, or otherwise does not necessarily constitute or imply its endorsement, recommendation, or favoring by the United States Government or any agency thereof. The views and opinions of authors expressed herein do not necessarily state or reflect those of the United States Government or any agency thereof."

Abstract

Cooling of commercial buildings contributes significantly to the peak demand placed on an electrical utility grid. Time-of-use electricity rates encourage shifting of electrical loads to off-peak periods at night and weekends. Buildings can respond to these pricing signals by shifting cooling-related thermal loads either by precooling the building's massive structure or the use of active thermal energy storage systems such as ice storage. While these two thermal batteries have been engaged separately in the past, this project investigated the merits of harnessing both storage media concurrently in the context of predictive optimal control.

To pursue the analysis, modeling, and simulation research of Phase 1, two separate simulation environments were developed. Based on the new dynamic building simulation program EnergyPlus, a utility rate module, two thermal energy storage models were added. Also, a sequential optimization approach to the cost minimization problem using direct search, gradient-based, and dynamic programming methods was incorporated. The objective function was the total utility bill including the cost of reheat and a time-of-use electricity rate either with or without demand charges. An alternative simulation environment based on TRNSYS and Matlab was developed to allow for comparison and cross-validation with EnergyPlus.

The initial evaluation of the theoretical potential of the combined optimal control assumed perfect weather prediction and match between the building model and the actual building counterpart. The analysis showed that the combined utilization leads to cost savings that is significantly greater than either storage but less than the sum of the individual savings. The findings reveal that the cooling-related on-peak electrical demand of commercial buildings can be considerably reduced. A subsequent analysis of the impact of forecasting uncertainty in the required short-term weather forecasts determined that it takes only very simple short-term prediction models to realize almost all of the theoretical potential of this control strategy.

Further work evaluated the impact of modeling accuracy on the model-based closed-loop predictive optimal controller to minimize utility cost. The following guidelines have been derived: For an internal heat gain dominated commercial building, reasonable geometry simplifications are acceptable without a loss of cost savings potential. In fact, zoning simplification may improve optimizer performance and save computation time. The mass of the internal structure did not show a strong effect on the optimization. Building construction characteristics were found to impact building passive thermal storage capacity. It is thus advisable to make sure the construction material is well modeled. Zone temperature setpoint profiles and TES performance are strongly affected by mismatches in internal heat gains, especially when they are underestimated. Since they are a key factor in determining the building cooling load, efforts should be made to keep the internal gain mismatch as small as possible. Efficiencies of the building energy systems affect both zone temperature setpoints and active TES operation because of the coupling of the base chiller for building precooling and the icemaking TES chiller. Relative efficiencies of the base and TES chillers will determine the balance of operation of the two chillers. The impact of mismatch in this category may be significant.

Next, a parametric analysis was conducted to assess the effects of building mass, utility rate, building location and season, thermal comfort, central plant capacities, and an economizer on the cost saving performance of optimal control for active and passive building thermal storage inventory. The key findings are:

- Heavy-mass buildings, strong-incentive time-of-use electrical utility rates, and large on-peak cooling loads will likely lead to attractive savings resulting from optimal combined thermal storage control.
- By using economizer to take advantage of the cool fresh air during the night, the building electrical cost can be reduced by using less mechanical cooling.
- Larger base chiller and active thermal storage capacities have the potential of shifting more cooling loads to off-peak hours and thus higher savings can be achieved.
- Optimal combined thermal storage control with a thermal comfort penalty included in the objective function can improve the thermal comfort levels of building occupants when compared to the non-optimized base case.

Lab testing conducted in the Larson HVAC Laboratory during Phase 2 showed that the EnergyPlus-based simulation was a surprisingly accurate prediction of the experiment. Therefore, actual savings of building energy costs can be expected by applying optimal controls from simulation results. However, it was also concluded that the Larson HVAC Laboratory has only marginal passive building thermal storage inventory and is therefore not representative of a heavy-mass commercial building.

Field testing (Phase 3) was conducted at two sites: In the Energy Resource Station (ERS) at the Iowa Energy Center in Ankeny, Iowa in September of 2003 and in the Energy Plaza facility in Omaha, Nebraska during the summer of 2005.

During the field tests, the novel supervisory controller successfully executed a three-step procedure consisting of 1) short-term weather prediction, 2) optimization of control strategy over the next planning horizon using a calibrated building model, and 3) post-processing of the optimal strategy to yield a control command for the current time step that can be executed in the test facility.

In the Energy Resource Station tests, the primary and secondary building mechanical systems were effectively orchestrated by the model-based predictive optimal controller in real-time while observing comfort and operational constraints. The findings revealed that even when the optimal controller is given imperfect weather forecasts and when the building model used for planning control strategies does not match the actual building perfectly, measured utility costs savings relative to conventional building operation can be substantial. This requires that the facility under control lends itself to passive storage utilization and the building model includes a realistic plant model. The savings associated with passive building thermal storage inventory proved to be small because the ERS facility is of relatively light-weight construction. Also, the facility's central plant revealed the idiosyncratic behavior that the chiller operation in the ice-making mode was more energy efficient than in the chilled-water mode.

During the second set of field experiments carried out in the Energy Plaza facility in Omaha, Nebraska during the summer of 2005 it was intended to 1) further explore the merits of harnessing the active and passive thermal storage inventories simultaneously by means of predictive optimal control, 2) validate the previous findings in the first (modeling and analysis), second (laboratory testing), and third (field testing in the ERS) project phases, and 3) provide experience and guidance for future application in real buildings. Yet, the second set of field tests had to be abandoned prematurely because of complications arising due to server failures. Though the developed weather predictor and predictive optimal control program had been running smoothly during the second field test period, there was a problem in the process of transmitting the optimal results into the building automation system (BAS). The limited data confirms that the optimal control values had been successfully transmitted into the BAS system provided each program is running, and the analysis of cooling load profiles during the test days reveals the effect of load shifting as expected.

In summary, the concept of predictive optimal control of active and passive building thermal storage inventory was analyzed by developing two separate simulation environments, individually investigating the effects of forecasting and modeling accuracy, conducting a parametric analysis of the primary parameters driving the controller performance, conducting lab tests to validate the performance predictions of the simulation tools, and finally by developing and incorporating a real-time predictive optimal control system in two commercial buildings.

Table of Contents

1 Introduction

1.1 Overview

This final report describes the accomplishments achieved in the three phases of a research project aiming to develop a software-based supervisory building controller for commercial buildings that utilizes the combined capacity of building thermal mass and thermal energy storage systems. This controller is designed to optimize cooling and ventilation equipment operation under real-time pricing and conventional electricity rates and by cooperating with the building automation system to minimize energy consumption and operating cost while ensuring human comfort. Due to the uncertain nature of future climate conditions, thermal loads, non-cooling electricity consumption and system performance, the whole-building global optimization approach is based on predictive optimal control. This load-management technology holds the promise of innovation in building automation and represents a novel approach to the control of building thermal storage.

The project was undertaken as a joint effort lead by the University of Nebraska – Lincoln, with support from the University of Colorado and Johnson Controls as the industrial partner.

The overriding **research goal** of this project was to transform a novel concept of supervisory building control into a load management and optimization system that operates in conjunction with a building's energy management and control system to optimize cooling and ventilation operation under dynamic and conventional electricity rates. To achieve this goal, these **research objectives** were pursued:

- Develop **physical models** for the building's energy systems and its dynamic thermal response.
- Conduct a **parametric study** to identify the preferred set of conditions under which the merits of the new technology is maximized and to isolate the key aspects affecting controller performance.
- Perform **model-based analysis** to identify a supervisory optimal control strategy capable of handling uncertainty in future variables and models while ensuring safe and comfortable operation.
- **Design, implement, and validate the supervisory controller** in a full-scale HVAC laboratory
- **Field-test the optimization system** in a suitable location (low humidity with large diurnal temperature swings) and equipped with a thermal energy storage system and a building automation system.

1.2 Organization of the Final Report

Phase 1 (Analysis, Modeling, and Simulation) of this project is covered in Chapters 2 through 0. Chapter 2 establishes the theoretical maximum performance of this novel control strategy and Chapter 3 explores how strongly prediction uncertainty in the required short-term weather forecasts affects the controller's cost saving performance. Chapter 4 investigates the impact of five categories of building modeling mismatch on the performance of model-based predictive optimal control of combined thermal storage using perfect prediction. The parametric study is presented in Chapter 0 to assess the effects of building mass, electrical utility rates, season and location, economizer operation, central plant size, and thermal comfort.

Phase 2 (Laboratory Testing) of this project was conducted at the Larson HVAC Laboratory of the University of Colorado and is described in Chapter 0.

Phase 3 (Field Testing) involved field tests conducted at the Energy Resource Station in Ankeny, Iowa as described in Chapter 5 as well as tests conducted at the Energy Plaza facility in Omaha, Nebraska as discussed in Chapter 6.

1.3 Content of the Final Report

This report cannot cover all of the results and insights gained in the context of this four-year project. For that reason, we explicitly reference the first two topical reports:

1. Henze, G.P. and M. Krarti (2002) "U.S. Department of Energy Cooperative Agreement DE-FC-26-01NT41255 – Predictive Optimal Control of Active and Passive Building Thermal Storage Inventory – Final

Report for Phase I: Analysis, Modeling, and Simulation." Architectural Engineering, Peter Kiewit Institute, University of Nebraska, Omaha, Nebraska.

2. Henze, G.P. and M. Krarti (2003) "U.S. Department of Energy Cooperative Agreement DE-FC-26-01NT41255 – Predictive Optimal Control of Active and Passive Building Thermal Storage Inventory – Final Report for Phase II: Laboratory Testing." Architectural Engineering, Peter Kiewit Institute, University of Nebraska, Omaha, Nebraska.

This final report intends to offer a unified view of the problem set out to be solved. Because not only one but two approaches to solving the problem were developed at the two primary institutions UNL and CUB in the course of the project, the PI decided to present mainly one of the approaches here (based on a coupling of Matlab and TRNSYS) and refer to references [50], [51] and [53] for further details on the second approach (based on EnergyPlus and integrated optimization routines).

2 Phase 1: Analysis – Evaluation of Optimal Control

2.1 Abstract

Cooling of commercial buildings contributes significantly to the peak demand placed on an electrical utility grid. Time-of-use electricity rates encourage shifting of electrical loads to off-peak periods at night and weekends. Buildings can respond to these pricing signals by shifting cooling-related thermal loads either by precooling the building's massive structure or by using active thermal energy storage systems such as ice storage. While these two thermal batteries have been engaged separately in the past, this chapter investigates the merits of harnessing both storage media concurrently in the context of optimal control. The objective function is the total utility bill including the cost of heating and a time-of-use electricity rate without demand charges. The evaluation of the combined optimal control assumes perfect weather prediction and plant modeling, which justifies the application of a so-called consecutive time block optimization that optimizes 24 hour horizons sequentially. The analysis shows that the combined utilization leads to cost savings that is significantly greater than either storage but less than the sum of the individual savings. The findings reveal that the cooling-related on-peak electrical demand of commercial buildings can be drastically reduced and justify the development of a predictive optimal controller that accounts for uncertainty in predicted variables and modeling mismatch in real time.

2.2 Introduction

The equipment and systems providing thermal comfort and indoor air quality for commercial buildings consume 42% of the total energy used in buildings [1]. Energy use and utility cost can be reduced significantly by increasing the efficiency of this equipment, by distributing thermal energy more efficiently and by more closely meeting the needs of building occupants. The energy efficiency of system components for heating, ventilating, and air-conditioning (HVAC) has improved considerably over the past 20 years. For example, shipment-weighted energy efficiency ratios of unitary air conditioners in the United States have increased by 54% [2]. The average efficiency of centrifugal chillers improved by 36% and the efficiency of the best chillers increased by 50% [3]. With similar improvements in the efficiencies of boilers, motors, fans, and pumps, outstanding opportunities exist for reducing energy use and cost in commercial sites. Yet, these opportunities depend on effective building operations: e.g., a building with coincident heating and cooling due to inferior control loop parameters wastes energy regardless of boiler and chiller efficiency.

In contrast to energy conversion equipment, less improvement has been achieved in thermal energy distribution, storage and control systems in terms of energy efficiency and peak load reduction potential. Advancements are also needed to improve thermal storage systems, improve control systems and improve systems integration from a whole building perspective while meeting occupant comfort and performance requirements [4]. In the definition of this project, 'active' denotes that thermal storage systems, such as ice storage, require an additional fluid loop to charge and discharge the storage tank or to deliver cooling to the existing chilled water loop. Building thermal capacitance is 'passive' since it requires no additional heat exchange fluid in addition to the conditioned air stream.

Active thermal energy storage (TES) is an electrical load management and building equipment utilization strategy which can reduce utility electricity demand and equipment first-costs. Typical applications of TES systems include medium-size to large office buildings, hotels, and retail stores. TES systems are designed to avoid high utility demand charges from cooling during the summer and level a building's electrical demand profile. Electrical demand and time-of-use rates have been tailored to reflect the significance of peak energy use periods. TES systems have gained acceptance in reducing peak electrical consumption and installed chiller capacity. Active TES is either a chilled-water tank or an ice tank. The basic operating strategy of an active TES system is to run electrical chillers during times of low electrical demand and energy prices (off-peak periods) to charge the storage medium. During expensive on-peak periods, either ice is melted or a chilled-water tank is discharged to provide cooling and reduce the use of mechanical cooling.

The building structural mass represents a passive building thermal storage inventory which can embody a substantial amount of thermal energy that can be harnessed to reduce operating costs. In conventional op-

eration, building zone conditions are usually controlled to maintain constant temperature and/or humidity setpoints that ensure acceptable comfort during occupancy. When unoccupied, the building energy equipment is turned off and the zone temperature is allowed to float; a strategy that is coined nighttime setup control. Several simulation and experimental studies have shown that proper precooling and discharge of building thermal storage inventory can attain considerable reductions of operating costs in buildings.

Phase 1 evaluated the merits of combined optimal control of both passive building thermal capacitance *and* active thermal energy storage systems to minimize an objective function of choice including total energy consumption, energy cost, occupant discomfort, or a combination of these.

Instead of merely satisfying instantaneous building cooling requirements, both active and passive storage inventories can be effectively harnessed in the framework of supervisory control:

a) To exploit the performance benefits of cooler ambient conditions during nighttime for central chilled water plants, allowing for optimal scheduling of chillers, cooling towers, fans and pumps;
b) To shape the next day's cooling load profile by precooling the building's massive structure at night;
c) To make best possible use of the cost savings potential offered by conventional time-of-use and dynamic utility rate structures, including real-time pricing options that are offered by an increasing number of utilities.

Several investigators have identified promising savings potentials when building operation has been optimized in buildings *without* storage [5] - [10]. Moreover, recent analyses suggest significant performance merits from *either* active [11] - [21] *or* passive [22] - [33] thermal storage inventory under optimal control.

The *combined* use of both storage media under optimal control has been investigated for a 24-hour deterministic simulation study which revealed that significant operating cost savings (~18%) and electrical demand reduction can be achieved [34]. Optimal building control proved most effective in dry climates with large diurnal temperature swings, in the presence of utility rates strongly encouraging load-shifting, and when cool storage systems allow more effective load-shifting than building precooling alone. These results suggest the investigation of combined optimal storage utilization facilitated by a predictive supervisory controller suitable for implementation in commercial buildings. This first chapter lays the groundwork for such a closed-loop model-based predictive optimal controller by investigating an overall solution approach that can be employed in real time.

Two essential assumptions are applied:

a) Weather, occupancy, non-cooling electrical loads are perfectly predicted.
b) The building thermal response is perfectly represented by the building model, i.e., there is no mismatch between the modeled and actual building behavior.

Given these assumptions, closed-loop optimal control is not necessary here as updated forecasts do not offer superior information and a consecutive time block optimization approach (described further below) is applied instead. The evaluation of the potential utility cost savings for a wide range of parameters are documented in Chapter 0.

2.3 Description of the Analysis

2.3.1 Investigated Building

We investigate a three-story office building as shown in Figure 1 with five thermal zones per floor, i.e., 15 thermal zones in total. The perimeter zones have an area of 288 m^2 each, while the core zone has an area of 576 m^2. Total area per floor is thus 1,728 m^2 and the building total is 5,184 m^2. Counting the exterior envelope, floor, and ceiling surfaces, the building mass is approximately 770 kg/m^2 of floor area, thus can be considered heavy-weight construction.

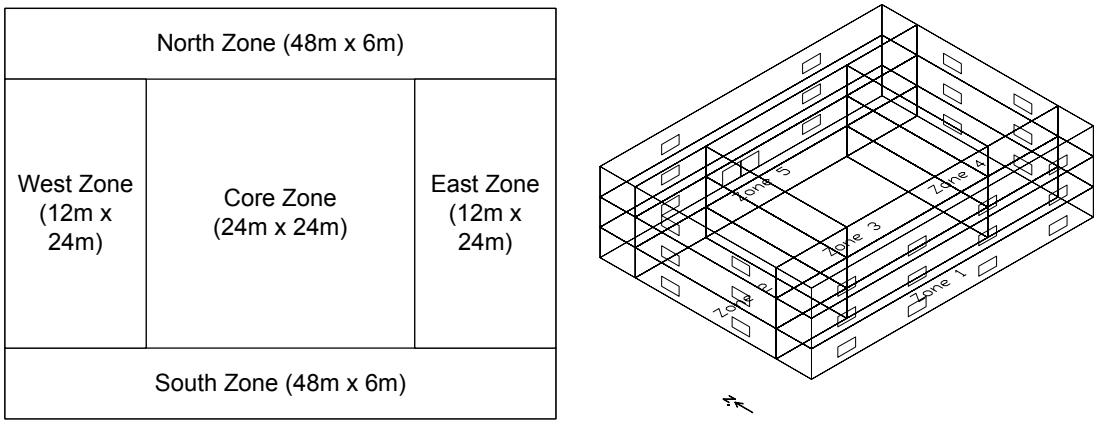

Figure 1: Plan View (left) and Isometric View (right) of Office Building

Peak building occupancy is 10 m^2/person. Each office worker contributes 132 W of internal gain, where 54% are assumed to be sensible and 46% latent. Peak lighting density is 20 W/m^2. The occupancy and lighting schedules for a weekday are shown in Figure 2, where hour 13 refers to the hour from 12 to 13. On week-ends and holidays building occupancy is zero and lighting density is 5% of the peak value.

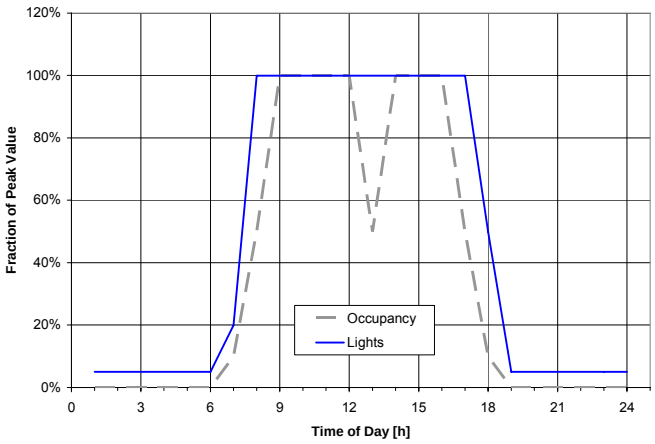

Figure 2: Weekday Occupancy and Lighting Schedule

The office building was first modeled in EnergyPlus [35] and subsequently a TRNSYS [36] model was derived and validated. For a series of identical days (July 21 in Phoenix, Arizona from TMY2 weather data), good agreement of the zone temperature and cooling load profiles for both dynamic simulation programs was achieved. Subsequent annual analysis revealed a building design cooling load of 470 kW.

The building is equipped with a central chilled water plant with a capacity of $CCAP_{base}$ = 250 kW including a thermal energy storage system with a capacity of *SCAP* = 2,500 kWh and a second dedicated chiller with a capacity of $CCAP_{TES}$ = 250 kW. Thus, the base chiller is downsized by 47% and the active TES tank can meet the peak load alone for 5.3 hours. The base chiller has a constant coefficient-of-performance (COP) of 4.5 and the dedicated TES chiller has constant COP of 3.0. The zones are conditioned using a variable air volume (VAV) air-handling unit with hot water reheat at the VAV terminal boxes. Outside air intake is controlled by an economizer cycle using return air temperature limit.

2.3.2 Base Case

We will state cost savings relative to a "base case," which is a chilled water system that experiences the same cooling load and weather profiles and uses the same HVAC systems subject to the same utility rate structure

as the corresponding optimized storage system. The active TES system is governed by the chiller-priority control strategy, i.e., the base chiller is used to serve the building cooling load up to its capacity $CCAP_{base}$, while the active storage is used to meet the cooling loads exceeding $CCAP_{base}$. The passive building thermal storage inventory is not utilized: During occupancy, a cooling zone setpoint of 24°C and a heating setpoint of 20°C is maintained; during unoccupied times, the HVAC systems are turned off and the temperatures are allowed to float.

The performance metric for all cases is the total utility cost for operating the office building over a selected time horizon, which includes electricity and heating costs. The electrical utility rate structures includes time-of-use differentiated energy charges ($/kWh), while the utility rate for purchased heating is considered constant.

2.3.3 Passive Thermal Storage System Modeling

The building structure responds to changes in zone temperature setpoints $T_{Z,SP}$. The zone temperature T_Z is directly affected only by the net convective heat flux according to the discrete-time energy balance on the zone air mass

$$C_Z \frac{\Delta T_Z}{\Delta t} = \sum_i \dot{Q}_{conv,i}, \tag{1}$$

where C_Z is the zone thermal capacitance. These convective heat fluxes include contributions from interior wall surfaces due to transmission and delayed release of solar gains, HVAC systems, internal gains, as well as infiltration. Of those, the current interior wall surfaces fluxes depend on a history of past inside and outside air and surface temperatures as well as inside and outside heat fluxes. The transient response of the building envelope is typically modeled by transforming the heat diffusion equation

$$\frac{\partial T_Z}{\partial t} = \alpha \frac{\partial^2 T_Z}{\partial x^2}, \tag{2}$$

(where α is the thermal diffusivity) into a conduction transfer function (CTF), where the inside and outside surface heat fluxes are determined with the help of construction-specific CTF coefficients *a, b, c*, and *d*.

$$\begin{aligned} \dot{q}_{s,o} &= \sum_{k=0}^{n_a} a_k T_{s,o,t-k\Delta t} - \sum_{k=0}^{n_b} b_k T_{s,i,t-k\Delta t} - \sum_{k=1}^{n_d} d_k \dot{q}_{s,o,t-k\Delta t} \\ \dot{q}_{s,i} &= \sum_{k=0}^{n_b} b_k T_{s,o,t-k\Delta t} - \sum_{k=0}^{n_c} c_k T_{s,i,t-k\Delta t} - \sum_{k=1}^{n_d} d_k \dot{q}_{s,i,t-k\Delta t}. \end{aligned} \tag{3}$$

The zone temperature setpoints can be varied between 15 and 30°C during unoccupied periods and between 20 and 24°C during occupied periods. Building precooling reduces the convective contributions from inside surfaces during occupied periods by depressing the average envelope temperature during unoccupied periods.

2.3.4 Active Thermal Storage System Modeling

The defining feature of any storage system is its ability to bridge a temporal gap between supply and demand. In an active thermal energy storage system, the temporal occurrence of electrical cooling-related loads can be separated from that of the thermal (cooling) loads. Figure 3 shows that the building cooling load can be met by any combination of contributions from the base chiller and the active TES system, while the dedicated chiller only serves to charge the active TES.

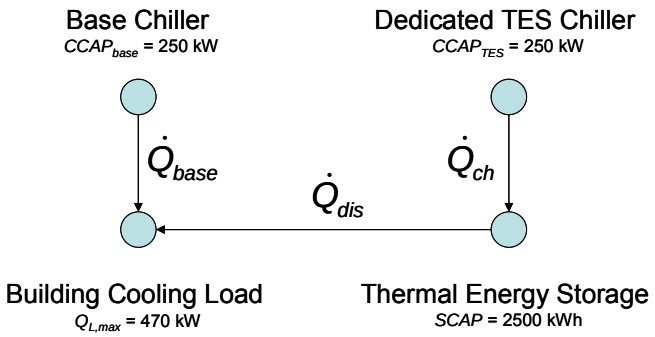

Figure 3: Central Chilled Water Plant Configuration

Changes in the state-of-charge x of the active TES system are described in discrete time by

$$x_{k+1} = x_k + u_k, \tag{4}$$

subject to the state constraints

$$x_{\min} = 0 \le x \le x_{\max} = 1, \tag{5}$$

where is u_k is the dimensionless TES charge/discharge rate subject to its own nonlinear constraints

$$u_{\min,k} \le u_k \le u_{\max,k}. \tag{6}$$

The charge and discharge capacities depend on the available thermal energy storage inventory and current cooling load. The constraints on the control variable u are formulated as

$$u_{\min,k} = \max\left\{-\dot{Q}_{L,k}\frac{\Delta t}{SCAP}, x_{\min} - x_k\right\} \tag{7}$$

and

$$u_{\max,k} = \min\left\{CCAP_{TES}\frac{\Delta t}{SCAP}, x_{\max} - x_k\right\}. \tag{8}$$

Thus, no actions can be taken that would lead to states-of-charge outside feasible limits, i.e., full and empty storage tank, respectively. Further, no more than the current load can be discharged and the TES chiller capacity $CCAP_{TES}$ limits the maximum charge rate $u_{max,k}$. There is no explicit ice or chilled-water tank model and heat transfer limitations on the charging and discharging rates are not considered, i.e., we assume an idealized loss-free thermal battery.

Depending on the current cooling load, a choice of active TES charging/discharging rate u determines the mode of operation of the central chilled water plant as shown in Table 1.

Table 1: Modes of Operation of Chilled Water Plant

Mode	Mode	TES charge/discharge rate	Consequence
PM1	Discharging	$u \le 0$	$\dot{Q}_{dis} = u\frac{SCAP}{\Delta t}; \dot{Q}_{ch} = 0; \dot{Q}_{base} = \dot{Q}_L - \dot{Q}_{dis}$
PM2	Charging	$u > 0$	$\dot{Q}_{dis} = 0; \dot{Q}_{ch} = u\frac{SCAP}{\Delta t}; \dot{Q}_{base} = \dot{Q}_L$

2.3.5 Optimal Control Modeling

2.3.5.1 Monthly Cost Function

Optimal control is defined as that control trajectory that minimizes the total monthly utility bill C_m for electricity and heating:

$$J_m = \min C_m = \min\left\{C_{elec,m} + C_{heat,m}\right\}, \text{ where}$$
$$C_{elec,m} = C_{energy,m} + C_{demand,m} = \sum_{k=1}^{K_m} r_{e,k} P_k \Delta t_h + \max_{1\le k\le K_m}\left\{r_{d,k} P_k\right\} \quad (9)$$
$$C_{heat,m} = \sum_{k=1}^{K_m} r_h \dot{Q}_{heat,k} \Delta t_h$$

where $r_{e,k}$ and $r_{d,k}$ are the energy and demand rates for electricity according to the utility tariff in effect for time k, K_m is the number of hours in the current month, P_k is the total facility electricity demand, Δt_h is a time increment of one hour, r_h is the unit cost of heat delivered, and $\dot{Q}_{heat,k}$ is the heating demand in hour k. For the analysis presented here, load-shifting to off-peak hours is encouraged only through a substantial energy rate differential; demand rates are not considered and the cost function simplifies to

$$J_m = \min C_m = \min\left\{C_{energy,m} + C_{heat,m}\right\}. \quad (10)$$

2.3.5.2 Consecutive Time Block Optimization

Consecutive time block optimization (CTBO) is employed, i.e., the predictive optimal controller carries out an optimization over a predefined planning horizon L and the complete generated optimal strategy is executed. At any time k^*, the required external variables (such as weather information) are predicted over a planning horizon L and the optimal policy that minimizes J_L is determined. The complete strategy is executed without correcting for improved forecasts available during $k^* < k < k^* + L$. After L time step the process is repeated. The planning horizon is L = 24 hours throughout this study.

The alternative approach is closed-loop optimization (CLO), i.e., the predictive optimal controller carries out an optimization over a predefined planning horizon L and of the generated optimal strategy only the first action is executed. At the next time step the process is repeated. The final control strategy of this near-optimal controller over a total simulation horizon of K steps is thus composed of K initial control actions of K optimal strategies of horizon L, where $L < K$. By moving the time window of L time steps forward and updating the control strategy after each time step, a new forecast is introduced at each time step and yields a policy which is different from the policy found without taking new forecasts into account.

In the limiting case of perfect forecasts, both CLO and CTBO can be expected to produce identical results. When the future is subject to uncertainty, i.e., in the case of an actual implementation, CLO-based predictive optimal control is expected to exhibit superior performance. Since the focal point of this chapter is to identify the relative performance of jointly optimizing the active and passive building thermal storage, we assume perfect predictions and use CTBO.

The optimal solution J_L found at current time k^* is associated with L global temperature setpoints $\left\{T_{Z,SP}\right\}_{k^*}^{k^*+L}$ and L active TES charge/discharge rates $\left\{u\right\}_{k^*}^{k^*+L}$.

2.3.5.3 Sequential Optimization and Building Modes

The cost of electrical energy $C_{energy,L}$ is affected by both the active and passive building thermal storage strategy. The choice of zone temperature setpoints will affect the cooling load, which has to be known for the active storage to be controlled properly. Therefore, there is a causal relationship from the passive to the active storage, which requires us to solve the passive storage first, followed by the optimization of the active thermal storage inventory on the basis of the previously determined optimal building cooling load profile.

Due to the presence of simple upper and lower zone temperature bounds, the passive thermal storage (building mass) component of the control problem proved to be solved effectively with the help of a common implementation of the quasi-Newton method, which is described below. The use of a direct search method (Nelder-Mead Simplex) led to an excessive number of function evaluations (TRNSYS runs) because of cost penalties arising from bound violations. To reduce the numerical complexity of the passive storage optimization problem, a simplification is introduced: Instead of optimizing L variables, only one global zone setpoint

$T_{Z,SP}$ is determined for each combination of occupancy (occupied, unoccupied) and utility rate periods (on-peak, off-peak), defined as building mode (BM), occurring over the next *L* time steps

- BM1: Unoccupied and off-peak rates
- BM2: Unoccupied and on-peak rates
- BM3: Occupied and off-peak rates
- BM4: Occupied and on-peak rates

During each building mode, the corresponding control variable is kept constant as shown in Figure 4a. Since these few variables describe stepped profiles for each control variable, we denote them as *solution parameters SP*. For the given occupancy and utility rate periods and assuming hourly time steps, the solution space for an $L = 24$ hour horizon is reduced from 24 dimensions to 5 dimensions. For any horizon *L*, the number of parameters can increase or decrease depending on how many distinct occupancy and rate periods are covered. Though this simplification causes the solution to become slightly suboptimal compared to the full solution, the problem now becomes computationally tractable.

The active storage (TES) optimization problem is characterized by complex and nonlinear constraints as expressed by Eq. (7) and (8), yet simple state transitions as characterized by Eq. (4). This class of problem is most readily solved using dynamic programming, which is described below, and yields *L* solution variables as shown in Figure 4b.

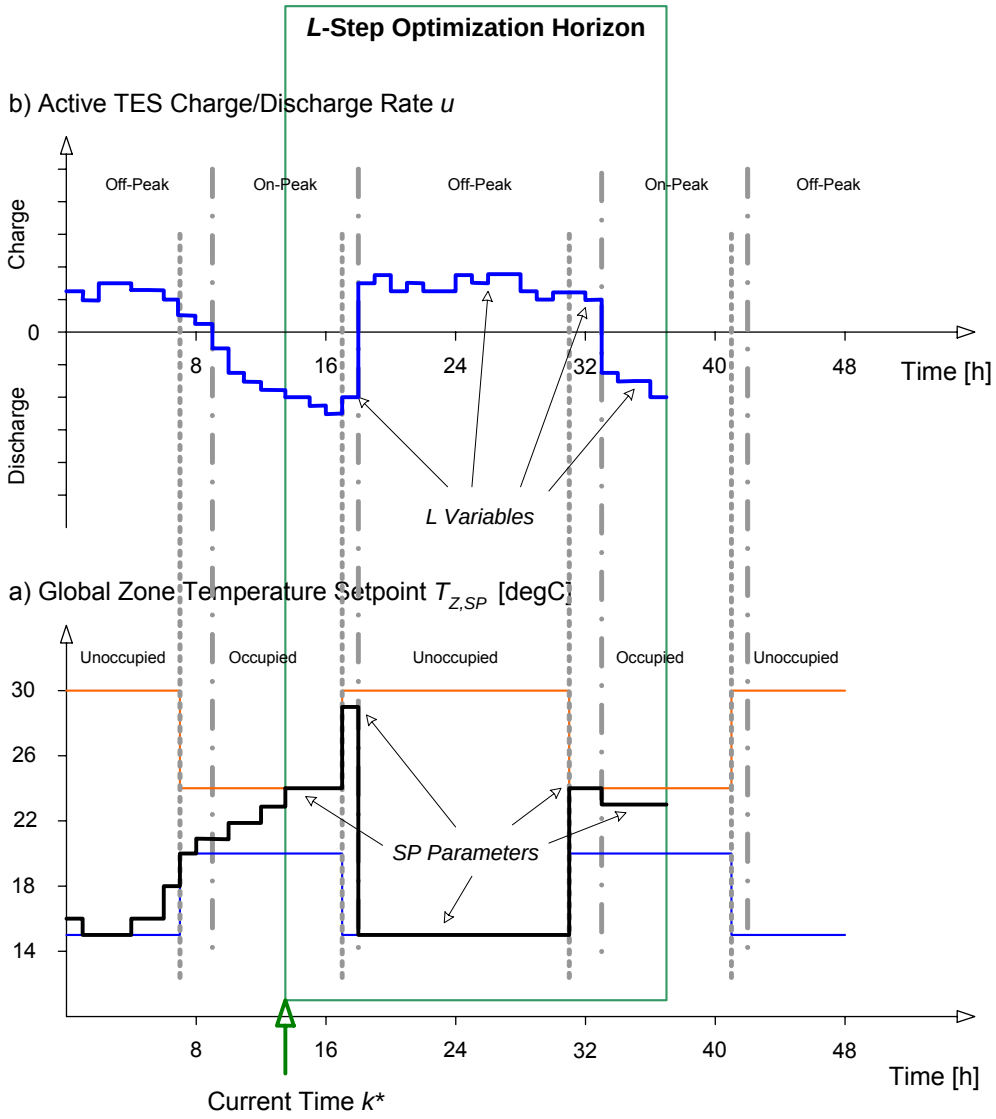

Figure 4: a) Simplified Stepped Optimization for Passive Storage and b) Active Storage Optimization

2.3.5.4 Iterative Sequential Optimization

Figure 5 illustrates how the least utility cost J_L over horizon L is determined. At time zero and starting with initial zone temperature setpoints $\{T_{Z,SP}\}_{init}$ halfway between the upper and lower bounds and no active storage utilization $\{u\}_{init} = 0$, the passive storage inventory is optimized to minimize C_L. As a result, the optimal building cooling load profile is computed and handed over to the active storage optimization, which calculates an optimal TES charge/discharge strategy. In a second pass, the optimal active storage utilization strategy and the previously found optimal zone temperature setpoint profile are employed to determine the new optimal zone temperature setpoint profile and optimal utility cost J_L. This cycle is repeated until the optimal cost J_L converges. Typically, convergence is attained after 2-3 iterations. Previously optimal solutions are stored as starting values for subsequent optimizations to reduce execution time.

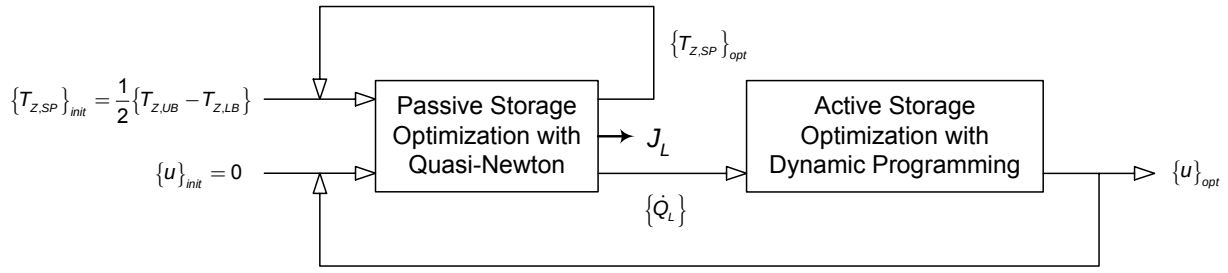

Figure 5: Iterative Sequential Optimization of Utility Cost C_L

2.3.6 Optimization Algorithms

We investigated two classes of optimization algorithms: a quasi-Newton method, which approximates the function gradient through finite differences, and dynamic programming for sequential decision making problems. Among those methods that utilize gradient information, quasi-Newton methods are the most popular. They collect curvature information on the cost function at each iteration to describe a quadratic model problem

$$\min_x \left\{ \frac{1}{2} x^T H x + c^T x + b \right\}, \tag{11}$$

where the Hessian matrix, H, is a positive definite symmetric matrix, c is a constant vector, and b is a constant. The optimal solution x^* occurs when the partial derivatives of x vanish, i.e.,

$$\nabla f(x^*) = Hx^* + c = 0 \;\Rightarrow\; x^* = -H^{-1}c. \tag{12}$$

Newton-type methods calculate the Hessian H directly, which is numerically very demanding. Quasi-Newton methods avoid the direct computation of the Hessian by extracting curvature information from observed behavior $f(x)$ and $\nabla f(x)$ and subsequently approximating the Hessian numerically [37]. We employ the popular method by Broyden, Fletcher, Goldfarb, and Shanno (BFGS):

$$H_{i+1} = H_i + \frac{q_i q_i^T}{q_i^T s_i} - \frac{H_i^T s_i^T s_i H_i}{s_i^T H_i s_i}, \text{ where } s_i = x_{i+1} - x_i \text{ and } q_i = \nabla f(x_{i+1}) - \nabla f(x_i) \tag{13}$$

In the presented case, the gradient information is derived by partial derivatives using numerical differentiation via finite differences: Each decision variable x is perturbed and the rate of change in the cost function is determined. Then at each iteration i, a line search is performed in the direction of

$$d = -H_i^{-1} \cdot \nabla f(x_i) \tag{14}$$

The task of minimizing operating cost using active thermal storage inventory is framed as a sequential decision-making process of decision variable u. The optimization technique *dynamic programming* commonly used for this type of problems was first formally introduced by the mathematician Richard Bellman in 1957. Bellman's *Principle of Optimality* [38] states that:

"An optimal policy has the property that whatever the initial state and initial decision are, the remaining decisions must constitute an optimal policy with regard to the state resulting from the first decision."

In other words, the optimal solution to an L-step process must come from the optimal solution of an L-1-step process that is based on the optimal outcome of the first step. The solution of one L-step process will thus be found recursively by optimizing L single-step processes in reverse time by starting at the end of time and moving back to "now". To apply, the cost function has to be incrementally additive and the dynamic system has to be discrete.

2.4 Results

The utility rate is assumed to be $0.20/kWh on-peak and $0.05/kWh off-peak; no demand charge is levied. The on-peak period is weekdays from 9 AM to 6 PM, off-peak all remaining hours. The building is occupied from 7 AM to 5 PM.

The viewgraphs in this section are created on the basis of simulations in which July 21 in Phoenix, AZ is repeated over and over again until steady-state conditions are attained after about 7 identical days. The outdoor ambient temperature swings from about 16°C early in the morning to over 38°C at 6 PM. Table 2 lists the nominal capacities of the base chiller and the active storage and chiller capacities for the five investigated cases.

Case 1 represents the basecase in which cooling loads have to be met without any storage available. Case 2 makes use of active thermal storage as governed by chiller-priority control, i.e., the downsized base chiller meets the cooling loads up to its capacity $CCAP_{base}$, thereafter the active storage contributes the remainder. The dedicated active storage chiller requires $SCAP/CCAP_{tes}$ = 10 hours to recharge an empty storage tank. Case 3 optimizes the passive storage capacity by properly precooling the building structure using a fully sized base chiller. In Case 4, the active storage is now optimized instead of governed by a simple rule such as chiller-priority. Finally, Case 5 optimizes both active and passive storage media and represents the focus of this research.

Case 5 is solved by optimizing each 24 hour interval sequentially, i.e. as a series of consecutive time blocks (CTBO) of 24 hours length each. The CTBO method does not allow for the consideration of newly available new information as it becomes available. However, it represents a reference scenario for comparison as we assume perfect prediction for this study.

Table 2: System Sizing for Investigated Control Strategies

Case No.	Optimization	Units	Sizing
1	**Basecase WITHOUT Active Storage**		
	CCAPbase	kW	500
	CCAPtes	kW	0
	SCAP	kWh	0
			Base chiller fully sized, no active storage; night setup.
2	**Basecase WITH Active Storage**		
	CCAPbase	kW	250
	CCAPtes	kW	250
	SCAP	kWh	2,500
			Base chiller downsized; chiller-priority active storage control; night setup.
3	**Passive Only**		
	CCAPbase	kW	500
	CCAPtes	kW	0
	SCAP	kWh	0
			Base chiller fully sized, no active storage; zone setpoints optimized.
4	**Active Only**		
	CCAPbase	kW	500
	CCAPtes	kW	250
	SCAP	kWh	2,500
			Base chiller fully sized; optimal active storage control; night setup.
5	**Active and Passive**		
	CCAPbase	kW	500
	CCAPtes	kW	250
	SCAP	kWh	2,500
			Base chiller fully sized; optimal active storage control; zone setpoints optimized.

The thick lines in Figure 6 represent the upper and lower temperature bounds for the operation of the office building on a weekday. It can be seen how passive only decides on substantial nighttime precooling down to about 21°C zone temperature averaged over all 15 zones. When the temperatures are allowed to float, the average zone temperature rises beyond 28°C during unoccupied times. The combined utilization of active and passive storage leads to less precooling than in the passive only case. All strategies involving passive storage allow for the temperatures to float from the end of occupancy at 5 PM to 6 PM because electricity prices are still high (on-peak) during this time. After 6 PM, electricity prices are low and the building is unoccupied.

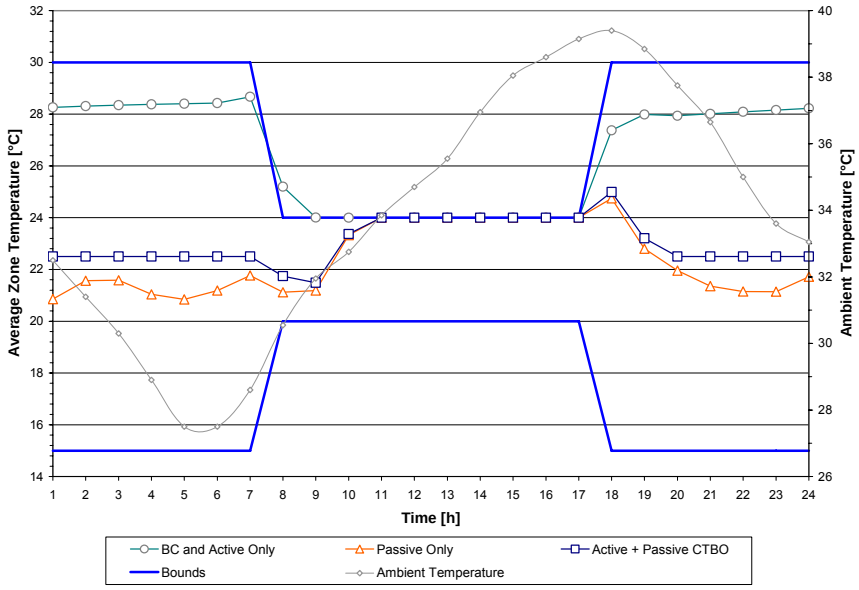

Figure 6: Average Zone Temperature Profiles

The inventory of state-of-charge of the active storage is shown in Figure 7 from midnight to midnight for those strategies involving active storage. For the base case with active storage under chiller-priority control, the storage is fully charged during off-peak hours and discharged by about 50% during the day. The active only optimization discharges fast as of 8 AM, but slows down during the early afternoon hours to end up empty by the end of occupancy. The combined storage utilization approach makes less use of the active storage.

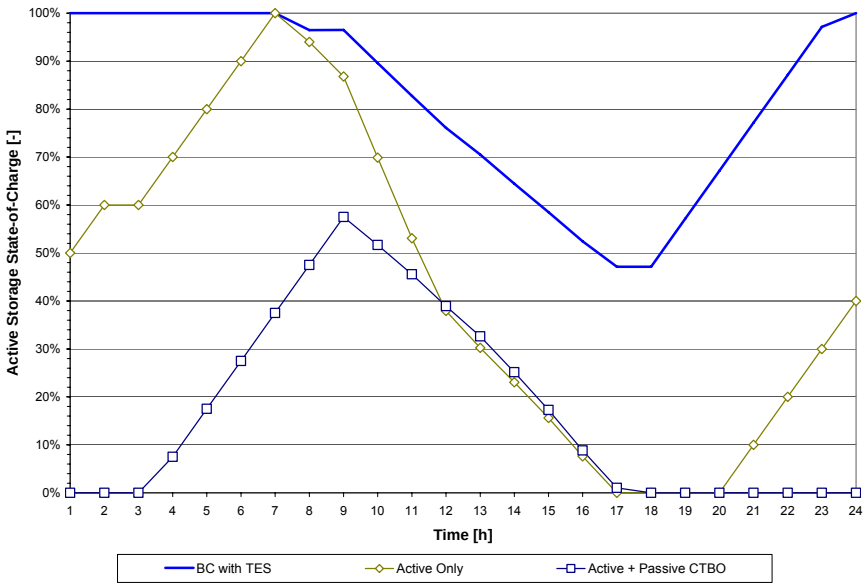

Figure 7: Active Storage State-of-Charge Profiles

Figure 8 illustrates the effect of precooling on the daytime cooling load profile and shows how the building cooling load is shifted away from the expensive on-peak period to the off-peak period for all cases involving

passive storage utilization. The passive only approach leads to the lowest on-peak cooling loads, next comes the CTBO approach to the combined case.

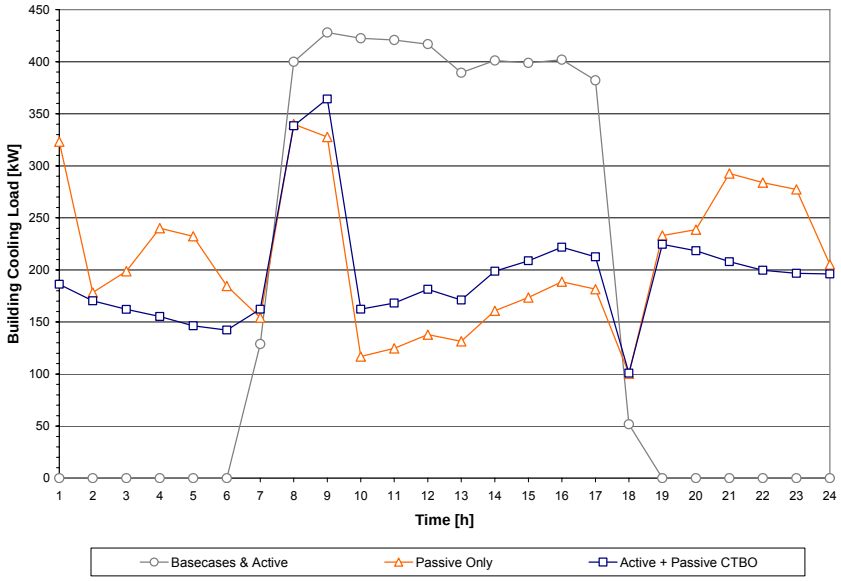

Figure 8: Building Cooling Load Profiles

Reducing on-peak electrical demand is a side effect of shifting expensive on-peak cooling loads to off-peak periods for energy only optimizations as can be seen in Figure 9. While the base case with active storage under chiller-priority control already reduces the demand by 20%, the combined optimization cuts the overall demand nearly in half. Active only and passive only are both superior to the base case with active storage, but inferior to the combined case solved by CTBO.

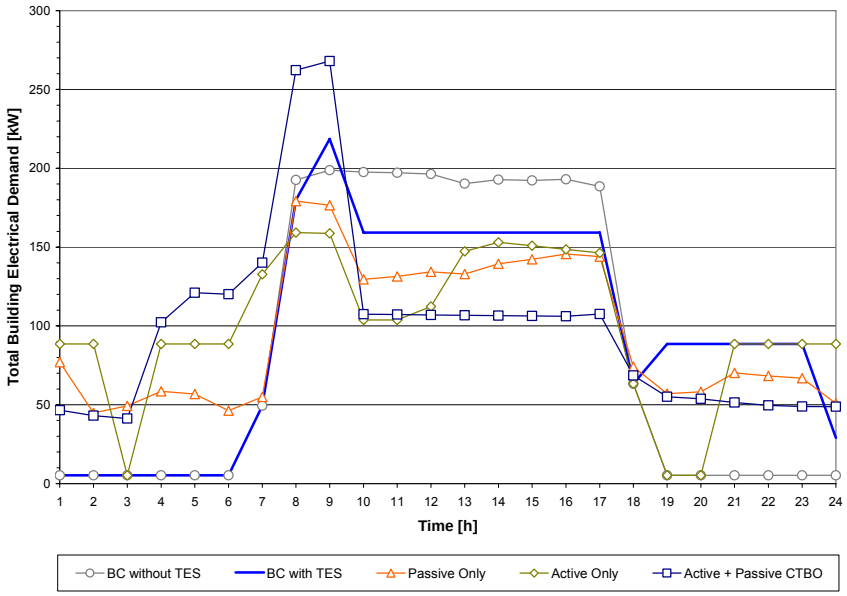

Figure 9: Total Building Electrical Demand Profiles

For a utility rate without demand charges, we can plot daily profiles of utility cost. The total hourly building operating cost including non-cooling cost is shown in Figure 10. The areas under each curve represent the

total daily operating cost. It is obvious that on-peak cost savings are traded off against nighttime expenses for recharging active and/or passive storage inventories.

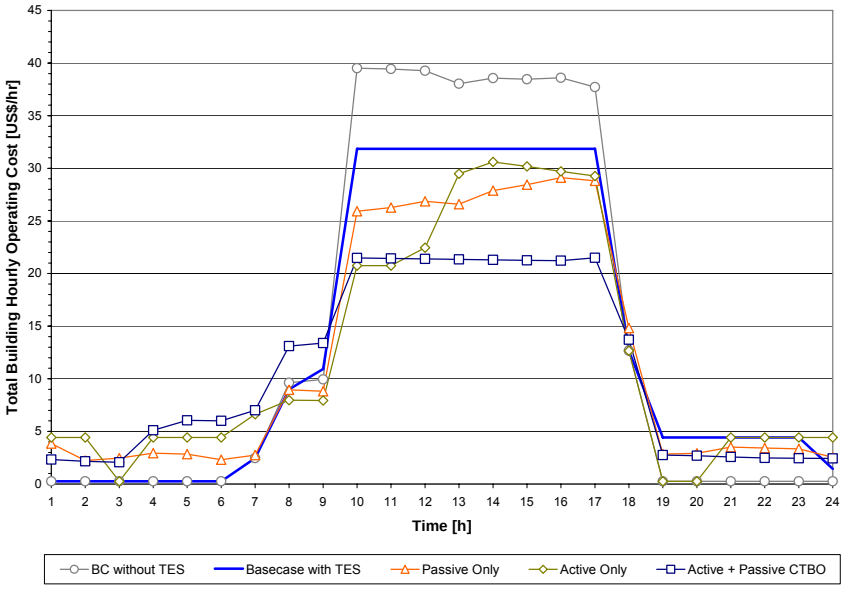

Figure 10: Total Hourly Building Operating Cost Profiles

Figure 11 illustrates how the cooling related costs are effectively shifted to nighttime periods. In fact, the combined storage cases lead to near-zero cooling costs during the on-peak period.

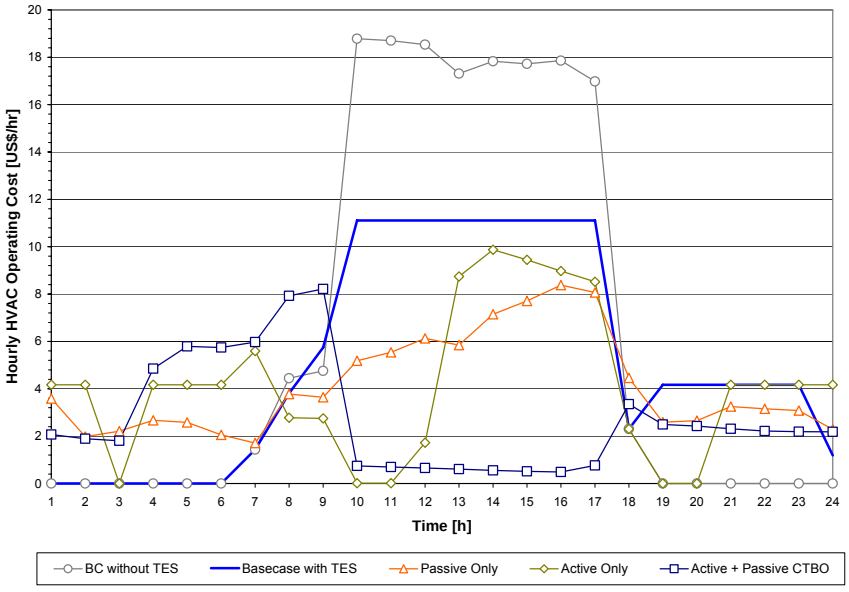

Figure 11: Hourly HVAC Operating Cost Profiles

Finally, Table 3 provides an overview of the daily cost savings achieved for this prototypical day in Phoenix, AZ. Based on total utility cost, savings of about 16% can be achieved for either passive or active only storage, and about 26% for the combined case when compared to the base case without storage. Compared to the base case with active storage under chiller-priority control, savings of about 8% can be achieved for either passive or active only storage and about 18% for the combined case. Based on cooling related utility cost

only, savings of about 37% can be achieved for either passive or active only storage, and about 57% for the combined case when compared to the base case without storage. Compared to the base case with active storage under chiller-priority control, savings of about 20% can be achieved for either passive or active only storage and about 46% for the combined case. These results show that given strong load-shifting incentives, the benefits of the proposed optimization system may be substantial.

Table 3: Summary of Daily Operating Costs

Total Building Hourly Operating Cost

Basecase without TES	Basecase with TES	Passive Only	Active Only	Active + Passive CTBO
$347.42	$314.97	$290.46	$289.00	$257.22
Savings	BC without TES:	16.4%	16.8%	26.0%
	BC with TES:	7.8%	8.2%	18.3%

HVAC Hourly Operating Cost

Basecase without TES	Basecase with TES	Passive Only	Active Only	Active + Passive CTBO
$156.65	$124.20	$99.69	$98.23	$66.45
Savings	BC without TES:	36.4%	37.3%	57.6%
	BC with TES:	19.7%	20.9%	46.5%

2.5 Conclusions and Future Work

This chapter investigated the potential of building thermal storage inventory, in particular the combined utilization of active and passive inventory, for the reduction of electrical utility cost using common time-of-use rate differentials. The findings reveal that when an optimal controller is given perfect weather forecasts and when the building model used for predictive control perfectly matches the actual building, utility cost savings and on-peak electrical demand reductions are substantial. While this work established the theoretical maximum performance, the next efforts need to determine how strongly prediction performance and model mismatch deteriorate the controller performance. Eventually, once an acceptable weather predictor is available and system identification routines calibrate the underlying model, lab and field experimentation will need to verify these savings figures during actual operation.

2.6 References

[1] Arthur D. Little, Inc. (1999) *Guide for Evaluation of Energy Savings Potential*. Prepared for the Office of Building Technology, State and Community Programs (BTS), U.S. Department of Energy.

[2] American Refrigeration Institute (ARI) (1999) *Statistical Profile of the Air-Conditioning, Refrigeration, and Heating Industry*. Page 28. 4301 North Fairfax Drive, Arlington, VA.

[3] American Standard, Inc. (1999) *EarthWise Today*, Vol. 24, p. 3. LaCrosse, Wisconsin.

[4] National Energy Technology Laboratory (NETL/DOE) (2000) *Federal Assistance Solicitation for Energy Efficient Building Equipment and Envelope Technologies Round II*. PS No. DE-PS26-00NT40781. Page 4. U.S. Department of Energy.

[5] Kaya, A., C.S. Chen, S. Raina, and S.J. Alexander (1982) "Optimum control policies to minimize energy use in HVAC systems." *ASHRAE Transactions* 88 (2).

[6] Braun, J.E., S.A. Klein, W.A. Beckman, and J.W. Mitchell (1989) "Methodologies for optimal control of chilled water systems without storage." *ASHRAE Transactions* 95 (1).

[7] House, J.M., T.F. Smith, J.S. Arora (1991) "Optimal Control of a thermal system." *ASHRAE Transactions*, *ASHRAE Transactions* 97 (1).

[8] Kasahara, M., T. Matsuba, Y. Hashimoto, I. Murasawa, A. Kimbara, K. Kamimura, and S. Kurosu (1998) "Optimal Preview Control for HVAC System." *ASHRAE Transactions* 104 (1).

[9] Braun, J.E., S.A. Klein, J.W. Mitchell, and W.A. Beckman (1989) "Applications of Optimal Control to Chilled Water Systems without Storage." *ASHRAE Transactions* 95 (1).

[10] Gibson, G.L. (1997) "A supervisory controller for optimization of building central cooling systems." *ASHRAE Transactions* 103 (1).

[11] Henze, G.P., M. Krarti, and M.J. Brandemuehl (1997a) "A Simulation Environment for the Analysis of Ice Storage Controls" *International Journal of HVAC&R Research*, 3 (2): 128–148.

[12] Henze, G.P., R.H. Dodier, and M. Krarti (1997b) "Development of a Predictive Optimal Controller for Thermal Energy Storage Systems." *Int. J. of HVAC&R Research*, 3 (3): 233–264.

[13] Henze, G.P. and M. Krarti (1998) "Ice Storage System Controls for the Reduction of Operating Costs and Energy." *J. of Solar Energy Engineering*, November 1998.

[14] Henze, G.P. and M. Krarti (1999) "The Impact of Forecasting Uncertainty on the Performance of a Predictive Optimal Controller for Thermal Energy Storage Systems." *ASHRAE Transactions* 105 (1).

[15] Krarti, M., M.J. Brandemuehl, and G.P. Henze (1995) "Final Project Report for ASHRAE 809-RP: Evaluation of Optimal Control for Ice Storage Systems." *ASHRAE Report*, American Society of Heating, Refrigerating, and Air-Conditioning Engineers, Atlanta, Georgia.

[16] Krarti, M., G.P. Henze, D. Bell, J.F. Kreider, M.J. Brandemuehl, and L.K. Norford (1997) "Model Based Optimizer Systems With TES: Final Report", JCEM Technical Report TR/97/15, University of Colorado, Boulder, CO.

[17] Krarti, M., G.P. Henze, and D. Bell (1999) "Planning Horizon for a Predictive Optimal Controller for Thermal Energy Storage Systems." *ASHRAE Transactions* 105 (1).

[18] Marken, A.V. (1997) "Control of Thermal Energy Storage Systems for Cost-Effectiveness." Internal Report, University of Colorado, Boulder, CO.

[19] Bell, D. (1998) "Evaluation of Optimal Controls for Ice-Based Thermal Energy Storage Systems." M.S. Thesis, University of Colorado, Boulder, CO.

[20] Massie, D. (1998) "Optimal Neural Network-Based Controller for Ice Storage Systems." Ph.D. dissertation, University of Colorado, Boulder, CO.

[21] Drees, K.H. and J.E. Braun (1996) "Development and evaluation of a rule-based control strategy for ice storage systems" *Int. J. of HVAC&R Research*, 2 (4): 312–336.

[22] Braun, J.E. (1990) "Reducing energy costs and peak electrical demand through optimal control of building thermal mass." *ASHRAE Transactions* 96 (2): 876-888.

[23] Rabl, A. and L.K. Norford (1991) "Peak load reduction by preconditioning buildings at night," *International Journal of Energy Research* 15: 781-798.

[24] Conniff, J.P. (1991) "Strategies for reducing peak air-conditioning loads by using heat storage in the building structure." *ASHRAE Transactions* 97 (1): 704-709.

[25] Andresen, I. and M.J. Brandemuehl (1992) "Heat storage in building thermal mass: a parametric study." *ASHRAE Transactions* 98 (1).

[26] Morris, F.B., J.E. Braun, and S.J. Treado (1994) "Experimental and simulated performance of optimal control of building thermal storage." *ASHRAE Transactions* 100 (1): 402-414.

[27] Keeney, K.R. and J.E. Braun (1996) "A simplified method for determining optimal cooling control strategies for thermal storage in building mass." *Int. J. of HVAC&R Research*, 2 (1): 59-78.

[28] Keeney, K.R. and J.E. Braun (1997) "Application of building precooling to reduce peak cooling requirements." *ASHRAE Transactions* 103 (1): 463-469.

[29] Mozer, M.C., L. Vidmar, and Robert H. Dodier (1997) "The Neurothermostat: Predictive optimal control of residential heating systems" *Advances in Neural Information Processing Systems*. MIT Press. Cambridge, MA.

[30] Chen, T.Y. (2001) "Real-time predictive supervisory operation of building thermal systems with thermal mass," *Energy and Buildings*, 33: 141-150.

[31] Braun, J.E., K.W. Montgomery, and N. Chaturvedi (2001) "Evaluating the performance of building thermal mass control strategies," *Int. J. of HVAC&R Research,* 7 (4): 403-428.

[32] Braun, J.E., T.M. Lawrence, C.J. Klaassen, and J.M. House (2002) "Demonstration of load shifting and peak load reduction with control of building thermal mass," *Proceedings of the 2002 ACEEE Conference on Energy Efficiency in Buildings*, Monterey, CA.

[33] Chaturvedi, N. and J.E. Braun (2002) "An inverse gray-box model for transient building load prediction," *Int. J. of HVAC&R Research*, 8 (1): 73-100.

[34] Kintner-Meyer, M. and A.F. Emery (1995) "Optimal control of an HVAC system using cold storage and building thermal capacitance." *Energy and Buildings* 23: 19–31.

[35] EnergyPlus v1.0.1 http://www.eren.doe.gov/buildings/energy_tools/energyplus.

[36] TRNSYS – A transient simulation program. SEL University of Wisconsin – Madison, http://sel.me.wisc.edu/trnsys/Default.htm.

[37] Matlab (1996) *Optimization Toolbox User's Guide*. The MathWorks, Inc.

[38] Bellman, Richard E. (1957) *Dynamic Programming*. Princeton, New Jersey: Princeton University Press.

3 Phase 1: Analysis – Impact of Forecasting Accuracy

3.1 Abstract

This chapter evaluates the benefits of combined optimal control of both passive building thermal capacitance and active thermal energy storage systems to minimize total utility cost in the presence of forecasting uncertainty in the required short-term weather forecasts. Selected short-term weather forecasting models are introduced and investigated with respect to their forecasting accuracy as measured by root mean square error, mean bias error, and the coefficient of variation. The most complex model, a seasonal autoregressive integrated moving average (SARIMA) shows the worst performance, followed by a static predictor model that references standard weather archives. The best prediction accuracy is found for bin models that develop a characteristic daily profile from observations collected over the past 30 or 60 days. The model that projects yesterday's patterns one day into the future, proved to be a surprisingly poor predictor. We test the predictor models in the context of a predictive optimal control task that optimizes building global temperature setpoints and active thermal energy storage charge/discharge rates in a closed-loop mode. For the four locations investigated in this parametric study, Chicago, IL, Denver, CO, Omaha, NE, and Phoenix, AZ, it was determined that the 30-day and 60-day bin predictor models lead to utility cost savings that are only marginally inferior compared to a hypothetical perfect predictor that perfectly anticipates the weather during the next planning horizon. In summary, the predictive optimal control of active and passive building thermal storage inventory using time-of-use electrical utility rates with significant on-peak to off-peak rate differentials and demand charges is a highly promising control strategy when perfect weather forecasts are available. The primary finding of this chapter is that it takes only very simple short-term prediction models to realize almost all of the theoretical potential of this technology.

3.2 Introduction

The *combined* use of both storage media under optimal control was investigated in the previous chapter for the reduction of electrical utility cost using common time-of-use rate differentials. The findings revealed that when an optimal controller is given perfect weather forecasts and when the building model used for predictive control perfectly matches the actual building, utility cost savings and on-peak electrical demand reductions are substantial. While this previous work established the theoretical maximum performance, the current chapter determines how strongly prediction performance affects the optimal controller's closed-loop performance. In this study, we assume that the building thermal response is perfectly represented by the building model, i.e., there is no mismatch between the modeled and actual building behavior. The next section will describe several short-term weather prediction models and investigate their prediction accuracy based on standardized statistical performance metrics. Thereafter, selected prediction models will be employed to the task of closed-loop predictive optimal control of active and passive building thermal storage.

3.3 Analysis of Short-Term Weather Prediction Models

The development of prediction models for ambient air temperature follows a 5-step procedure recommended in [39]: data collection, data examination (analysis of time series), data evaluation, prediction model construction, and prediction model evaluation.

3.3.1 Data Collection

The first step to be taken is the collection of as much relevant data on the prediction task as possible. The amount of data should be kept low as determined by relevance, reliability and recentness [39]. The *National Oceanic and Atmospheric Administration (NOAA)* runs an Interactive Weather Information Network, accessible at http://nndc.noaa.gov, where a considerable amount of historical and current weather data is available. Thus, measurements for the most recent years 2000 and 2001 were collected for the following four cities:

Chicago, IL; Denver, CO; Omaha, NE; Phoenix, AZ. The available database was reduced to hourly observations, i.e., 8,760 values per year are available.

3.3.2 Data Examination

In order to select an appropriate prediction model, the characteristic of the temperature time series for Omaha, Nebraska for the year 2001 was examined with respect to its main features: stationary behavior, trend, seasonal component, apparent changes and outlying observations. The investigation tools employed are the graph of the time series and the following additional measurements; sample autocorrelation function (SACF), sample partial autocorrelation function (SPACF), sample mean $\mu_x(t)$ and sample variance $\sigma_x^2(t)$.

Visual inspection of the SACF and SPACF revealed that the time series is non-stationary. A positive trend from winter to summer and a negative trend from summer to winter were observed, which of course, is not a trend but rather a periodic behavior with an annual cycle. Furthermore, there is a periodic behavior with a daily cycle. Few outlying observations were found, which are attributed to abrupt changes within the weather development and which are considered rare.

3.3.3 Description of Prediction Models

As discussed in greater detail in Section 5.3, the predictors are required to provide short-term forecasts of ambient weather for the next L = 24 hours starting at the current time k^*.

3.3.3.1 Methods Based on a Reference Day

The assumption underlying this procedure is that the actual time series will exhibit a behavior similar to a reference pattern, which is developed by rendering historical data, TMY2 data or bin estimates. In each case requiring prediction over the planning horizon L = 24 hours, a forecast is made for the next L hours, and the L-hour profile is shifted such that the predicted value for the current hour k^* coincides with the actual measured value. The prediction therefore yields a characteristic L-hour profile which is anchored at the current known value.

(A) TMY2 Predictor

First, a prediction with a static reference pattern consisting of TMY2 data is considered and explained. The TMY2 weather database describes a typical meteorological year for 239 stations derived from the 1961-1990 National Solar Radiation Data Base (NSRDB) [44]. The TMY2 data files consist of months that were selected from individual years and then concatenated to form a complete year. The TMY2 database therefore only represents typical conditions. Mathematically, the predictor is expressed by:

$$\left\{\hat{X}_t\right\} = \left\{Y_t\right\}, \qquad t \in [k^*, k^* + L] \tag{15}$$

where time $k^* \in [1,\ 8760 - L]$, $\left\{\hat{X}_t\right\} = \hat{X}_1, \ldots, \hat{X}_t$ are the predicted values of the times series of year 2001 and $\left\{Y_t\right\}$ is the time series of the TMY2 year.

(B) Same-as-Yesterday Predictor

This predictor follows a similar concept of prediction by reference; however, the difference is the dynamic reference pattern of the time series, i.e., a continuous update of the reference day. Assuming that the weather conditions "today" will be similar to "yesterday", the profile of the previous 24 hours is transferred to the current time step according to:

$$\left\{\hat{X}_t\right\} = \left\{X_{t-24}\right\},\ t \in [k^*, k^* + L] \tag{16}$$

(C) Bin Predictor

The reference time series consists of bin values, one for every hour h of the day. The methodology presented distinguishes between a static and a dynamic reference day. In the static case, a representative reference day, which represents all q days of a month, is created from bin values for each month. Thus, there are 12 reference days per year. In essence, the bin day provides an average daily profile for a particular month. Consequently, the bin time series can be expressed as:

$$\left\{\hat{X}_h\right\}_M = \frac{1}{q}\sum_{n=0}^{q-1} X_{h+24n}, \quad h \in [1, 24] \tag{17}$$

Here, $q \in [28, 30, 31]$ is the number of days in the month M that is used to construct the characteristic daily profile, which can either be the previous month or the same month of the previous year. The dynamic type of the bin model develops the characteristic profile of the next L hours on the basis of the past d days relative to the current time k*. Hence, the bin values are computed from

$$\left\{\hat{X}_t\right\} = \frac{1}{d}\sum_{n=1}^{d} X_{t-24n}, \quad t \in [k^*, k^* + L] \tag{18}$$

where the cases investigated in this project are d = 1, 7, 30, 60, and 90 days. The case d = 1 leads to the same-as-yesterday predictor described in the previous subsection.

3.3.3.2 Unbiased Random Walk

This predictor is very simple. If the present temperature is T_{k^*}, then one predicts that the future temperatures T_{k^*+1}, T_{k^*+2}, T_{k^*+3}, . . . are all equal to T_{k^*}. It turns out that this prediction is best in the least-squares sense if the process generating the sequence of temperatures is an unbiased random walk—that is, if the temperature at the next hour is with equal probability either somewhat greater or somewhat less than the present temperature. This forecasting model is perhaps the simplest interesting model and provides a base case against which one can test more sophisticated predictors. This model is mathematically described as:

$$\left\{\hat{X}_t\right\} = \left\{X_{k^*}\right\}, \quad t \in [k^*, k^* + L] \tag{19}$$

where L is the length of the prediction and planning horizon, here L = 24 hours.

3.3.3.3 SARIMA

The seasonal autoregressive and moving average prediction model is a flexible tool with a wide range of applications that belongs to the family of Box-Jenkins methods. It is mathematically demanding and entails time-consuming procedures for model identification, parameter estimation, diagnosis, and prediction for every time series. Since the development of a SARIMA model is not within the scope of this project, the results of these four stages are only summarized briefly and the reader is referred to [41], [42], [43]. Because the presented time series is not stationary, it has to be transformed into a stationary time series which is achieved by eliminating the trend and the seasonal component. Among the different methods of transformation (smoothing with a finite moving-average filter, exponential smoothing, polynomial fitting [41]), the so-called differencing is commonly used. In the studied cases, first regular differencing and first seasonal differencing [43] according to

$$z_t = X_t - X_{t-1} - X_{t-24} + X_{t-25} \tag{20}$$

proved effective in creating a stationary time series with neither trend nor daily or seasonal periodicity. Here, the periodicity is the diurnal cycle with a period of 24 hours. Using standard guidelines, the sample autocorrelation functions (SACF and SPACF) is determined from the differenced time series to select the proper orders p and q of the ARIMA(p,q) model.

Precise estimates of the model parameters are found using either a *nonlinear least-squares* (NLS) approach or the *maximum likelihood* (ML) criterion favored by Box and Jenkins, which was applied in this project. The equation for the ARIMA model can be expressed as:

$$z_t = \phi_1 z_{t-1} + \phi_2 z_{t-2} + \phi_3 z_{t-3} + \phi_4 z_{t-4} + \phi_5 z_{t-5} + \phi_6 z_{t-6} + \phi_7 z_{t-7} - \theta_1 a_{t-24} + a_t \tag{21}$$

Since Eq. (21) predicts temperatures, z_t has to be transformed back to temperatures using Eq. (20). Finally, the forecast equation is:

$$\hat{X}_t = X_{t-1} + X_{t-24} - X_{t-25} + \phi_1[X_{t-1} - X_{t-2} - X_{t-25} + X_{t-26}] + \ldots + \phi_7[X_{t-7} - X_{t-8} - X_{t-31} + X_{t-32}] \tag{22}$$

Table 4: SARIMA model parameters for four investigated locations

	Omaha, NE	Chicago, IL	Denver, CO	Phoenix, AZ
Order of AR *p*	3	3	2	3
Order of MA *q*	1	1	1	1
Estimates *φ*	φ1 = 0.3833 φ2 = 0.0735 φ3 = 0.0234 φ4 =φ5 = φ6 = φ7 = 0	φ1 = 0.2200 φ2 = 0.0843 φ3 = 0.0374 φ4 =φ5 = φ6 = φ7 = 0	φ3 = -0.0398 φ5 = -0.0594 φ1 =φ2 = φ4 = φ6 = φ7 = 0	φ1 = -0.0221 φ6 = 0.0704 φ7 = -0.0505 φ2 =φ3 = φ4 = φ5 = 0
Estimates *θ*	θ = 0.2712	θ = -0.1008	θ = 0.0852	θ =-0.9998

This model is fitted by the parameters ϕ listed in

Table 4. Because both the periodicity of the time series and the prediction horizon are 24 hours, parameter θ_1 cancels out of the model and is not used. The accuracy of the final model can be assessed using standard procedures as outlined in [43].

3.3.4 Prediction Model Evaluation

The selection of an appropriate prediction model for weather forecasting has to be preceded by a detailed examination and comparison of the various possible models with respect to their accuracy and reliability.

3.3.4.1 Standard Metrics for Error Examination

The accuracy of the prediction model is quantified using standard metrics: mean bias error MBE, root mean square error RMSE, and the coefficient of variation of the RMSE, CV-RMSE. A function of observed measurements $x_1,\ldots,x_n$ produces an average value equal to

$$\overline{x} = \frac{1}{n}\sum_{i=1}^{n} x_i \tag{23}$$

The mean bias error (MBE) for a time series with the same observed measurements may be expressed by

$$MBE = \frac{1}{n}\sum_{i=1}^{n}(\hat{x}_i - x_i) \tag{24}$$

where $\hat{x}_i$ is the *i*-th predicted value, x_i represents the *i*-th actual measured data, and *n* is the total number of observations in the sample. The root mean square error of a time series (RMSE) is an average measure of the deviation of the data from the model; it is also called the standard error of the estimate.

$$RMSE = \sqrt{\frac{\sum_{i=1}^{n}(x_i - \hat{x}_i)^2}{n-p}} \tag{25}$$

where *n* is the number of observations defined previously as 8760, and *p* is the number of degrees of freedom in the model. The coefficient of variation of the root mean square error (CV-RMSE) is a normalized (non-dimensional) measure that is found by dividing the RMSE by the mean value of the observation.

3.3.4.2 Analysis of Prediction Results

Table 5 provides an overview of the annual average values for MBE, RMSE and CV-RMSE (8760 prediction cycles) as well as the cumulative error for all prediction models applied to Denver and Phoenix. These locations were chosen since Phoenix is the location with the smallest cumulative and average errors and Denver is the location with the highest errors. The differences of the errors between the locations are obvious, espe-

cially for the same-as-yesterday predictor. Within the prediction models, the bin-month predictor gives the smallest errors in any of the listed results. The SARIMA model delivers the highest average and cumulative values.

This trend is reinforced by the plot of the statistical metrics versus time. Figure 12 illustrates the monthly average RMSE for selected prediction models developed for Phoenix, AZ. The SARIMA, the random walk and the TMY2 models predict with lower accuracy as expressed by higher average RMSE. This can be explained by the static nature of the model, which is not updated in response to the current weather patterns. The accuracy for the SARIMA model tested against year 2002 decreases significantly since the model was built upon the time series for 2001. The monthly RMSE values of the other models are similar to each other. Contrary to intuition, it turned out that using the previous day's weather does not yield the best predictor. This may be explained by the high volatility of the weather patterns from one day to the next.

Mean bias errors were found to be very small for all predictor models, indicating that they did not systematically under- or overestimate future weather patterns.

Subsequent investigation of the prediction accuracy of the bin predictors for all four locations revealed that the dynamic bin procedure as expressed by Eq.(18) provides the best prediction performance, in particular the 30-day and 60-day bin models as shown by Figure 13, and is recommended for further use.

Table 5: Cumulative RMSE and CV-RMSE error and the annual average value of MBE, RMSE and CV-RMSE for Denver and Phoenix

Predictor	**TMY2**		**Yesterday**		**Bin-month**		**SARIMA**		**Random Walk**	
Location	**Denver**	**Phoenix**	**Denver**	**Phoenix**	**Denver**	**Phoenix**	**Denver**	**Phoenix**	**Denver**	**Phoenix**
cum. RMSE	45365	28347	41408	22414	31334	19704	71618	81876	54403	48216
cum.CV-RMSE	160.70	95.78	146.90	75.61	111.00	66.42	252.23	274.99	190.94	161.80
average MBE	-0.004	-0.003	-0.006	0.003	0.010	0.007	-0.003	0.004	0.001	-0.002
average RMSE	5.19	3.24	4.74	2.57	3.59	2.26	8.23	9.38	6.23	5.52
average CV-RMSE	0.018	0.011	0.017	0.009	0.013	0.008	0.029	0.032	0.022	0.019

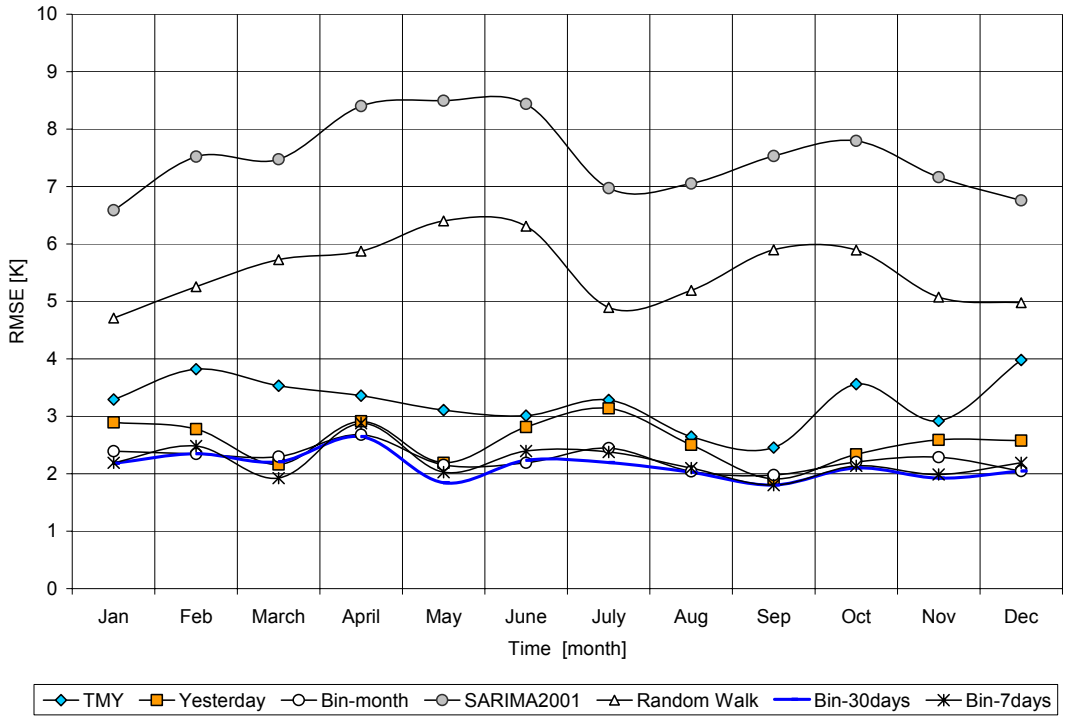

Figure 12: Monthly average RMSE for selected prediction models for Phoenix, AZ

Figure 14 is a cumulative histogram of the RMS errors for a selection of predictors as applied to Omaha, Nebraska. It is apparent that the SARIMA predictor has a large fraction of prediction events (>60%) with high RMS errors of 6 K and higher. While the TMY and same-as-yesterday predictors significantly improve upon the SARIMA model, the bin models for 7-days, 30-days, and the preceding calendar month far outperform these.

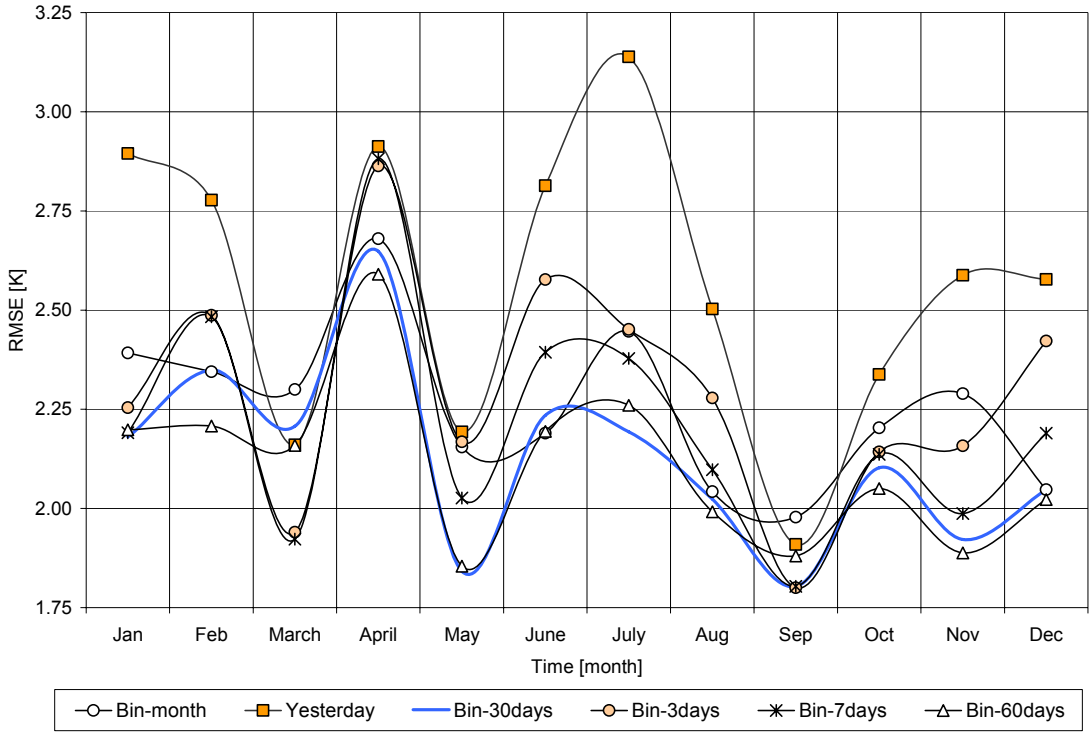

Figure 13: Monthly average RMSE for bin predictors for Phoenix, AZ

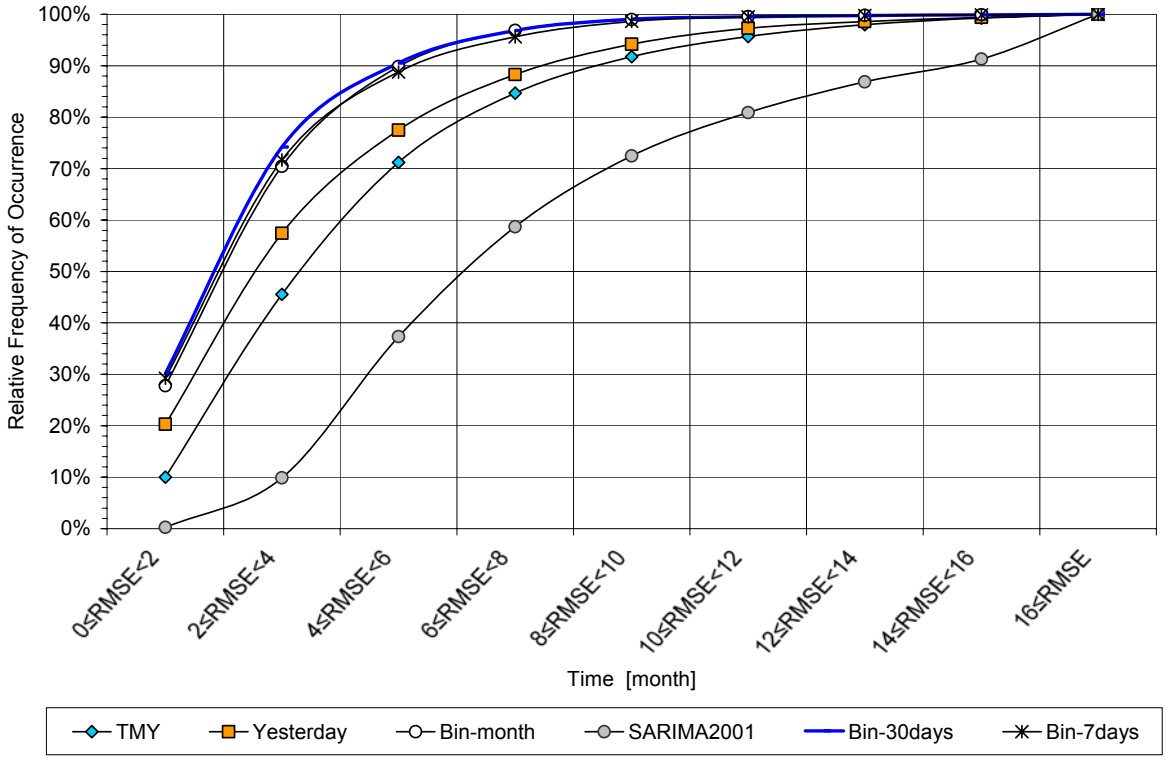

Figure 14: Cumulative histogram of RMS errors for selected predictors for Omaha, NE

3.4 Application of Prediction Models to Predictive Control Task

The prediction models investigated in Section 3.3, will now be employed for the purpose of providing short-term temperature predictions for the next L = 24 hours.

3.4.1 Utility Cost and Energy Consumption

The results in this section are created on the basis of monthly simulations for the month of July in the following four locations: Chicago, IL, Denver, CO, Omaha, NE, and Phoenix, AZ. The utility rate is assumed to be \$0.20/kWh on-peak and \$0.05/kWh off-peak; a demand charge of \$10 is levied during the on-peak hours, none during the off-peak hours. The on-peak period is weekdays from 9 AM to 6 PM, off-peak all remaining hours. The building is occupied from 7 AM to 5 PM.

Case 1 represents the reference case in which cooling loads have to be met without any storage available. Case 2 represents the base case that makes use of active thermal storage as governed by chiller-priority control, i.e., the downsized base chiller meets the cooling loads up to its capacity $CCAP_{base}$, thereafter the active storage contributes the remainder. The dedicated active storage chiller requires SCAP/$CCAP_{tes}$ = 10 hours to recharge an empty storage tank. Case 3 optimizes both active and passive storage media under closed-loop predictive control and represents the focus of this research.

Table 6: System Sizing for Investigated Locations

Case No.	Optimization	Units	Chicago, IL	Denver, CO	Omaha, NE	Phoenix, AZ
1	**Reference Case Without Any Storage**					
	CCAPbase	kW	600	600	600	600
	CCAPtes	kW	0	0	0	0
	SCAP	kWh	0	0	0	0
	Note: Base chiller fully sized, no active storage; night setup.					
2	**Basecase With Active Storage Under Chiller-Priority**					
	CCAPbase	kW	250	150	250	250
	CCAPtes	kW	250	250	250	250
	SCAP	kWh	2,500	2,500	2,500	2,500
	Note: Base chiller downsized; chiller-priority active storage control; night setup.					
3	**Predictive Optimal Control of Active and Passive Building Storage**					
	CCAPbase	kW	250	150	250	250
	CCAPtes	kW	250	250	250	250
	SCAP	kWh	2,500	2,500	2,500	2,500
	Note: Base chiller fully sized; optimal active storage control; zone setpoints optimized.					

The following five tables show the monthly operating costs and savings achieved for each of the four geographic locations in the United States for the three cases described above. Case 3 will be further broken down to reflect the influence of short-term weather prediction accuracy by employing selected forecasting models discussed in Section 3.3.

The first two tables describe the location of Phoenix, AZ. Table 7 shows the total utility cost, while Table 8 illustrates the cost of operating the heating, ventilating, and air-conditioning (HVAC) systems, which is the cost portion that is influenced by the investigated predictive optimal control strategy. In the latter table, HVAC demand charges are not shown because the HVAC electrical peak may not coincide with the total electrical demand and therefore may not contribute to the total demand charge.

It is important to realize that the predictive controller does not minimize total electrical utility cost, but electrical energy cost subject to a constraint on the electrical demand charge, i.e., the target demand charge. From Table 7 it can be seen that in all cases involving thermal energy storage, total electrical utility cost is reduced by 11-24% while energy consumption increases by 8-16%. Relative to the reference case without any thermal storage usage, the base case reduces total electrical utility bill by 11% at the expense of 8% higher energy use. Predictive optimal control of active and passive building thermal storage inventory under perfect prediction raises the utility cost savings to 24% while incurring an increase in energy use of 14%. The same-as-yesterday and 7-day bin predictors suffer a noticeable but acceptable degradation in savings performance

relative to the perfect prediction case. The 30-day and 60-day bin predictors are subject to only marginal penalties compared to the case of perfect prediction and significantly improve upon the same-as-yesterday and 7-day bin predictors. The very crude random walk predictor, simply assuming the current temperature to persist over the next *L* hours, leads to cost savings of 15% and energy increases of 13%, which lies between the base case and the perfect prediction case. From these results for Phoenix, AZ it can be concluded that simple 30-day or 60-day bin predictors are sufficient to achieve most of the theoretically attainable cost savings benefits.

Table 7: Monthly total electrical utility cost comparison for Phoenix, AZ

Case	Units	Reference Case	Basecase	Predictive Optimal Control of Active and Passive Storage					
Predictor		None	None	Perfect	Yesterday	7day Bin	30day Bin	60day Bin	Random Walk
On-Peak Demand	kW	209	159	151	153	156	157	157	171
Δ relative to Reference Case	%	-	-24%	-28%	-27%	-26%	-25%	-25%	-18%
Δ relative to Basecase	%	31%	-	-5%	-4%	-2%	-2%	-1%	8%
Off-Peak Demand	kW	215	239	310	296	321	374	374	242
Δ relative to Reference Case	%	-	11%	44%	38%	49%	74%	57%	12%
Δ relative to Basecase	%	-10%	-	30%	24%	35%	57%	21%	1%
On-Peak Energy Consumption	MWh	49	41	30	33	32	30	31	36
Δ relative to Reference Case	%	-	-16%	-40%	-33%	-34%	-38%	-37%	-26%
Δ relative to Basecase	%	19%	-	-28%	-20%	-21%	-26%	-25%	-12%
Off-Peak Energy Consumption	MWh	15	28	44	42	42	45	44	37
Δ relative to Reference Case	%	-	84%	187%	170%	171%	188%	183%	137%
Δ relative to Basecase	%	-46%	-	56%	47%	47%	57%	54%	29%
Total Energy Consumption	MWh	65	70	74	75	74	75	75	73
Δ relative to Reference Case	%	-	8%	14%	15%	15%	16%	16%	13%
Δ relative to Basecase	%	-7%	-	6%	7%	7%	8%	7%	5%
Demand Charge	$	$2,094	$1,592	$1,511	$1,531	$1,559	$1,566	$1,572	$1,713
Δ relative to Reference Case	%	-	-24%	-28%	-27%	-26%	-25%	-25%	-18%
Δ relative to Basecase	%	31%	-	-5%	-4%	-2%	-2%	-1%	8%
On-Peak Energy Charge	$	$9,833	$8,250	$5,909	$6,570	$6,495	$6,082	$6,196	$7,273
Δ relative to Reference Case	%	-	-16%	-40%	-33%	-34%	-38%	-37%	-26%
Δ relative to Basecase	%	19%	-	-28%	-20%	-21%	-26%	-25%	-12%
Off-Peak Energy Charge	$	$774	$1,424	$2,221	$2,091	$2,100	$2,233	$2,193	$1,837
Δ relative to Reference Case	%	-	84%	187%	170%	171%	188%	183%	137%
Δ relative to Basecase	%	-46%	-	56%	47%	47%	57%	54%	29%
Total Energy Charge	$	$10,607	$9,674	$8,129	$8,661	$8,595	$8,315	$8,389	$9,110
Δ relative to Reference Case	%	-	-9%	-23%	-18%	-19%	-22%	-21%	-14%
Δ relative to Basecase	%	10%	-	-16%	-10%	-11%	-14%	-13%	-6%
Total Cost	$	$12,701	$11,266	$9,640	$10,192	$10,154	$9,881	$9,961	$10,822
Δ relative to Reference Case	%	-	-11%	-24%	-20%	-20%	-22%	-22%	-15%
Δ relative to Basecase	%	13%	-	-14%	-10%	-10%	-12%	-12%	-4%

Table 8 reveals that in all cases involving thermal energy storage, cooling-related electrical energy charges are reduced by 20-53% while energy consumption increases by 18-37%. Relative to the reference case without any thermal storage usage, the base case reduces electrical energy charges by 20% at the expense of 18% higher energy use. Predictive optimal control of active and passive building thermal storage inventory under perfect prediction raises the electrical energy cost savings to 53% while incurring an increase of energy use of 33%. Again, the same-as-yesterday and 7-day bin predictors suffer a noticeable but tolerable degradation in savings performance relative to the perfect prediction case. Again, the 30-day and 60-day bin predictors are subject to only marginal penalties compared to the case of perfect prediction and noticeably improve upon the same-as-yesterday and 7-day bin predictors. The crude random walk predictor leads to cost savings of 15% and energy increases of 13%, i.e., between the base case and the perfect prediction case. It is evident that by employing both active and passive thermal storage inventories, substantial cost savings can be achieved, however, at the cost of increased total electrical energy use.

Table 8: Monthly HVAC electrical utility cost comparison for Phoenix, AZ

Case	Units	Reference Case	Basecase	Predictive Optimal Control of Active and Passive Storage					
Predictor		None	None	Perfect	Yesterday	7day Bin	30day Bin	60day Bin	Random Walk
On-Peak Demand	kW	106	56	99	99	99	99	99	99
Δ relative to Reference Case	%	-	-47%	-6%	-6%	-6%	-6%	-6%	-6%
Δ relative to Basecase	%	90%	-	79%	78%	79%	79%	78%	79%
Off-Peak Demand	kW	111	135	304	291	316	369	369	235
Δ relative to Reference Case	%	-	21%	173%	162%	184%	231%	231%	111%
Δ relative to Basecase	%	-18%	-	125%	115%	134%	173%	173%	74%
On-Peak Energy Consumption	MWh	22	14	2	6	5	3	4	9
Δ relative to Reference Case	%	-	-36%	-90%	-75%	-76%	-86%	-83%	-59%
Δ relative to Basecase	%	57%	-	-84%	-60%	-63%	-78%	-74%	-35%
Off-Peak Energy Consumption	MWh	6	19	35	33	33	36	35	28
Δ relative to Reference Case	%	-	200%	446%	406%	409%	450%	437%	328%
Δ relative to Basecase	%	-67%	-	82%	68%	69%	83%	79%	42%
Total Energy Consumption	MWh	28	33	38	38	38	39	39	37
Δ relative to Reference Case	%	-	18%	33%	35%	35%	37%	36%	30%
Δ relative to Basecase	%	-15%	-	13%	15%	14%	16%	15%	10%
On-Peak Energy Charge	$	$4,369	$2,786	$445	$1,106	$1,032	$618	$732	$1,809
Δ relative to Reference Case	%	-	-36%	-90%	-75%	-76%	-86%	-83%	-59%
Δ relative to Basecase	%	57%	-	-84%	-60%	-63%	-78%	-74%	-35%
Off-Peak Energy Charge	$	$324	$974	$1,771	$1,641	$1,650	$1,783	$1,743	$1,387
Δ relative to Reference Case	%	-	200%	446%	406%	409%	450%	437%	328%
Δ relative to Basecase	%	-67%	-	82%	68%	69%	83%	79%	42%
Total Energy Charge	$	$4,693	$3,760	$2,216	$2,747	$2,681	$2,401	$2,475	$3,196
Δ relative to Reference Case	%	-	-20%	-53%	-41%	-43%	-49%	-47%	-32%
Δ relative to Basecase	%	25%	-	-41%	-27%	-29%	-36%	-34%	-15%

Similar trends can be identified for Chicago, IL as shown in Table 9. However, in this case all bin predictors appear to perform similarly well. Yet, it is the 60-day bin predictor that leads to the lowest violation of the target demand charge. For this location, the target demand is 0.95*159 = 151 kW. While the perfect predictor honors that constraint, all other predictors lead to demand charges in excess of 151 kW. Of these, the excess demand for the 60-day predictor is only 2 kW.

Table 9: Monthly total electrical utility cost comparison for Chicago, IL

Case	Units	Reference Case	Basecase	Predictive Optimal Control of Active and Passive Storage					
Predictor		None	None	Perfect	Yesterday	7day Bin	30day Bin	60day Bin	Random Walk
On-Peak Demand	kW	237	159	151	156	155	158	153	166
Δ relative to Reference Case	%	-	-33%	-36%	-34%	-35%	-33%	-35%	-30%
Δ relative to Basecase	%	49%	-	-5%	-2%	-3%	-1%	-4%	5%
Off-Peak Demand	kW	214	238	243	270	334	265	264	333
Δ relative to Reference Case	%	-	11%	13%	26%	56%	24%	11%	55%
Δ relative to Basecase	%	-10%	-	2%	13%	40%	11%	9%	39%
On-Peak Energy Consumption	MWh	43	41	28	32	31	31	31	35
Δ relative to Reference Case	%	-	-5%	-34%	-26%	-28%	-27%	-28%	-18%
Δ relative to Basecase	%	6%	-	-31%	-22%	-24%	-23%	-24%	-13%
Off-Peak Energy Consumption	MWh	13	17	34	29	31	31	31	26
Δ relative to Reference Case	%	-	31%	163%	125%	138%	138%	139%	96%
Δ relative to Basecase	%	-23%	-	102%	72%	82%	82%	83%	50%
Total Energy Consumption	MWh	56	58	63	61	62	62	62	61
Δ relative to Reference Case	%	-	3%	12%	9%	11%	11%	11%	9%
Δ relative to Basecase	%	-3%	-	9%	6%	8%	8%	8%	6%
Demand Charge	$	$2,370	$1,592	$1,511	$1,555	$1,545	$1,580	$1,530	$1,664
Δ relative to Reference Case	%	-	-33%	-36%	-34%	-35%	-33%	-35%	-30%
Δ relative to Basecase	%	49%	-	-5%	-2%	-3%	-1%	-4%	5%
On-Peak Energy Charge	$	$8,579	$8,116	$5,640	$6,378	$6,205	$6,226	$6,178	$7,047
Δ relative to Reference Case	%	-	-5%	-34%	-26%	-28%	-27%	-28%	-18%
Δ relative to Basecase	%	6%	-	-31%	-21%	-24%	-23%	-24%	-13%
Off-Peak Energy Charge	$	$652	$851	$1,715	$1,467	$1,549	$1,549	$1,560	$1,278
Δ relative to Reference Case	%	-	31%	163%	125%	138%	138%	139%	96%
Δ relative to Basecase	%	-23%	-	102%	72%	82%	82%	83%	50%
Total Energy Charge	$	$9,231	$8,966	$7,356	$7,845	$7,754	$7,775	$7,738	$8,324
Δ relative to Reference Case	%	-	-3%	-20%	-15%	-16%	-16%	-16%	-10%
Δ relative to Basecase	%	3%	-	-18%	-13%	-14%	-13%	-14%	-7%
Total Cost	$	$11,601	$10,559	$8,866	$9,400	$9,299	$9,355	$9,268	$9,989
Δ relative to Reference Case	%	-	-9%	-24%	-19%	-20%	-19%	-20%	-14%
Δ relative to Basecase	%	10%	-	-16%	-11%	-12%	-11%	-12%	-5%

It turned out that Denver, CO is a significantly milder location with lower reference case on-peak demands. Consequently, the system was downsized to a base chiller of 150 kW instead of 250 kW of cooling capacity as shown in Table 6. The active thermal storage capacity and associated chiller were not altered. The savings from the investigated control strategy are generally slightly lower, 20% instead of 24% for the perfect prediction case. Again, the 60-day bin predictor most closely observed the target demand limit of 0.95*137 kW = 130 kW and led to near-optimal savings performance.

Table 10: Monthly total electrical utility cost comparison for Denver, CO

Case	Units	Reference Case	Basecase	Predictive Optimal Control of Active and Passive Storage					
Predictor		None	None	Perfect	Yesterday	7day Bin	30day Bin	60day Bin	Random Walk
On-Peak Demand	kW	177	137	130	138	139	141	138	178
Δ relative to Reference Case	%	-	-23%	-27%	-22%	-21%	-20%	-22%	0%
Δ relative to Basecase	%	29%	-	-5%	1%	2%	3%	1%	30%
Off-Peak Demand	kW	168	181	237	359	384	323	277	297
Δ relative to Reference Case	%	-	8%	41%	114%	129%	93%	53%	77%
Δ relative to Basecase	%	-7%	-	31%	99%	112%	79%	17%	65%
On-Peak Energy Consumption	MWh	41	36	28	29	29	29	28	36
Δ relative to Reference Case	%	-	-13%	-31%	-28%	-29%	-30%	-30%	-12%
Δ relative to Basecase	%	15%	-	-21%	-18%	-18%	-20%	-20%	1%
Off-Peak Energy Consumption	MWh	11	20	31	30	30	30	30	20
Δ relative to Reference Case	%	-	72%	168%	161%	163%	164%	162%	79%
Δ relative to Basecase	%	-42%	-	56%	51%	53%	53%	52%	4%
Total Energy Consumption	MWh	52	55	59	59	59	59	58	56
Δ relative to Reference Case	%	-	6%	12%	13%	13%	12%	12%	8%
Δ relative to Basecase	%	-5%	-	6%	7%	7%	6%	6%	2%
Demand Charge	$	$1,774	$1,370	$1,302	$1,381	$1,393	$1,412	$1,379	$1,782
Δ relative to Reference Case	%	-	-23%	-27%	-22%	-21%	-20%	-22%	0%
Δ relative to Basecase	%	29%	-	-5%	1%	2%	3%	1%	30%
On-Peak Energy Charge	$	$8,181	$7,117	$5,615	$5,855	$5,826	$5,705	$5,688	$7,167
Δ relative to Reference Case	%	-	-13%	-31%	-28%	-29%	-30%	-30%	-12%
Δ relative to Basecase	%	15%	-	-21%	-18%	-18%	-20%	-20%	1%
Off-Peak Energy Charge	$	$570	$983	$1,530	$1,486	$1,498	$1,507	$1,496	$1,021
Δ relative to Reference Case	%	-	72%	168%	161%	163%	164%	162%	79%
Δ relative to Basecase	%	-42%	-	56%	51%	52%	53%	52%	4%
Total Energy Charge	$	$8,752	$8,100	$7,144	$7,340	$7,324	$7,212	$7,185	$8,188
Δ relative to Reference Case	%	-	-7%	-18%	-16%	-16%	-18%	-18%	-6%
Δ relative to Basecase	%	8%	-	-12%	-9%	-10%	-11%	-11%	1%
Total Cost	$	$10,525	$9,470	$8,446	$8,722	$8,717	$8,623	$8,564	$9,970
Δ relative to Reference Case	%	-	-10%	-20%	-17%	-17%	-18%	-19%	-5%
Δ relative to Basecase	%	11%	-	-11%	-8%	-8%	-9%	-10%	5%

Finally, Omaha, Nebraska was found to be associated with theoretical maximum savings of 23% for the perfect prediction case, which is similar to Phoenix and Chicago. However, unlike the other locations, the 7-day bin predictors best honors the target demand limit of 0.95*159 kW = 151 kW. In fact, the 30-day bin predictor leads to slightly lower total energy charges than the perfect predictor. This is possible because it uses an electrical demand margin above the target demand limit that is actually not available for use. Inspection of the on-peak electrical demand revealed that the violation is a one-time occurrence in the month of July.

Table 11: Monthly total electrical utility cost comparison for Omaha, NE

Case	Units	Reference Case	Basecase	Predictive Optimal Control of Active and Passive Storage					
Predictor		None	None	Perfect	Yesterday	7day Bin	30day Bin	60day Bin	Random Walk
On-Peak Demand	kW	224	159	151	161	155	163	171	170
Δ relative to Reference Case	%	-	-29%	-33%	-28%	-31%	-27%	-24%	-24%
Δ relative to Basecase	%	41%	-	-5%	1%	-2%	2%	7%	7%
Off-Peak Demand	kW	235	243	242	242	246	236	244	309
Δ relative to Reference Case	%	-	3%	3%	3%	5%	1%	0%	32%
Δ relative to Basecase	%	-3%	-	0%	0%	2%	-3%	0%	28%
On-Peak Energy Consumption	MWh	44	41	29	29	29	29	29	34
Δ relative to Reference Case	%	-	-8%	-35%	-34%	-35%	-35%	-35%	-23%
Δ relative to Basecase	%	9%	-	-29%	-28%	-29%	-29%	-29%	-16%
Off-Peak Energy Consumption	MWh	14	20	37	38	37	37	37	31
Δ relative to Reference Case	%	-	47%	166%	171%	171%	170%	171%	125%
Δ relative to Basecase	%	-32%	-	81%	85%	85%	84%	84%	54%
Total Energy Consumption	MWh	58	61	66	67	66	66	66	65
Δ relative to Reference Case	%	-	5%	13%	15%	14%	14%	14%	12%
Δ relative to Basecase	%	-4%	-	8%	10%	9%	8%	9%	7%
Demand Charge	$	$2,241	$1,592	$1,511	$1,607	$1,553	$1,629	$1,705	$1,700
Δ relative to Reference Case	%	-	-29%	-33%	-28%	-31%	-27%	-24%	-24%
Δ relative to Basecase	%	41%	-	-5%	1%	-2%	2%	7%	7%
On-Peak Energy Charge	$	$8,874	$8,129	$5,785	$5,871	$5,774	$5,749	$5,806	$6,839
Δ relative to Reference Case	%	-	-8%	-35%	-34%	-35%	-35%	-35%	-23%
Δ relative to Basecase	%	9%	-	-29%	-28%	-29%	-29%	-29%	-16%
Off-Peak Energy Charge	$	$692	$1,016	$1,839	$1,876	$1,874	$1,869	$1,873	$1,560
Δ relative to Reference Case	%	-	47%	166%	171%	171%	170%	171%	125%
Δ relative to Basecase	%	-32%	-	81%	85%	85%	84%	84%	54%
Total Energy Charge	$	$9,566	$9,145	$7,623	$7,747	$7,649	$7,618	$7,680	$8,399
Δ relative to Reference Case	%	-	-4%	-20%	-19%	-20%	-20%	-20%	-12%
Δ relative to Basecase	%	5%	-	-17%	-15%	-16%	-17%	-16%	-8%
Total Cost	$	$11,807	$10,737	$9,134	$9,354	$9,201	$9,246	$9,385	$10,100
Δ relative to Reference Case	%	-	-9%	-23%	-21%	-22%	-22%	-21%	-14%
Δ relative to Basecase	%	10%	-	-15%	-13%	-14%	-14%	-13%	-6%

3.4.2 Description of Control Strategies

Figure 15 shows the average zone temperature over all 15 zones for July 2 in Denver, Colorado. The thick lines represent the upper and lower temperature bounds for the operation of the office building on a week-

day. It can be seen that under perfect and same-as-yesterday prediction the building is precooled to a relatively constant value of 22-23°C zone temperature averaged over all 15 zones. Using the 30-day bin predictor, precooling before occupancy is not as pronounced as for the perfect case but similar for the evening hours following occupancy. The random walk predictor recommends spurious cooling below the cooling setpoint during occupancy and very little precooling during the night before and after occupancy compared to the base case and reference cases without passive storage utilization. Obviously, the predictive optimal controller makes very poor control decisions given this exceedingly crude predictor.

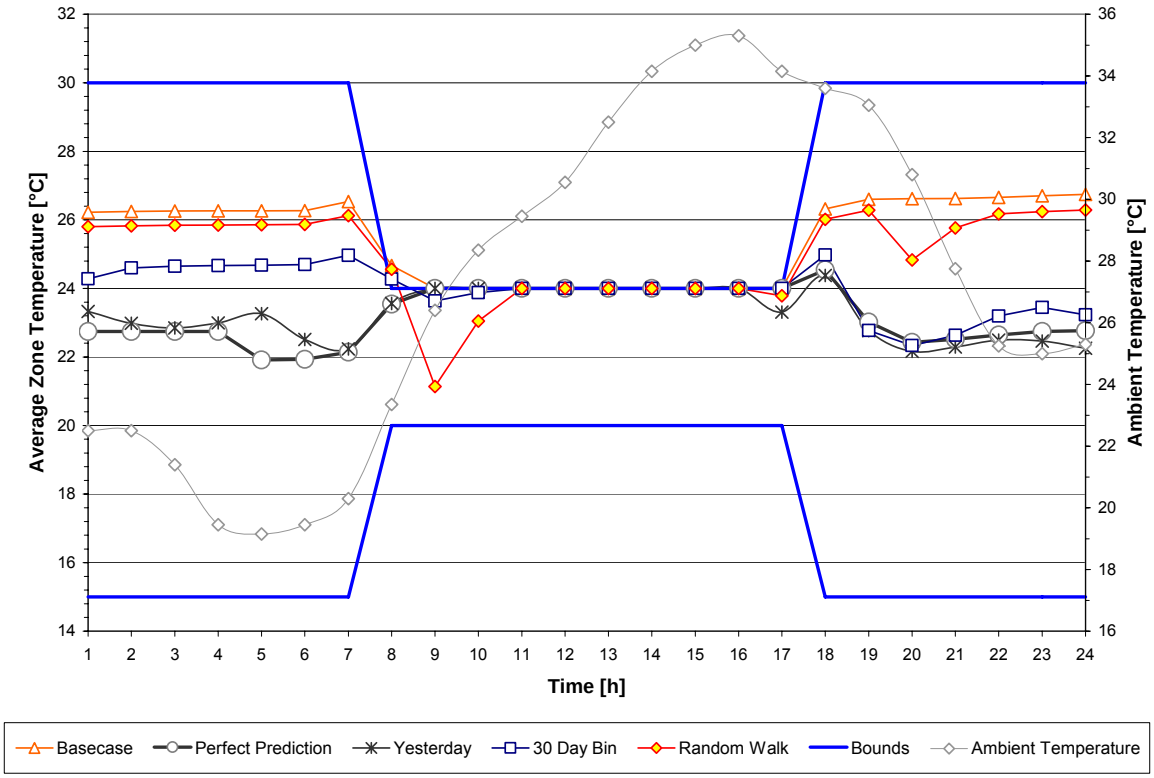

Figure 15: Average Zone Temperature Profiles for Denver, CO

The inventory of state-of-charge of the active storage is shown in Figure 16 from midnight to midnight on July 2 for those strategies involving active storage, i.e., not the reference case. For the base case with active storage under chiller-priority control, the storage is fully charged during off-peak hours and discharged to about 63% during the day. Under perfect prediction, the storage remains empty until 4 AM. Thereafter, the storage is charged for five hours to about 45% state-of-charge. Both, same-as-yesterday and 30-day bin predictors begin recharging earlier and to higher terminal states-of-charge at the beginning of the on-peak period. In all cases, the entire active storage is used over the extent of the on-peak period and the active storage tanks are depleted at the end of the on-peak period. Even under random walk weather prediction, the same conclusions hold, except that the TES system is not charged as much (42%) as for the other cases and recharging occurs in the early evening hours already. The conclusion we can draw from this is that the predictive controller makes robust decisions even when furnished with highly inferior weather forecasts.

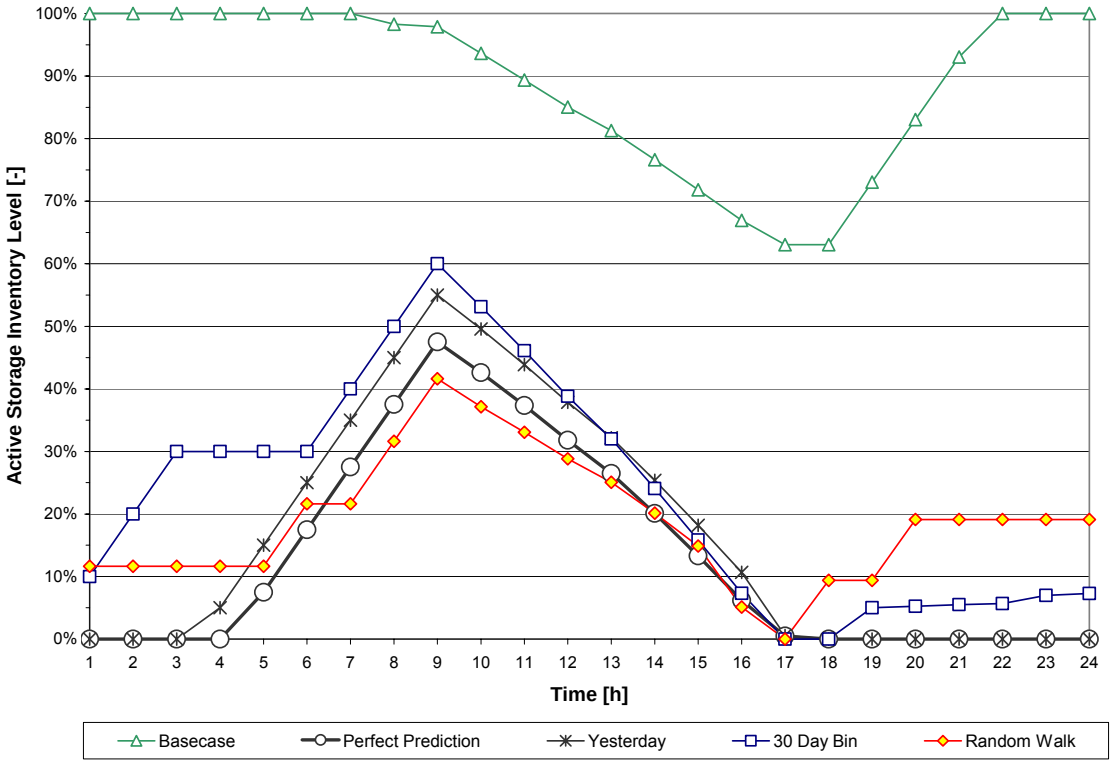

Figure 16: Active Storage State-of-Charge Profiles for Denver, CO

Finally, reducing on-peak electrical demand is a highly desirable side effect and often the dominant reason for shifting expensive on-peak cooling loads to off-peak periods as can be seen in Figure 17. While the base case with active storage under chiller-priority control already reduces the demand by 15% relative to the reference case without storage for this particular day, the combined optimization lowers the overall demand by about 36%. Of course, the demand reduction during any one day has little bearing on the demand reduction during the peak day of the billing period. Predictive optimal control using a random walk predictor proves to be less effective in terms of shifting on-peak loads to off-peak periods.

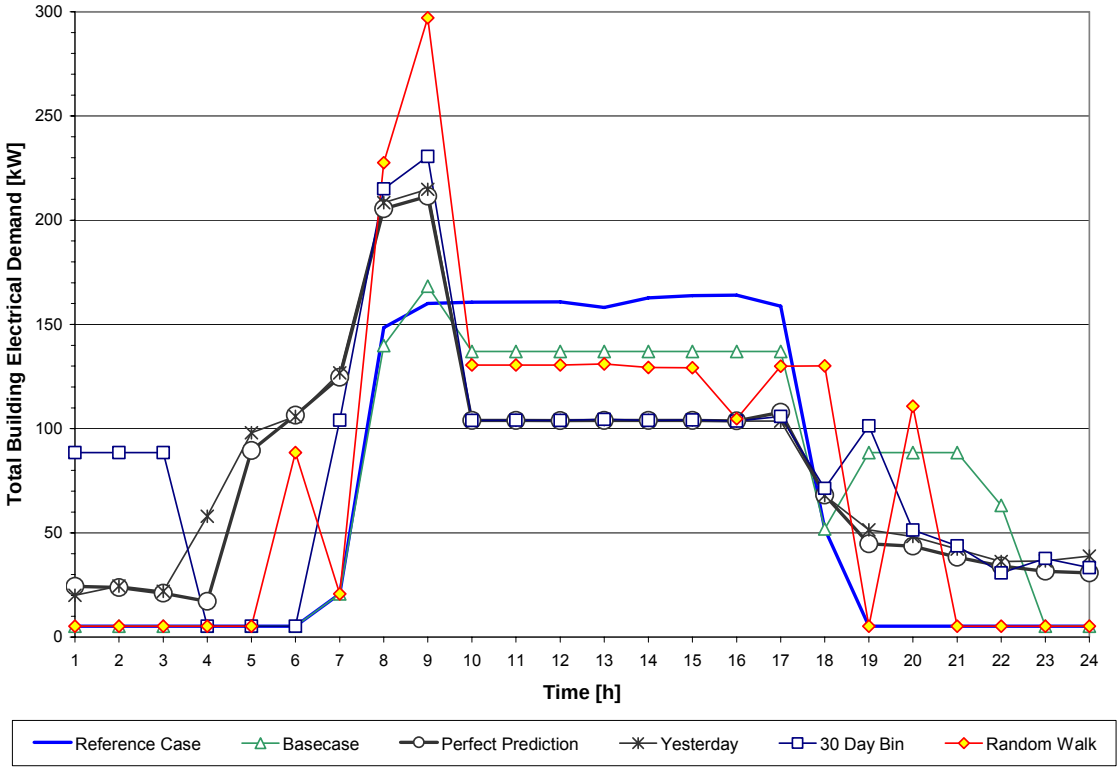

Figure 17: Total Building Electrical Demand Profiles for Denver, CO

3.5 Conclusions and Future Work

In this chapter we evaluated the benefits of combined optimal control of both passive building thermal capacitance *and* active thermal energy storage systems to minimize total utility cost in the presence of forecasting uncertainty in the required short-term weather forecasts.

Selected short-term weather forecasting models were introduced and investigated with respect to their forecasting accuracy as measured by RMS error, mean bias error, and the coefficient of variation. The most complex model, a seasonal autoregressive integrated moving average (SARIMA) exhibited the worst performance, followed by a static predictor model that references standard weather archives (TMY). The best prediction accuracy was computed for the bin models that develop a characteristic daily profile from observations collected over the past 30 or 60 days, followed by those that look back only 7 days. The model that projects yesterday's patterns one day into the future, proved to be a surprisingly poor predictor.

Next, we tested the predictor models in the context of the predictive optimal control task that optimizes building global temperature setpoints and active thermal energy storage charge/discharge rates in a closed-loop mode. For the four locations investigated in this parametric study, Chicago, IL, Denver, CO, Omaha, NE, and Phoenix, AZ, it was determined that the 30-day and 60-day bin predictor models lead to utility cost savings that are only marginally inferior compared to a hypothetical perfect predictor that perfectly anticipates the weather during the next planning horizon. Both same-as-yesterday and 7-day bin forecasting models performed significantly worse. The random walk predictor, assuming the current weather to remain constant over the extent of the planning horizon, served as a benchmark for the other predictors. Interestingly, in three out of four locations the random walk predictor led to utility cost savings that were higher than the base case of a building with thermal storage controlled by chiller-priority control.

In summary, the predictive optimal control of active and passive building thermal storage inventory using time-of-use electrical utility rates with significant on-peak to off-peak rate differentials and demand charges, appears to be a promising building control strategy when perfect weather forecasts are available. The good

news is that it takes only very simple short-term prediction models to realize almost all of the potential of this technology. The next chapter will assess the impact of modeling accuracy, i.e., to find out how accurately the building under predictive control has to be represented in the building model. Upon the completion of this next chapter, lab and field experimentation will be described to support the simulation results.

3.6 References

[39] Henze, G.P., C. Felsmann, and G. Knabe (2004) "Evaluation of Optimal Control for Active and Passive Building Thermal Storage." *International Journal of Thermal Sciences,* Vol. 43, No. 2, pp. 173-183, Elsevier Science, New York, New York.

[40] Gilchrist W. (1977) *Statistical Forecasting*, John Wiley & Sons, New York.

[41] Brockwell, P.J. and Davis R.A. (1996) *Introduction to Time Series and Forecasting*, Colorado State University, Springer-Verlag New York Inc.

[42] Bowermann B.L. and O'Conell R T. (1997) *Forecasting and Time Series: An applied Approach*, 3/e, Miami University, Ohio, Wadsworth Publishing Company.

[43] Pankratz A. (1983) *Forecasting with univariate Box-Jenkins models: concepts and cases*, DePauw University, John Wiley & Sons, Inc.

[44] TMY2 Database http://www.finite-tech.com/ftidoe/weatherfiles/manuals/tmymanual.pdf

[45] EnergyPlus v1.0.1 http://www.eren.doe.gov/buildings/energy_tools/energyplus.

[46] TRNSYS – A transient simulation program. SEL University of Wisconsin – Madison, http://sel.me.wisc.edu/trnsys/Default.htm.

[47] ASHRAE Handbook of Applications (1999) "Supervisory Control Strategies and Optimization" Chapter 40, p.25.

[48] Matlab (1996) *Optimization Toolbox User's Guide*. The MathWorks, Inc.

[49] Bellman, Richard E. (1957) *Dynamic Programming*. Princeton, New Jersey: Princeton University Press.

4 Phase 1: Analysis – Impact of Modeling Accuracy

4.1 Abstract

This chapter evaluates the impact of modeling accuracy on the model-based closed-loop predictive optimal control of both passive building thermal capacitance and active thermal energy storage systems to minimize utility cost. The following guidelines have been derived: For an internal heat gain dominated commercial building, the deviation of building geometry and zoning from the reference building only marginally affects the optimal control strategy; reasonable simplifications are acceptable without loss of cost savings potential. Building construction characteristics determine the building passive thermal storage capacity. Zone temperature setpoints are affected more than TES operation by this construction mismatch, and a loss of cost savings potential is found in some cases. It is advisable to make sure the construction material is well modeled. Zone temperature setpoint profiles and TES performance are strongly affected by mismatches in internal heat gains, especially when they are underestimated. Since they are a key factor determining the building cooling load, efforts should be invested to keep the internal gain mismatch as small as possible. Efficiencies of the building energy systems have no direct impact on building cooling load, but they affect both zone temperature setpoints and active TES operation because of the coupling of the base chiller and the TES chiller. Relative efficiencies of the base and TES chillers will determine the balance of operation of the two chillers. Mismatch in this category may be significant. To avoid critical modeling mismatch, system identification techniques may be useful in improving the modeling process.

4.2 Introduction

This chapter evaluates the impact of modeling accuracy on the predictive optimal control of both passive building thermal capacitance and active thermal energy storage systems to minimize an objective function of choice including total energy consumption, energy cost, occupant discomfort, or a combination thereof.

The accuracy of the building model used for the model-based optimal control relative to the actual building behavior is of great importance to the quality of the optimal strategy. The modeling process entails the truthful representation of the actual characteristics of a specific building. Modeling accuracy may be increased by either improving the simulation program itself or by accurately collecting data and information on the building to be modeled. However, it is impossible and impractical to collect complete, accurate information for modeling purposes. Some degree of mismatch is unavoidable with respect to building geometry, construction material properties, internal heat gain, and performance characteristics of the building energy systems. Therefore, it is important to quantify the impact of various modeling mismatches on predictive optimal control. Investigations have been carried out in five different categories of modeling mismatch that are likely to occur in the modeling process. This chapter summarizes and analyzes the results and provides a comprehensive assessment and guidelines for modeling.

4.3 Assumption and Restrictions

There are two categories of factors affecting the model-based optimal control of the active and passive building thermal storage inventory. The building independent category includes climate, location and utility rate structure. These are factors that cannot be changed or manipulated. They cannot be mismatched in the optimization simulation. The building dependent category includes all aspects related to building modeling. In the simulation environment, the building model is generated by the user in the form of an input file where mismatches occur. It is important to know what happens if a mismatched model is employed in the context of real-time control and its "optimal" result is applied to the real building. In this chapter, model-related factors are summarized into the following five categories of parameters:

1. Geometry
2. Zoning
3. Construction materials including external and internal construction

4. Internal heat gains including light, equipment and occupancy
5. Characteristics of the plant including the base chiller and TES system

In order to focus on these factors only, all building independent factors (e.g., climate, location and utility rate) are kept the same in all simulation cases. Table 12 lists the building independent factors.

Table 12: Summary of building independent factors in the simulation cases

Location	Phoenix, AZ
Weather	Phoenix, AZ, TMY2 file used in the simulation
Utility rate structure	On-peak period: 9 a.m. – 6 p.m. On-peak energy rate: 0.20 $/kWh Off-peak energy rate: 0.05 $/kWh On-peak demand rate: 10.00 $/kW Off-peak demand rate: 0.00 $/kW

To examine the effects of model variation on optimization, the weather data file has been modified. Ten identical days are generated by repeating the weather patterns of July 21 ten times from July 21 to 30, thus eliminating the effects of weather variation on the optimization. Another consideration is the thermal history of the building. Zhou et al. (2003) [50] pointed out that different assumptions of the thermal history could generate widely different results during the early part of the simulation. To eliminate the start-up effects on the optimization mentioned above, all simulations in this analysis are conducted from July 21 to 30, but results from the beginning will not be considered and presented in the following discussion.

4.4 Definition of Terms

Before implementing the predictive optimal controller in a field or lab application, simulation studies were carried out to analyze the impact of the five categories of modeling variations listed above. Two simulation environments were set up: the first one was used to carry out the optimization for all simulation cases using the mismatched models. After the optimal solution was generated by the first simulation environment, the optimal strategy in the form of hourly zone temperature setpoints (passive storage) and TES charge/discharge rates (active storage) was applied in the second simulation environment. Here, a reference building model carried out the simulation (without optimization) and the associated results including cost and energy consumption were calculated. This second environment was meant to represent the application of the controller in a real building.

4.4.1 Execution Model

The execution model (EM) represents the real building and is intended to execute the optimal strategy previously found by the optimizer to calculate the energy cost and other related simulation results. In this analysis, the EM represents a one-story office building with five thermal zones. The building is occupied from 8:00 a.m. to 5:00 p.m. with 0.1 person/m^2 and 45 W/m^2 of internal heat gain.

4.4.2 Planning Model

The planning model (PM) refers to the mismatched building model used in the optimization simulation environment. Figure 18 gives an overview of the planning models for the five categories of mismatch.

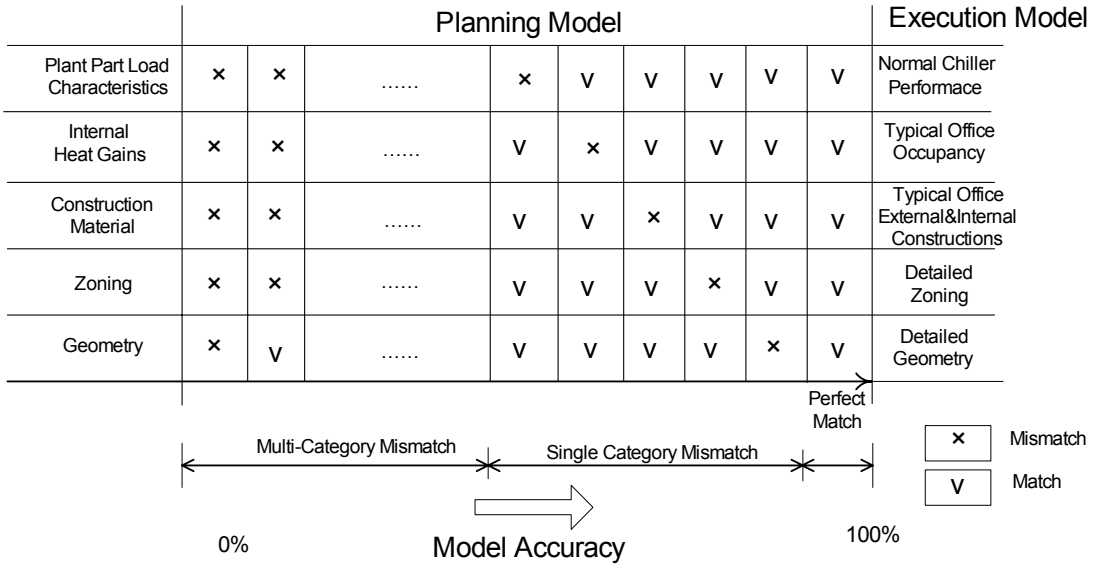

Figure 18: Overview of the execution model and planning models

For a specific building, model accuracy decreases with the number of parameter categories that vary from the execution model. In the perfect match case, the planning model is identical to the execution model. Although optimization results calculated using this model are considered as a theoretical benchmark, the existence of local minima means the results are not necessarily the best of all the planning models. All other optimization results of mismatch planning models will be compared with the perfect match case, and the deviations will be identified.

4.4.3 Cost Savings Ratio

Since the analysis in this chapter is based on the comparison of daily optimal results of different planning models, daily energy cost is selected as the objective function in the optimizations; demand cost is not included in this analysis. The saving potential of each planning model is discussed in terms of a cost savings ratio (CSR). The optimal control strategy generated by each planning model will be applied to the execution model; cost savings are calculated by comparing the cost with those of conventional nighttime setback control. Cost savings achieved by optimization of the perfect match model are considered as the benchmark value. The cost savings ratio (CSR) of each planning model is defined as the ratio of cost savings achieved by the planning model compared to the benchmark value.

Before investigating the mismatched planning models, simulations of conventional nighttime setback control and optimization of the perfect match planning model were carried out. Table 13 gives the summary of energy consumption and cost savings of these two cases.

Table 13: Summary of cost and energy consumption of night setback control and optimization of perfect match case

Case	Nighttime setback control	Optimization of perfect match PM
Daily energy consumption [kJ] (average)	5,048,878	5,154,819
Daily energy cost [$] (average)	231.62	183.80
Cost saving	-	20.6%
CSR	-	100%

4.5 Analysis and Discussion

4.5.1 Geometry

One of the biggest improvements in building simulation software is the capability of visualizing the building model. Users can now generate a building model which closely mirrors the actual building. However, it is still impossible to accurately model every aspect of the building's behavior. In addition, there is always a trade-off between the increased realism and cost of modeling efforts. As far as the optimal controller is concerned, we need to identify how much "realism" is required when setting up a building model and applying it to our optimization environment, and what kind of consequences result from a particular mismatch.

In the analysis of the geometry category, the execution model (EM) is set up as a cross-shaped building with five zones. Mismatched planning models (PMs) vary in shape and area of fenestration. Figure 19 offers a schematic of the geometry of both EM and PM.

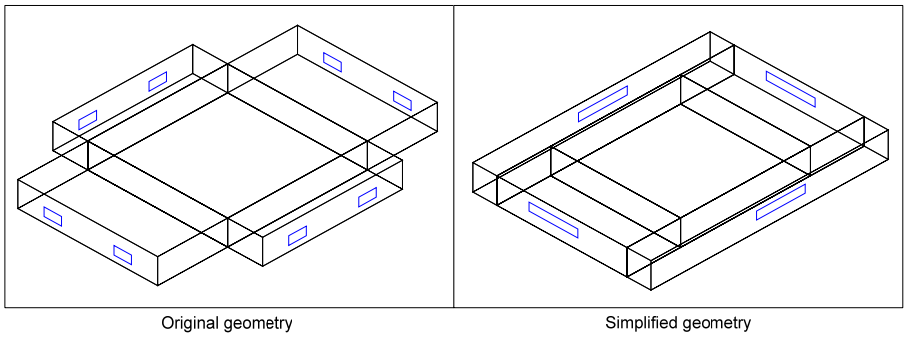

Figure 19: Geometries of the original building and the simplified building model

From Figure 19 we can see that in the geometry mismatched PM, the building shape is modeled as a simple box, which is the simplest representation of a building. Two simplification approaches were investigated. One approach was to keep the total external surface area the same as the original (referred to as PM-A in Figure 20 and Figure 21), and the other approach was to keep the total volume constant (referred to as PM-V in Figure 20 and Figure 21). Figure 20 and Figure 21 compare the optimization results for three consecutive days between the perfect matched model and the mismatched PMs.

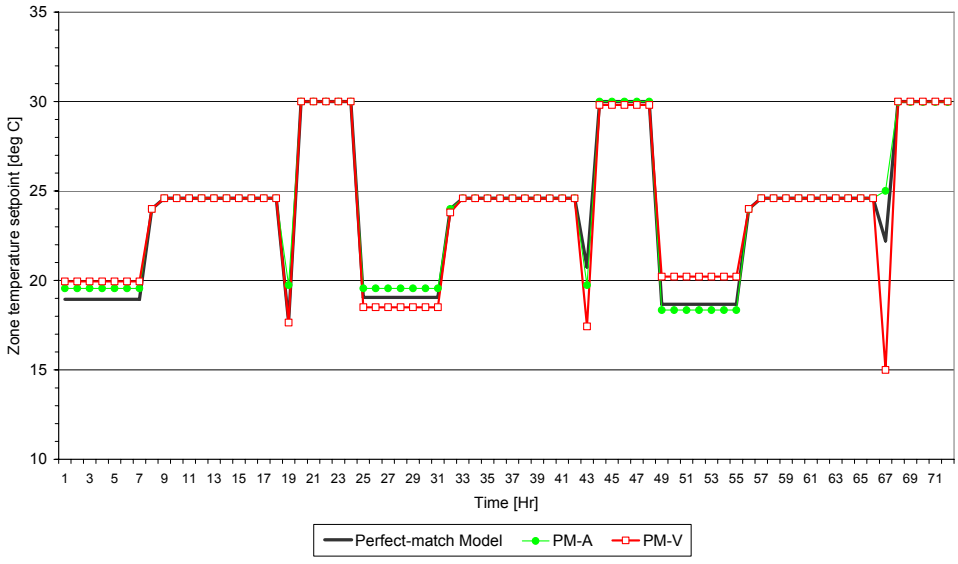

Figure 20: Optimization zone temperature setpoint profiles for the perfect match model case and two geometry simplification PMs

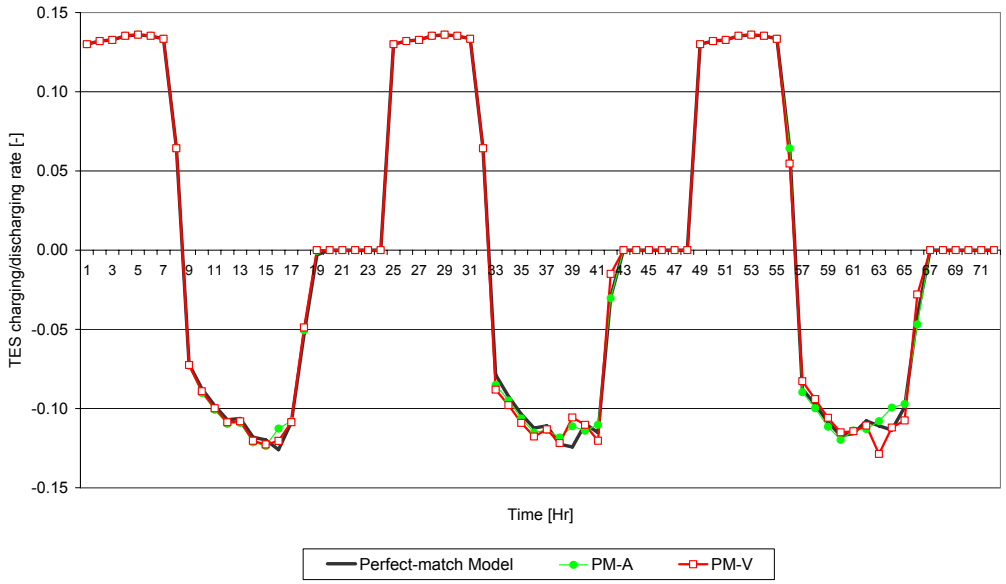

Figure 21: Optimization TES charging/discharging profiles for the perfect match model case and two geometry simplification PMs

From Figure 19 and Figure 20 we can see that the simplifications of the building geometry result in a limited variation of the optimal results for the zone temperature setpoints and thermal energy storage (TES) operation. For TES optimization, variation of the geometry appears to be irrelevant because the optimal profiles of the three cases are nearly identical. The differences in zone temperature setpoints between the perfect match model and the two geometry simplification PMs primarily occur during the precooling period. In terms of the profile of the perfect match model, geometry simplification with constant total external surface area appears to provide greater "similarity". Another noticeable effect is the instability in the profile of the PMs. Over a ten-day period of identical simulations, the optimizer usually finds a consistent pattern for the optimization after several days. However, as shown in the results of the PMs above, the optimal zone temperature setpoint profiles differ from day to day. This also happens in several other cases, but the magnitude of the daily variation is limited. Table 15 gives the summary of energy consumption and CSR of these two PMs.

Table 14: Summary of cost and energy consumption of geometry mismatched PMs

Case	PM-A	PM-V
Daily energy consumption [kJ]	5,193,731	5,233,801
Daily energy cost [$]	184.43	185.58
Cost saving	20.38%	19.88%
CSR	98.68%	96.26%

The area of fenestration is a key factor in determining the cooling load caused by direct solar radiation introduced through the fenestration. Two planning models representing overestimated and underestimated total fenestration area by 50% were investigated. The optimization results do not show significant differences compared to the perfect match model. Our investigations of the building geometry variation yield the following two conclusions:

- Geometry mismatch in the building model leads to only minor deviations in the solution of predictive optimal control.
- Deviations caused by geometry mismatch have a greater effect on zone temperature setpoints than on TES operation.

4.5.2 Zoning

A building zone is normally defined as a space controlled by an individual thermostat. In most applications, the zoning of the building mirrors the layout of the building construction. For a typical office building, which is the application that the predictive optimal controller aims at, most spaces are designed for the same purpose and the required indoor air conditions are similar. When applying predictive optimal control, the thermostat setpoints of all building zones are controlled by a single optimal controller. In this case, a straightforward simplification of the building model is to combine all the physical zones of the building into a single thermal zone.

In this section, two possible simplifications of building zoning are investigated. The first approach simply combines all of the spaces in the building into one zone without considering the internal structure and furnishing. The other approach is based on the first one, but an artificial internal structural object has been added into the space to represent the internal structure and furnishing of the real building. Figure 22 illustrates these two approaches.

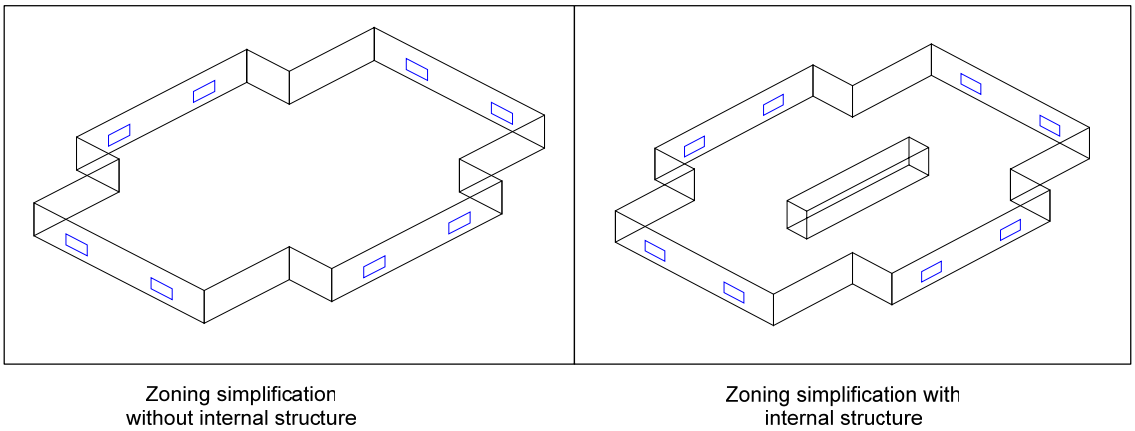

Figure 22: Schematics of zoning simplifications

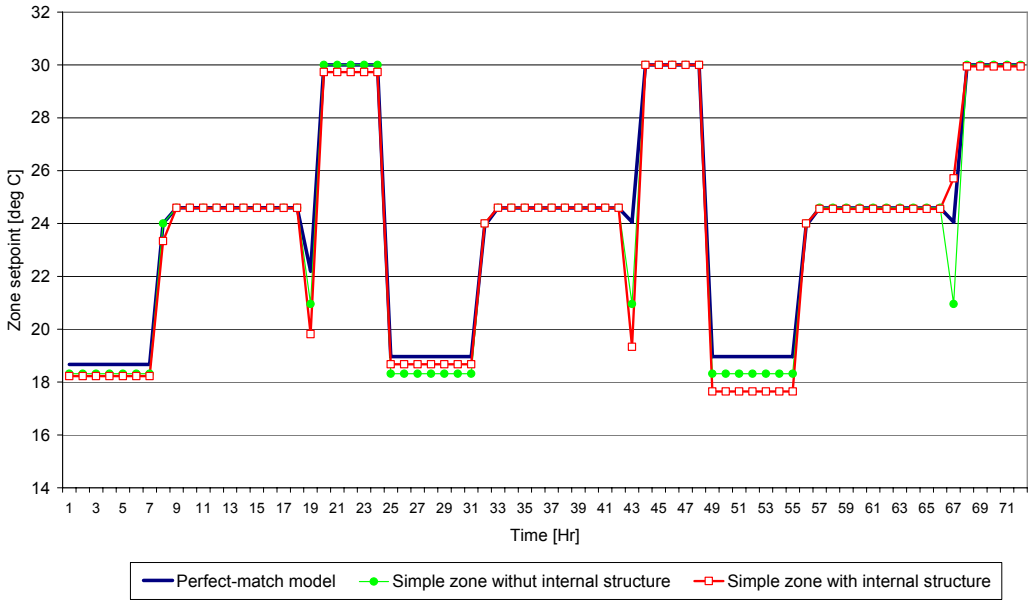

Figure 23: Optimal zone temperature setpoint profiles for perfect match model case and two zoning simplification PMs

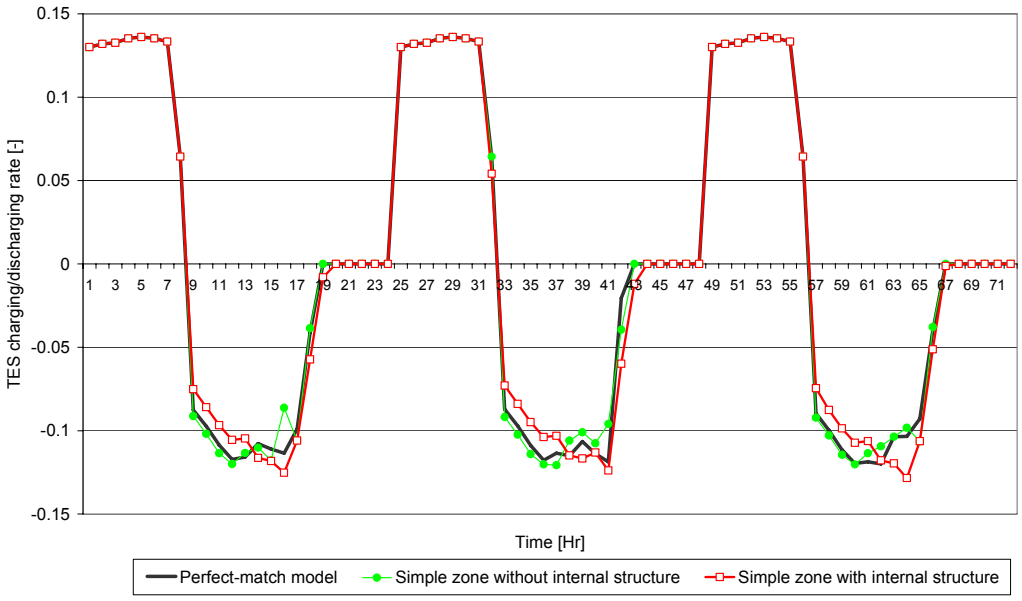

Figure 24: Optimal thermal energy storage charge/discharge profiles for perfect match model case and two zoning simplification PMs

Figure 23 and Figure 24 compare the optimal results of two zoning simplified planning models and the perfect match model. From the figures above, we can see that simplification of building zoning affects both the optimization of zone temperature setpoints and TES operation. Both simple zone planning models result in lower zone temperature setpoints during the precooling period. Instability also occurs in the simple zone planning model with internal structure, which generates a discharging strategy that is different compared with the planning model without the internal structure. Adding internal structure changes the cooling load profile by providing more thermal capacitance, which delays the occurrence of the peak cooling load.

In this analysis, the execution model has limited internal structure; thus the addition of internal structure does not allow the zoning simplified model to match the load profile of the execution model. Consequently, false information is given to the controller, leading to improper operation of the active storage (TES) system. Most office buildings have significant internal structure. This affects their cooling load profile, especially with respect to the peak cooling load. When system identification techniques are applied to properly estimate the internal structure, better modeling can be expected.

Table 15: Summary of cost and energy consumption of zoning mismatched PMs

Case	PM without internal structure	PM with internal structure
Daily energy consumption [kJ]	5,142,997	5,250,857
Daily energy cost [$]	182.29	185.47
Cost saving	21.30%	19.92%
CSR	103.16%	96.49%

Table 15 provides a summary of the energy consumption and CSR of the zoning simplification models. It is interesting to see that the first planning model achieves even higher savings than the perfect model. The results for the simplified planning model imply that decreasing complexity of the building model simplifies the optimization task and reduces the chance of being caught in a local minimum. Computation time in the first planning model is also reduced by an average of one third compared with the perfect match model.

4.5.3 Construction Material

Prior research has demonstrated that the thermal storage potential of buildings depends on building construction characteristics. The heavier the weight, the more thermal storage can be achieved. In this section, the impact of external and internal construction materials on energy optimization potential is investigated. External and internal construction materials are divided into three classes based on mass: heavy, medium, and light. Section 4.8 lists details of the construction material of the building model. The execution model uses medium level construction materials. By combining different mass level of external and internal constructions, eight planning models have been set up to cover all possibilities of mismatch in the building construction category. Table 16 lists the mismatched PMs and the simulation results.

Table 16: Summary of construction mismatched PMs

PMs	PM1	PM2	PM3	PM4	PM5	PM6	PM7	PM8
External construction	Light	Heavy	Normal	Normal	Light	Heavy	Light	Heavy
Internal construct	Normal	Normal	Light	Heavy	Light	Heavy	Heavy	Light
Average precooling temperature	17.64	19.03	18.48	19.08	17.89	20.85	18.16	19.55
Average daily energy cost	183.73	185.9	184.17	184.65	184.44	186.86	184.40	187.60
Cost savings	20.68%	19.74%	20.49%	20.28%	20.37%	19.33%	20.39%	19.01%
CSR	100.15%	95.61%	99.23%	98.21%	98.65%	93.59%	98.74%	92.04%

The simulation results show that mass level variation has an effect on optimization results. All planning model optimal temperature setpoint profiles have the same pattern as the perfect match model. Zone temperature setpoints are affected mostly during the precooling period. Table 16 lists the average precooling temperatures of each planning model during the ten-day simulation. The results show that the precooling temperature varies according to the mass level; the lighter the weight of construction, the lower the setpoint needed. Because more thermal capacitance is available with heavy construction, the building does not need to be cooled down as much to shift the on-peak cooling load to off-peak time periods. The zone temperature setpoint optimization appears to be more sensitive to the mass level of the external construction because the external structure dominates in our analysis.

Active storage charging profiles are not affected, however, discharging rate profiles change with variations in cooling load profiles caused by variations in construction weight. As shown in Appendix 1, all construction mass levels have nearly identical thermal resistance. Different mass levels only shift the occurrence of the peak cooling load; correspondingly, the optimizer shifts the discharging strategy to level the cooling load.

When the optimal strategy of the planning models is applied to the execution model, most cases show lower cost savings than the perfect match model. The optimizer incorporates erroneous information about the mass level of the building and subsequently develops erroneous precooling and discharging strategies. However, PM1 achieves even higher savings than the perfect match model. By underestimating the mass level of the internal structure, the optimizer further lowers the precooling zone temperature setpoint, then shifts more load away from the on-peak time period. This is a unique phenomenon which cannot be extrapolated to other cases. If the setpoint is lowered even further, cost penalties will be incurred because more energy is consumed for precooling. Consequently, more costs are incurred than are saved by on-peak load reduction.

In summary, a mismatch of construction material in the building model affects the optimal results of the setpoint and TES performance. The potential for cost savings decreases in most cases.

4.5.4 Internal Heat Gain

In this section, the effect of building internal heat gain on the optimization results is investigated. Two planning models are devised, representing models with either overestimated or underestimated internal heat gains compared with the execution model. Table 17 lists the internal heat gain for these two planning models and the perfect match model.

Table 17: Internal heat gains for investigated planning models

PM	Underestimated PM	Perfect Match PM	Overestimated PM
Number of people [1/m^2]	0.05	0.10	0.15
Lighting power density [W/m^2]	23	45	68

Figure 25 and Figure 26 show the optimal results of these two planning models and the perfect match model.

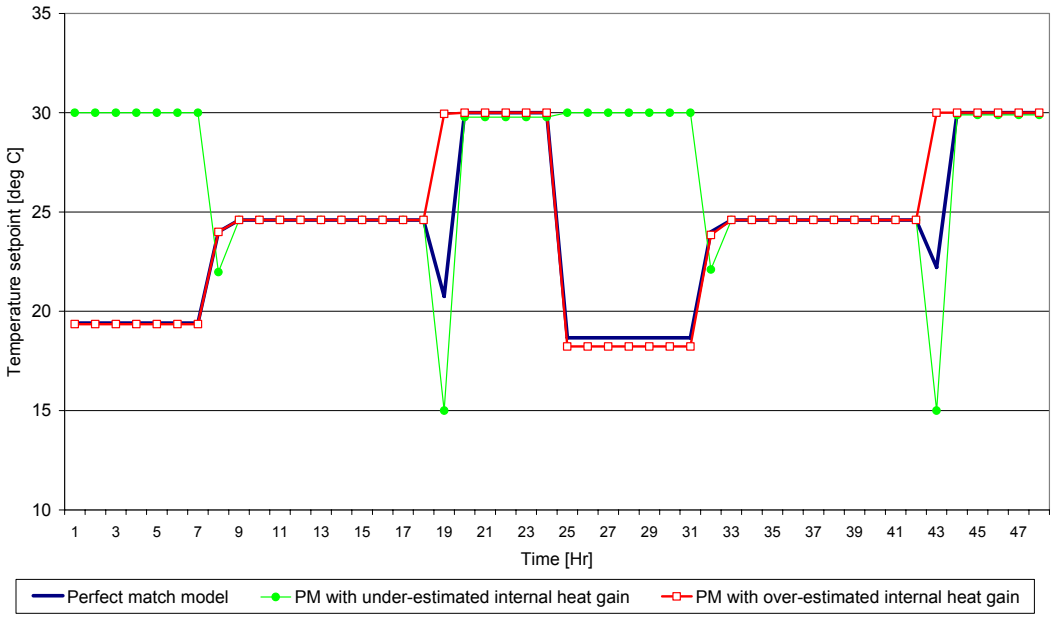

Figure 25: Optimal zone temperature setpoint profiles for perfect match model and internal heat gain mismatched PMs

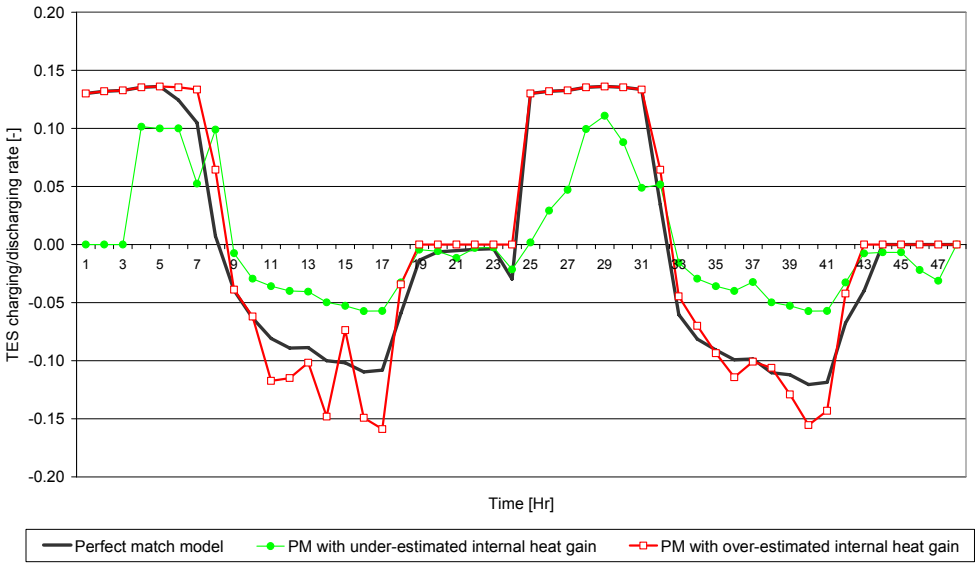

Figure 26: Optimal TES charging/discharging profiles for perfect match model and internal heat gain mis-matched PMs

Figure 25 and Figure 26 show that mismatch in internal heat gains strongly affects the optimal results. For the planning model with underestimated heat gains, the optimizer allows the zone temperatures to float up during most of the unoccupied time period and precools only slightly before the onset of occupancy. At the same time, the active storage is not fully charged because of underestimated cooling loads. On the other hand, in the overestimated scenario, the optimizer further lowers the zone temperature setpoints, fully charges the TES tank, and discharges faster than the perfect match model. Figure 27 shows the state-of-charge of the TES tank in each case.

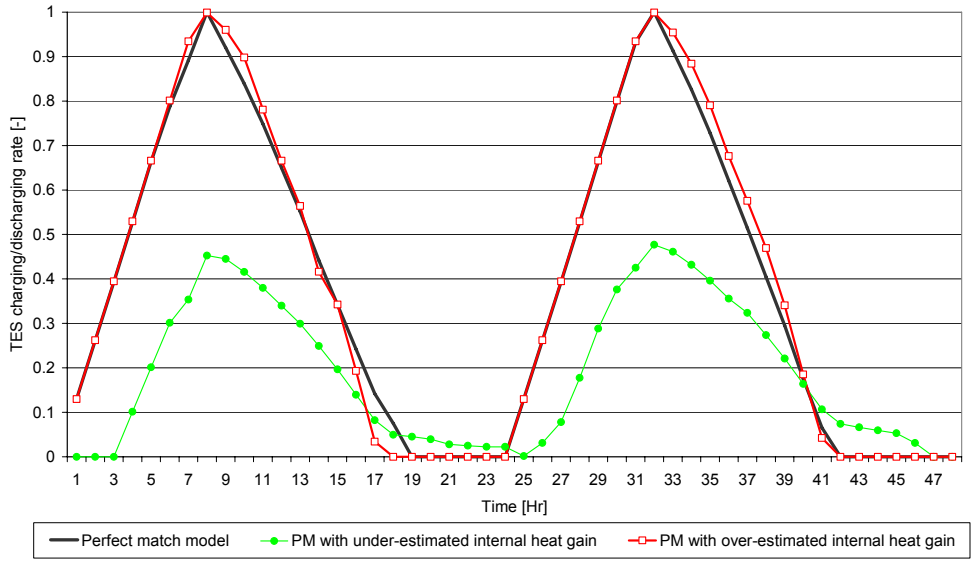

Figure 27: Optimization TES state of charge profiles in perfect-match model and internal heat gain mis-matched PMs

Table 18 provides an overview of cost savings and energy consumption of the internal heat gain mismatched planning models and the perfect match model. Obviously, the false information on internal gains leads to

significant cost penalties in the planning model with underestimated internal gains. The potential of building active and passive thermal storage cannot be fully utilized, even the total energy consumption is decreased compared with the perfect match case, but a cost penalty occurs because more energy is consumed during the on-peak time period. On the other hand, overestimating the internal heat gains encourages the building to be substantially precooled, fully utilizing the potential of TES and leading to higher cost savings in this case. It should also be noted that the energy consumption is slightly lower than in the perfect match case.

Table 18: Summary of cost and energy consumption of internal heat gain mismatched PMs

Case	PM with underestimated internal heat gain	PM with overestimated internal heat gain
Daily energy consumption [kJ]	5,010,903	4,988,260
Daily energy cost [$]	198.91	183.18
Cost saving	14.13%	20.92%
CSR	68.41%	101.30%

4.5.5 Coefficient-of-Performance (COP) of the Plant

Up to this point in our analysis, the mismatches we have investigated affect the optimal solution by changing the cooling load profile of the building. In this section, a mismatch in the energy system is investigated. This mismatch has no direct impact on the building cooling load, but is crucial for the optimizer to determine how to best utilize both active and passive building thermal storage potentials. The coefficients-of-performance (COP) of the plant, including the base chiller and the dedicated TES chiller, are selected to quantify the efficiency of the entire central chilled water system. For each chiller, three COP values are established to represent high, medium and low efficiencies. The execution model is assumed to be equipped with two medium efficiency chillers representing the normal plant setting. Eight combinations of base chillers and TES chillers with varying efficiency levels have been set up to cover a wide range of mismatches (base chiller COP: high: 5, medium: 4, low: 3; TES chiller COP: high: 3.5, medium: 3, low: 2.5).

Table 19: List of planning models in energy system efficiency mismatch

Planning Model	PM1	PM2	PM3	PM4	PM5	PM6	PM7	PM8
COP of Base Chiller	Low	High	Medium	Medium	Low	High	Low	High
COP of TES Chiller	Medium	Medium	Low	High	Low	High	High	Low

The results show that efficiency mismatch of the energy system affects both the optimization of the zone temperature setpoints and the TES performance, and accurate modeling of the base chiller appears to be more important than that of the TES chiller. Figure 28 and Figure 29 show the optimal results of PM1 and PM2.

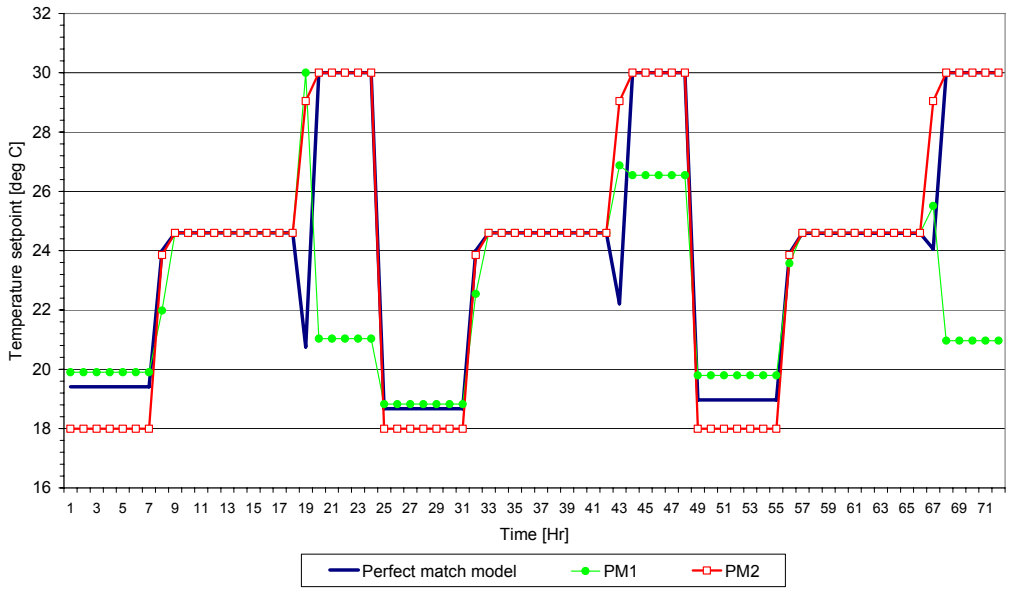

Figure 28: Optimal setpoint profiles for perfect match model and COP mismatched PMs

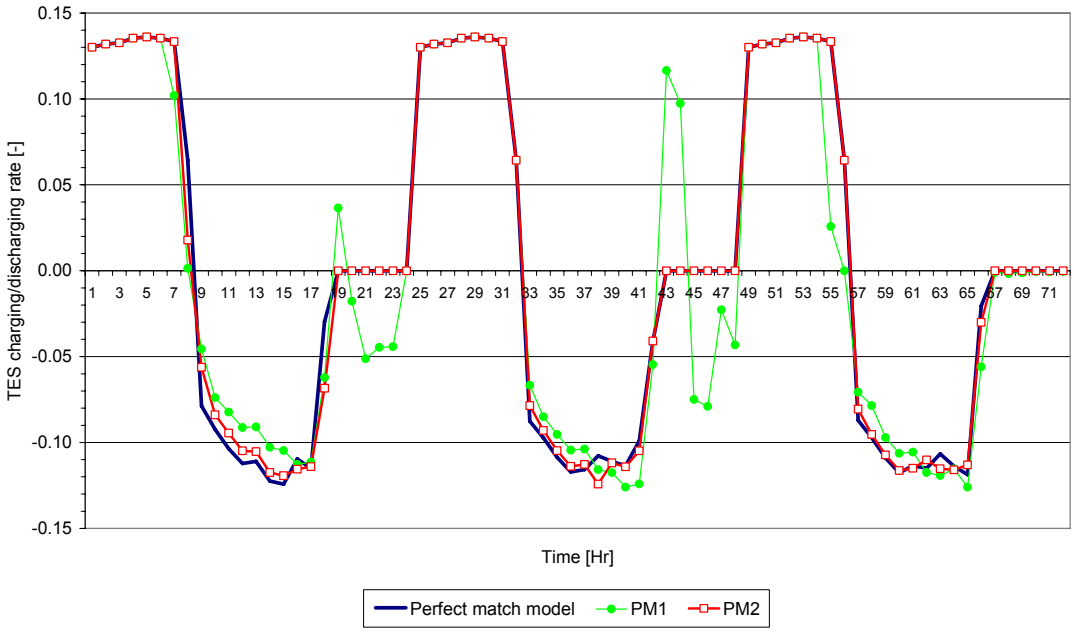

Figure 29: Optimal TES charging/discharging profiles in perfect match model and COP mismatched PMs

In PM1 and PM2, the efficiency of the base chiller varies from low to high while the TES chiller COP remains constant. From Figure 28 and Figure 29 we can see that with improved base chiller efficiency (PM2), the optimizer lowers the precooling zone temperature setpoint because the optimizer assumes the building can store more cooling without an energy penalty. Because PM1 has a poor base chiller COP, zone temperature setpoints are usually higher from 1 a.m. to 7 a.m. than in the perfect match model. They do not rise as much as in the perfect match model and PM2 during the evening hours; instead, the optimizer chooses to keep down the zone temperature setpoints. As a result, the cooling load of PM2 during occupied times is usually lower than the perfect match case and PM1. With respect to the operation of the TES, all planning models charge the tank from 1 a.m. until the beginning of occupancy, the TES discharge strategies depend on the

planning models. For PM2, the TES performance does not change much compared with the perfect match model. But for PM1, the TES system operates from 7 p.m. until midnight, while it is dormant in both PM1 and in the perfect match case.

The same features were found in PM4 to PM8 where a mismatch in the base chiller efficiency exists. For PM3 and PM4, not much difference was found compared with the solution of the perfect match case. This is because the precooling load is typically met by the base chiller; zone temperature setpoint profiles determine the cooling load profile of the building. Given a cooling load profile, the TES operates according to on-peak and off-peak time periods and charges and discharges as much as it can. Table 20 summarizes fractions of cooling load demand for the base chiller and TES chiller in each PM, where:

$$F_{main} = \frac{\text{Cooling demand for base chiller}}{\text{Total cooling demand}}$$

$$F_{TES} = \frac{\text{Cooling demand for TES chiller}}{\text{Total cooling demand}}$$

Table 20: Summary of results of efficiency mismatched PMs

PM	Daily energy consumption [kJ]	F_{main}	F_{TES}	Daily energy cost [$]	Cost saving	CSR
Perfect match model	5,154,819	56.1%	43.9%	183.80	20.6%	100%
PM1	5,452,680	55.8%	44.2%	186.2	19.6%	94.9%
PM2	5,313,072	57.2%	42.8%	186.86	19.33%	93.6%
PM3	5,144,993	56.7%	43.3%	186.07	19.67%	95.25%
PM4	5,169,963	55.3%	44.7%	183.47	20.79%	100.68%
PM5	5,257,110	57.3%	42.7%	185.50	19.92%	96.45%
PM6	5,313,072	57.2%	42.8%	186.86	19.33%	93.60%
PM7	5,634,867	52.8%	47.2%	187.82	18.91%	91.58%
PM8	5,300,435	56.6%	43.4%	186.47	19.49%	94.41%

From Table 20, it can be clearly seen that chiller efficiency affects the fraction of duty of each chiller in the optimizations. Cost penalties are induced by excessive precooling and/or improper operation of the TES. The highest cost savings lost occur in PM7 when the base chiller efficiency is underestimated and that of the TES chiller is overestimated. It is also found that the total energy consumption increases when the efficiency is mismatched, especially in the case of the base chiller.

4.6 Conclusions

This chapter investigated the impact of five categories of building modeling mismatch on the performance of model-based closed-loop predictive optimal control of active and passive building thermal storage. Based on the simulation results, the following conclusions are reached:

For an internal heat gain dominated commercial building, the deviation of building geometry and zoning from the reference building only marginally affects the optimal control strategy. These factors should be considered secondary elements in the building modeling process; reasonable simplifications are acceptable without loss of cost savings potential. In fact, zoning simplification may be an efficient way to improve the optimizer performance and save computation time. The mass of the internal structure did not show a strong ef-

fect on the optimization in our simulation analysis; however, it did change the building cooling load profile, which in turn will affect the operation of the active storage system.

Building construction characteristics were found to impact building passive thermal storage capacity. Zone temperature setpoints are affected more than TES operation by the construction mismatch, and a loss of cost savings potential was found in some cases. It is advisable to make sure the construction material is well modeled.

Zone temperature setpoint profiles and TES performance are strongly affected by mismatches in internal heat gains, especially when they are underestimated. Since they are a key factor in determining the building cooling load, efforts should be made to keep the internal gain mismatch as small as possible.

Efficiencies of the building energy systems have no direct impact on building cooling load, but they affect both zone temperature setpoints and active TES operation because of the coupling of the base chiller and the TES chiller. Relative efficiencies of the base and TES chillers will determine the balance of operation of the two chillers. Mismatch in this category may be significant.

Field experimentation is needed to validate the conclusions derived in this simulation analysis. To avoid critical mismatch, system identification techniques may be useful in improving the modeling process.

4.7 References

[50] Zhou, G., P. Ihm, M. Krarti, S. Liu, and G.P. Henze (2003) "Integration of Optimization Routines Within EnergyPlus", Proceedings of the Eighth International IPBSA Conference Building Simulation 2003, pp. 1475-1482, Eindhoven, Netherlands.

4.8 Appendix: Material Properties

Table 21: Construction Material Summary

External wall				
		Heavy	Medium	Light
Thickness	[mm]	320.00	270.00	270.00
Thermal conductivity	[W/(m*K)]	0.10	0.09	0.08
Density	[kg/m3]	1348.09	1176.63	562.11
Specific heat	[kJ/(kg*K)]	0.84	0.84	0.84
Thermal resistance	[(m2*K)/W]	3.08	3.06	3.26
Mass	[kg/m2]	431.39	317.69	151.77
Roof				
		Heavy	Medium	Light
Thickness	[mm]	273.00	173.00	173.00
Thermal conductivity	[W/(m*K)]	0.20	0.13	0.12
Density	[kg/m3]	1767.88	1472.49	513.41
Specific heat	[kJ/(kg*K)]	0.88	0.91	1.05
Thermal resistance	[(m2*K)/W]	1.35	1.29	1.50
Mass	[kg/m2]	482.63	254.74	88.82
Partition wall				
		Heavy	Medium	Light
Thickness	[mm]	240.00	140.00	140.00
Thermal conductivity	[W/(m*K)]	1.42	1.26	0.44
Density	[kg/m3]	2155.29	2067.00	881.86
Specific heat	[kJ/(kg*K)]	0.84	0.84	0.84
Thermal resistance	[(m2*K)/W]	0.17	0.11	0.32
Mass	[kg/m2]	517.27	289.38	123.46

Phase 1: Analysis – Parametric Study

4.9 Abstract

A parametric study is presented in this chapter and documented in [51] utilizing an EnergyPlus-based simulation environment to assess the effects of building mass, electrical utility rates, season and location, economizer operation, central plant size, and thermal comfort. The findings reveal that the cooling-related on-peak electrical demand and utility cost of commercial buildings can be substantially reduced by harnessing both thermal storage inventories using optimal control for a wide range of conditions.

4.10 Introduction

This chapter systematically evaluates the merits of combined optimal control of both passive building thermal capacitance *and* active thermal energy storage systems to minimize an objective function of choice including total energy consumption, energy cost, occupant discomfort, or a combination of these. The evaluation is conducted by means of a parametric analysis utilizing a simulation environment developed using the state-of-the-art simulation program EnergyPlus. In the analysis, the effects of building mass, electrical utility rates, building location and climate, chiller and tank capacities, and economizer operation on the cost and energy performance of a commercial building are assessed.

Control of both active and passive thermal storage systems describes the process of shaping and shifting the cooling load from daytime to nighttime hours by charging and discharging the two available thermal storage batteries. Knowledge of the active TES system performance, the passive storage behavior, and building energy system characteristics is crucial to ensure the successful design, installation, and operation of this load-shifting technology. Therefore, this chapter studies the impact of selected parameters on the energy and cost saving performance of a prototypical commercial building under utility cost minimizing optimal control modeled using the building simulation program EnergyPlus.

4.11 Description of the Analysis

4.11.1 Building Energy Simulation Environment

The simulation environment used for this investigation is based on EnergyPlus. In particular, the simulation environment consists of a detailed TES model and optimization routines internally integrated into EnergyPlus. EnergyPlus is built on the most popular features and capabilities of BLAST and DOE-2 while including many innovative simulation capabilities such as time steps of less than an hour, modular systems and plant integrated with heat balance-based zone simulation, multi-zone air flow, thermal comfort, and photovoltaic systems. It is a valuable tool to simulate building energy flows and study the controls of building mechanical systems to save both building energy consumption and costs [51]. The implementation of the active building thermal storage system within EnergyPlus is documented in [53], while the overall optimization approach used by the simulation environment is documented in [50].

4.11.2 Investigated Building

Throughout the analysis presented in this chapter, we consider a three-story office building as shown in Figure 1 with five thermal zones per floor, i.e., 15 thermal zones in total. The perimeter zones have an area of 288 m^2 each, while the core zone has an area of 576 m^2. Total area per floor is thus 1,728 m^2 and the building total is 5,184 m^2. Peak building occupancy is 12 m^2/person. Each office worker contributes 132 W of internal gain, where 54% are assumed to be sensible and 46% latent. Peak lighting density is 20 W/m^2, equipment power density is 21.7 W/m^2, i.e., the total electrical power density is 41.7 W/m^2. The occupancy and lighting schedules for a weekday are shown in Figure 2, where hour 13 refers to the hour from 12 to 13. On weekends and holidays building occupancy is zero and lighting density is 5% of the peak value.

Counting the exterior envelope, floor, and ceiling surfaces, the building mass is approximately 1,000 kg/m^2 of floor area, and thus can be considered heavy-weight construction. Table 22 shows the wall construction of the exterior walls, interior partitions, ceilings and floors for this heavy-mass case.

Table 22: Construction of heavy-mass building

Construction Name	Layers (from outside to inside)
Exterior Wall	ASHRAE Wall Type #28: 25mm stucco, 100mm insulation, 300mm heavy weight concrete, 20mm plaster
Roof	ASHREA Roof Type #25: 12 mm slag/stone, 10 mm felt and mambrane, 100mm insulation, 150mm heavy weight concrete, air space and acoustic tile
Floor	300mm earth, 200mm heavy weight concrete
Ceiling	20mm plaster or gyp.board, 200mm heavy weight concrete, 20mm plaster or gyp. board
Internal Wall	20mm plaster, 100mm heavy weight concrete, 20mm plaster

Three electrical utility rate structures are considered: strong-incentive rate, normal-incentive rate, and weak-incentive rate. In the strong incentive rate, the energy cost is 0.05 $/kWh during off-peak periods and 0.20 $/kWh during on-peak periods; the demand cost is 10 $/kW during on-peak periods and zero during off-peak periods. In the normal-incentive rate, the energy cost is 0.10 $/kWh during off-peak periods and 0.20 $/kWh during on-peak periods; the demand cost is 10 $/kW during on-peak periods and 5 $/kW during off-peak periods. Finally, in the weak-incentive rate, the energy cost is 0.20 $/kWh throughout the day and demand cost is same as in the normal incentive rate. The on-peak period is 9:00-18:00; the off-peak period is the rest of the day.

A variable air volume HVAC system with terminal reheat is used to meet the cooling load. Zone temperatures are controlled by a dual setpoint with dead band controller. For conventional nighttime setback control, the system is off during the unoccupied hours and the indoor temperature is floating; the system is on during occupied hours (8:00-19:00) and keeps the indoor temperature at the higher limit of cooling setpoints of 24°C.

The outdoor air flow rate is controlled by a return air temperature based economizer that adjusts the outdoor air fraction from 0% to 100% by comparing the temperature of return air and outdoor air. At the same time, the outdoor air fraction must meet the schedule of minimal outdoor air fraction of 15% during occupied periods.

The central plant is made up of one large base chiller and an ice-based active TES system. The base chiller is modeled as a constant-COP electrical chiller and meets all the cooling loads alone during nighttime setback controls. Its nominal capacity is 500 kW and COP is 4.5. The ice-based TES system is configured in parallel with the chiller. It is made up of a 1,500 kWh ice tank, a dedicated small chiller with a capacity of 250 kW and COP of 3.0 and its own dedicated cooling tower. In nighttime setback controls, the active thermal storage system is dormant. Under optimal control, the active storage is controlled to be charged during off-peak hours and discharged during on-peak hours; the cooling load is met jointly by the base chiller and the active thermal energy storage.

Three seasons of three locations are studied in this parametric study. These are winter (January 17), spring (April 2), and summer (July 20) in Phoenix, Arizona, Minneapolis, Minnesota, and Boulder, Colorado. The updated typical meteorological year (TMY2) weather data is used. Table 23 summarizes the outdoor dry bulb temperature of these locations to give a brief summary of the weather.

Table 23: Dry-bulb temperatures during spring, summer and winter in Phoenix, Minneapolis and Boulder

		Min (C)	Max (C)	Average (C)	Swing (C)
Summer	Phoenix	27.8	41.1	34.3	13.3
	Minneapolis	16.7	26.7	22.7	10.0
	Boulder	16.1	26.7	20.0	10.6
Spring	Phoenix	14.4	32.8	23.9	18.4
	Minneapolis	15.0	24.4	19.8	9.4
	Boulder	-0.6	13.3	7.2	13.9
Winter	Phoenix	8.9	19.4	12.3	10.5
	Minneapolis	-7.8	1.1	-4.3	8.9
	Boulder	-7.2	-2.9	-4.8	4.3

4.11.3 Base Case Scenarios

Before studying optimal combined thermal storage control, it is necessary to establish a reference case for comparison. This reference or base case is defined by the operation of the commercial building under night-time setback control, i.e., no passive storage utilization, and non-optimized conventional active storage (TES) control. Conventional TES control includes storage-priority control or chiller-priority control. In storage-priority control, the ice tank is charged to 100% during the nighttime off-peak hours; during the on-peak hours, the building cooling load is met first by melting ice, and then, if the ice melting cannot providing enough cooling to meet the load, the base chiller is started to meet the remainder of the cooling load. Here, a 1,500 kWh ice tank and a 500 kW primary chiller are simulated. In chiller-priority control, during off-peak time, the ice tank is charged to 100% state-of-charge; during the on-peak hours, the building cooling load is first met by operating the primary chiller (the chiller can therefore be downsized); when the chiller cannot meet all of the cooling load, the ice is melted to make up for the rest of the load. Here, a 1500 kWh ice tank and a downsized 300 kW chiller are simulated.

From the above description, it can be concluded that several important factors need to be determined for conventional TES controls to achieve cost savings. First, it has to be determined how much ice has to be charged during off-peak time or how large the ice tank should be. If the ice tank is too small, it may not be able to meet the load; if the ice tank is too large, energy and costs incurred to charge the tank are going to be wasted. Secondly, it has to be determined how much should the chiller be downsized. An inappropriately downsized chiller will either be too big and recover the initial investment or be too small to meet the cooling load. Without optimization, the TES system may actually result in more energy use and costs than a system without TES. This can be clearly seen in Table 24.

Table 24 shows the comparison among nighttime setback control without TES, storage-priority controlled TES, and chiller-priority controlled TES. Different building mass levels, i.e., H (heavy: 1,000 kg/m^2), M (medium: 350 kg/m^2) and L (light: 200 kg/m^2) and different electrical utility rate structure, i.e., 1 (normal incentive) and 2 (strong incentive), are compared.

Table 24: Cost comparison [US$] of non-optimized storage-priority control, chiller-priority control with ice tank dormant nighttime setback control

	H-1			H-2		
	Winter	Spring	Summer	Winter	Spring	Summer
No TES	655.11	808.27	907.67	589.48	732.28	815.60
Storage-Priority	661.75	780.80	891.00	568.97	679.81	815.60
Savings	1.0%	-3.4%	-1.8%	-3.5%	-7.2%	0.0%
Chiller-Priority	705.11	853.58	887.75	614.48	752.59	815.60
Savings	7.6%	5.6%	-2.2%	4.2%	2.8%	0.0%
	M-1			M-2		
	Winter	Spring	Summer	Winter	Spring	Summer
No TES	658.46	812.07	912.31	592.87	735.87	819.22
Storage-Priority	663.92	784.60	895.64	571.18	683.40	777.55
Savings	0.8%	-3.4%	-1.8%	-3.7%	-7.1%	-5.1%
Chiller-Priority	708.46	855.87	888.95	617.87	754.67	777.26
Savings	7.6%	5.4%	-2.6%	4.2%	2.6%	-5.1%
	L-1			L-2		
	Winter	Spring	Summer	Winter	Spring	Summer
No TES	661.08	813.16	913.22	595.56	736.96	819.88
Storage-Priority	665.44	785.69	896.55	572.78	684.50	778.21
Savings	0.7%	-3.4%	-1.8%	-3.8%	-7.1%	-5.1%
Chiller-Priority	711.08	856.19	889.07	620.56	755.00	777.35
Savings	7.6%	5.3%	-2.6%	4.2%	2.4%	-5.2%

From Table 24, it can be observed that without optimal control, the chiller-priority control or storage- priority control can only save about 5% of the costs in some cases; in several cases, they may actually incur higher costs than a system without TES.

4.12 Parametric Study

Factors that will affect the performance of building thermal storage inventory are numerous. Building mass determines the thermal capacity of the building passive storage. A strong-incentive time-of-use (TOU) utility rate structure allows increased energy consumption to be traded off by the cost savings. In this chapter we investigate the effect of a total of six parameters on the performance of a model-predictive controller harnessing the active and passive building thermal storage inventory.

4.12.1 Effect of Building Mass

The amount of heat that can be stored in the passive building storage inventory is determined by the building's total thermal capacity to which the supply air stream is coupled. Since the specific heat of most of the building construction material is within a narrow band of 0.8-2.5 kJ/kg°C, the thermal capacity of the building is mainly determined by the mass of the construction. Without a change to the architectural design and construction of the building model, the building mass can be altered by varying either the thickness of the wall material or the density of the material. Table 25 summarizes the results of optimizing the passive building thermal storage inventory for three building mass levels under three utility rate structures and seasons. The operating cost shown in the following tables is broken down into chiller operating cost only, total primary and secondary HVAC system operating cost for cooling and total building cost including non-cooling electricity cost. The non-cooling related cost portion can be determined by subtracting the cooling electricity cost from the total cost.

Table 25: Comparison of optimal control of passive TES with different mass levels

Effect of Mass		Strong TOU			Normal TOU			Weak TOU		
		Heavy	Medium	Light	Heavy	Medium	Light	Heavy	Medium	Light
Base Case	Chiller Elec. ($)	226	229	230	249	253	254	263	269	270
	Cooling Elec. ($)	309	313	313	341	345	346	362	367	368
	Non-Cooling ($)	507	507	507	567	567	567	616	616	616
	Total Cost ($)	816	819	820	908	912	913	978	983	984
Opt. Case	Chiller Elec. ($)	154	161	168	204	212	217	262	268	269
	Cooling Elec. ($)	227	236	245	287	297	302	361	367	368
	Non-Cooling ($)	507	507	507	567	567	567	616	616	616
	Total Cost ($)	734	743	751	854	864	869	976	983	984
Savings	Chiller Saving	-31.9%	-29.6%	-26.7%	-18.1%	-16.1%	-14.6%	-0.5%	-0.4%	-0.1%
	Cooling Saving	-26.6%	-24.4%	-21.9%	-15.7%	-14.0%	-12.7%	-0.4%	-0.1%	-0.1%
	Total Saving	-10.1%	-9.3%	-8.4%	-5.9%	-5.3%	-4.8%	-0.2%	0.0%	0.0%

As can be observed in Table 25, by using optimal control of passive thermal storage inventory only, the total electrical cost of the building can be reduced by up to 10% and the cooling electrical cost can be reduced by up to 26%. Building constructed with higher mass has larger saving potentials than building with light mass. However, even with a light mass, 8.4% of total electrical cost and 21.9% of cooling electrical cost can be saved under optimized control.

Figure 30 shows the indoor air temperature and cooling energy use of optimal controlled passive storage of a light mass building and a heavy mass building.

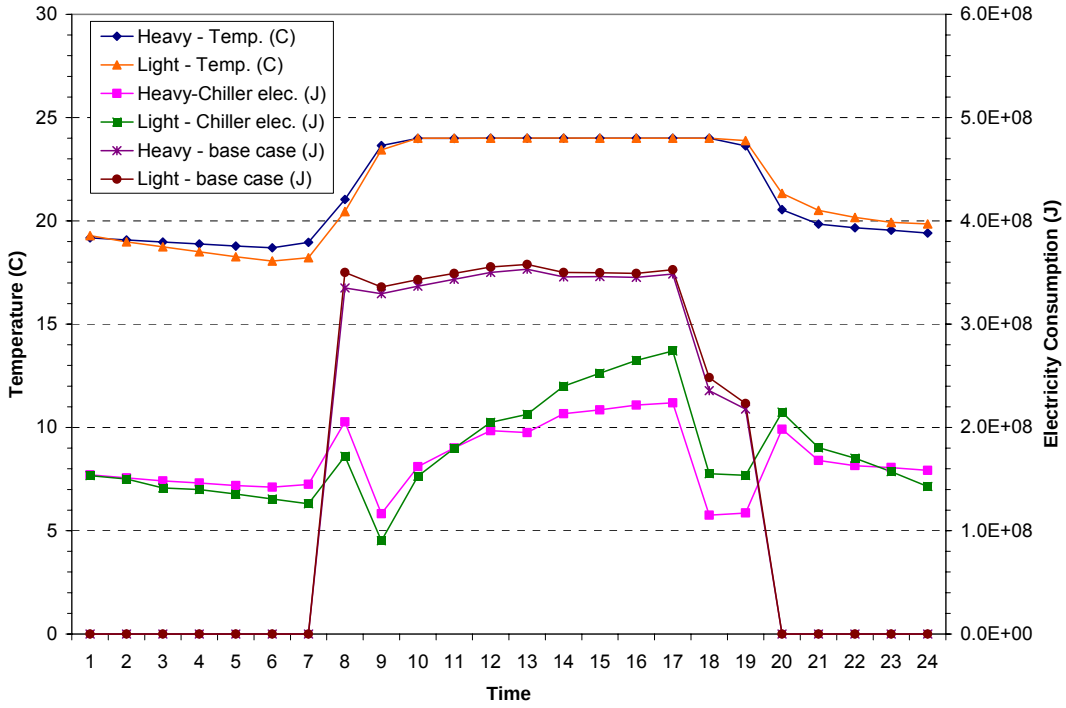

Figure 30: Temperature and electricity consumption profile of a light mass and a heavy mass building

It can be observed from Figure 30 that the chiller of both the heavy-mass building and light-mass building consumes about the same amount of the electricity with a peak value of 98-99 kW under nighttime setback control (base case). The optimal control of the heavy mass building precools the building mass during the night and early morning to about 18.7°C; the light building precools the mass to about 18.0°C. Since the thermal capacity of the heavy-mass building is much larger than that of the light-mass building, chiller electricity use of the heavy mass building is higher during nighttime than that of the light-mass building. During

the day, the precooled heavy-mass building absorbs more heat than the light-mass building so that the peak electrical demand during the occupied hours is reduced to 62.2 kW, lower than that of the light mass building, 75.2 kW.

There are thermal losses associated with the storage of cooling energy. In passive building thermal storage inventory, the cooling energy is lost by radiation and convection of building mass to the higher environmental temperature; in active TES systems, the cooling energy is lost from heat transmission through the exterior tank surface and the potential efficiency degradation of the dedicated chiller in the icemaking mode. Therefore, if the efficiency of the dedicated TES chiller working under a cool nighttime environment is not significantly higher than under a hotter daytime environment, using active TES is bound to be energy expensive. Moreover, when the outdoor air temperature cools down only marginally during the night and the building mass cannot be fully cooled by ventilation only; passive building storage utilization will likely consume more energy as well. Therefore, the reason that TES can actually save electrical cost lies in the time-of-use (TOU) electrical rate structure.

Three electrical rate structures are considered in this study, i.e. weak-incentive, normal-incentive and strong-incentive. Table 26 summarizes the savings of optimal control of both passive and active building thermal storage inventory under different TOU rate structures.

Table 26: Comparison of optimal combined thermal storage control performance for different utility rates

Effect of TOU rate		Heavy Mass			Medium Mass			Light Mass		
		Strong	Normal	Weak	Strong	Normal	Weak	Strong	Normal	Weak
Base Case	Chiller Elec. ($)	226	249	249	229	253	269	230	254	270
	Cooling Elec. ($)	309	341	362	313	345	367	313	346	368
	Non-Cooling ($)	507	567	616	507	567	616	507	567	616
	Total Cost ($)	816	908	978	819	912	983	820	913	984
Opt. Case	Chiller Elec. ($)	76	124	262	85	134	268	87	138	269
	Cooling Elec. ($)	173	257	361	183	265	367	187	269	368
	Non-Cooling ($)	505	567	616	502	567	616	505	567	616
	Total Cost ($)	678	824	976	685	832	983	692	836	984
Savings	Chiller Saving	-66.3%	-50.3%	5.0%	-63.1%	-47.0%	-0.4%	-62.0%	-45.6%	-0.1%
	Cooling Saving	-44.0%	-24.7%	-0.4%	-41.5%	-23.4%	-0.1%	-40.3%	-22.4%	-0.1%
	Total Saving	-16.9%	-9.3%	-0.2%	-16.4%	-8.9%	0.0%	-15.6%	-8.5%	0.0%

Figure 31(a) and (b) show indoor air temperature, active storage state-of-charge, and total cooling energy consumption of optimal combined thermal storage control under strong and normal incentive rate as well as base case.

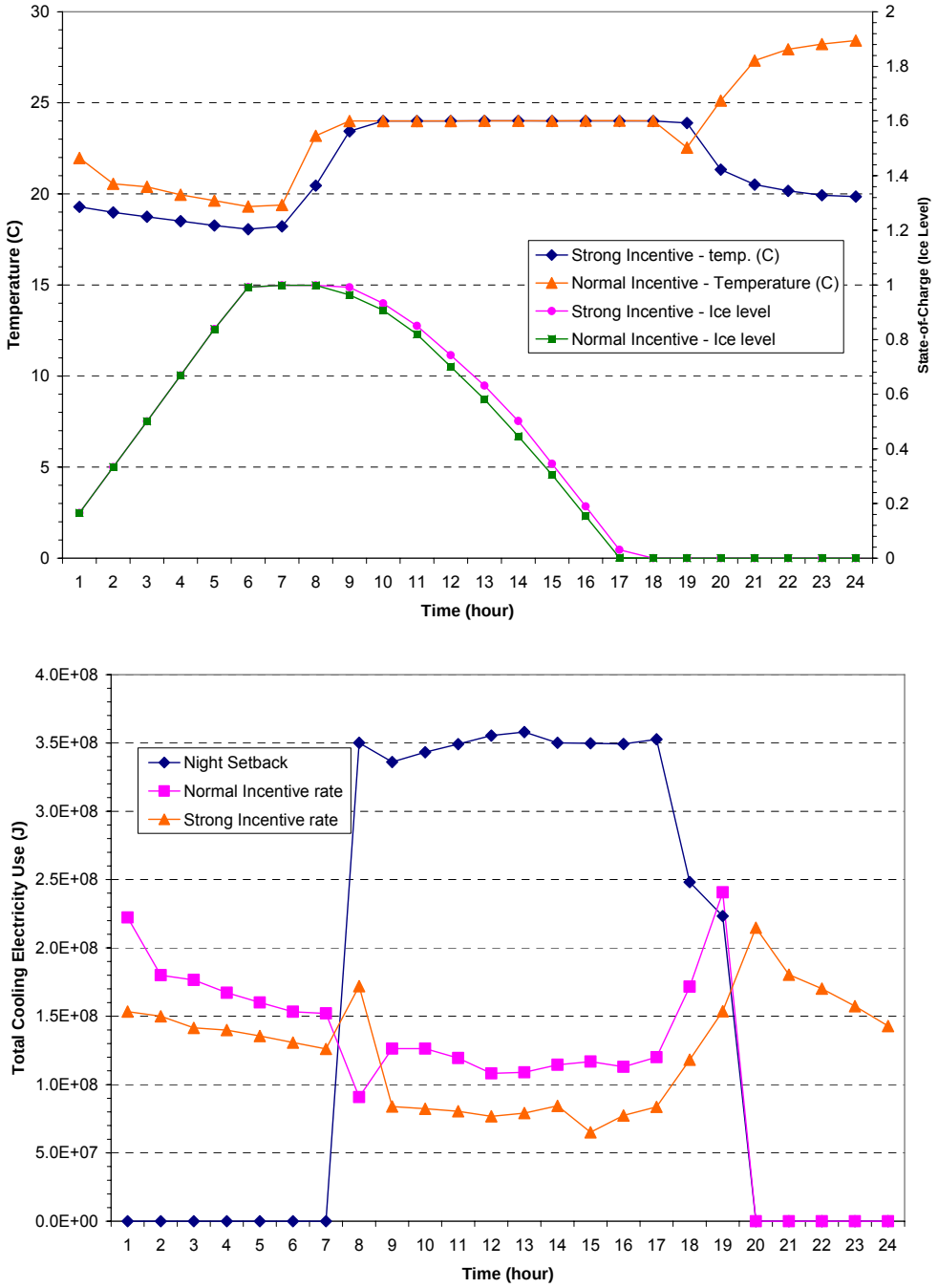

Figure 31: a) Temperature, state-of-charge, and b) electricity use profile of optimal combined thermal storage control under strong and normal incentive rates

It can be observed from Figure 31 that under strong electrical rate incentives, both passive and active thermal storage inventories are made fully use of. Before the building is occupied at 8:00, the building is precooled to 18-20°C during the night and the active TES tank is charged full. When building begins to be occupied and the electrical utility rate switches to on-peak, zone air temperature is kept at the highest allowable setpoints of 24°C. The ice tank is not discharged immediately but is discharged during the entire on-peak period. Therefore, a large portion of on-peak energy is shifted to off-peak periods and the on-peak electrical demand

is reduced significantly. Under the normal-incentive electrical rate, the building is not precooled significantly compared with the strong-incentive rate.

Table 26 summarizes the results of optimizing both the passive and active thermal inventory for different electrical utility rate structures. Comparing the optimally controlled building with a system under nighttime setback control, it can be observed that the higher the incentive in the rate structure, the more savings can be obtained by shifting on-peak load to off-peak period by using both passive and active thermal inventories. Comparing the optimally controlled building with either of the two conventional controls in Table 24, it can also be observed that optimal combined thermal storage control saves more than chiller-priority control does. For the chiller-priority control, there are numerous instances where it incurred higher costs than without an active TES system. However, using optimal combined thermal storage control can always achieve some savings or at least will never cost more than an active thermal storage system.

4.12.2 Effect of Building Location and Seasons

Three seasons are considered, i.e. summer, spring, winter; three locations are compared, i.e. Phoenix, AZ, Minneapolis, MN, and Boulder, CO.

Table 27: Summary of optimal combined thermal storage control savings for various locations and seasons

Effect of Season & Location		Phoenix			Minneapolis			Boulder		
		Winter	Spring	Summer	Winter	Spring	Summer	Winter	Spring	Summer
Base Case	Chiller Elec. ($)	24	156	229	0	120	187	0	2	141
	Cooling Elec. ($)	86	229	313	15	176	254	16	42	213
	Total Cost ($)	593	736	819	522	683	761	522	549	720
Opt. Case	Chiller Elec. ($)	0	29	85	0	14	36	0	1	18
	Cooling Elec. ($)	51	123	183	15	78	125	15	36	108
	Total Cost ($)	558	629	685	521	584	631	522	543	615
Savings	Chiller Saving	-99.5%	-81.3%	-63.1%	0.0%	-88.1%	-80.9%	0.0%	-66.8%	-87.2%
	Cooling Saving	-40.8%	-46.5%	-41.5%	-4.2%	-55.9%	-50.9%	-3.5%	-14.6%	-49.1%
	Total Saving	-5.9%	-14.6%	-16.4%	-0.1%	-14.4%	-17.0%	-0.1%	-1.1%	-14.5%

It can be observed from Table 27 that the total electricity cost savings achieved by optimal combined thermal storage control varies from 0.1% to 17.0%, and cooling electricity cost savings varies from 3.5% to 55.9%, from season to season and from location to location.

In the winter, the savings that can be achieved are lower than those during the spring or summer for all three locations. This is because the cooling electrical load in the winter is very low, about 10% of the total electrical load, while in spring and summer the cooling electrical load is higher, about 40-45% of the total electrical load. When the ratio of cooling load in the total load is low, the potential of savings derived from shifting cooling loads is low. For example, this occurs in spring in Boulder, Colorado. Because the weather of April 2 in Boulder is still very cool and the cooling load under nighttime setback is nearly zero, there is not much that can be saved.

Generally, it can be observed that locations with higher cooling loads have a larger potential for savings. The savings achieved in Phoenix and Minneapolis are larger than those in Boulder. Also, savings in Phoenix are larger than those in Minneapolis, except during the summer. Figure 32 shows the temperature and electricity profiles of optimal combined thermal storage control in summer in Phoenix and Minneapolis.

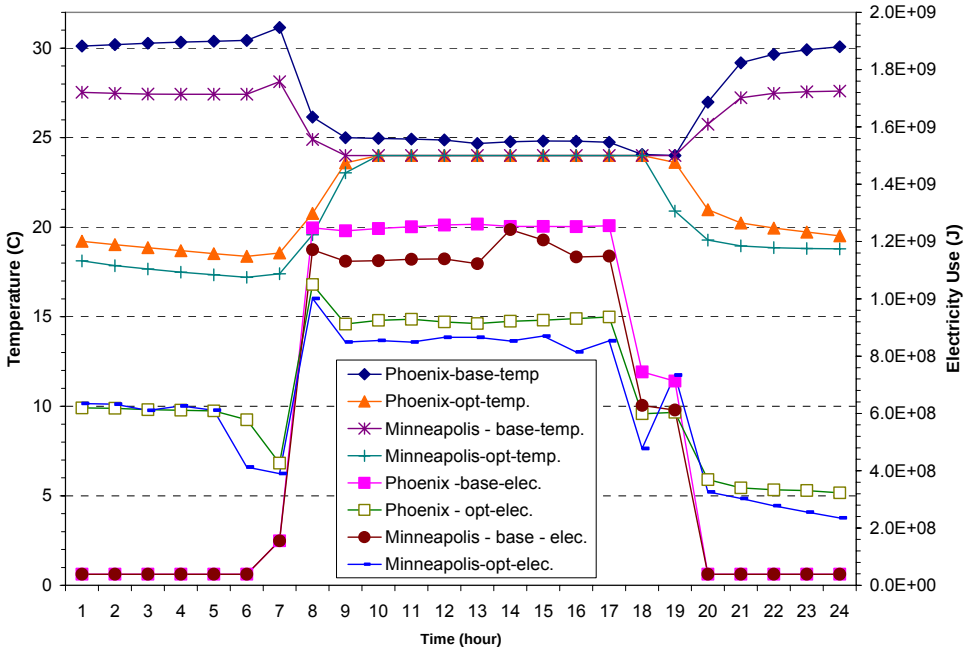

Figure 32: Temperature and electricity use profile of optimal combined thermal storage control in Phoenix and Minneapolis

It can be observed from Figure 32 that under nighttime setback control, indoor temperature in Phoenix is about 25°C, which is 1°C higher than the setpoint 24°C (not shown in the figure), while the indoor temperature in Minneapolis is within 24°C. This indicates that the system capacity is not large enough for Phoenix. Therefore, the base case electrical cost in Phoenix should be higher if the system capacity is large enough to meet the setpoint. This means that the savings in Phoenix will be higher if the system capacity is large enough to meet the setpoint in the base case. Second, looking at inspecting the base case electrical cost for Minneapolis, the demand cost has a higher fraction of the total cost due to the peak at 14:00. Therefore, the optimal control in Minneapolis achieved higher savings by decreasing the demand peak in the base case. These two reasons combine to let the optimal combined thermal storage control achieve higher savings in Minneapolis than in Phoenix.

This analysis shows that the effects of season and location on optimal control savings are hard to predict. However, the trend can be observed that higher cost savings can be achieved when there are higher cooling loads that can be shifted to off-peak hours.

4.12.3 Effect of Thermal Comfort

Based on previous analysis, it was observed that without considering thermal comfort in the optimization, the optimal control of passive building thermal storage inventory tends to maintain the indoor air temperature at the higher limit of the cooling setpoint, 24°C, in this study, in order to reduce the cooling load. In most of the cases, this causes the zone to be less comfortable. As recommended by ASHRAE [54], the predicted mean vote (PMV) of the zone should be within the limits of ±0.5. In this section, the impact of maintaining zone thermal comfort on the optimal control performance is studied.

The impact of thermal comfort is realized by adding a thermal comfort penalty into the cost function. Therefore, the cost function of the optimization routine becomes:

$$CostFunctionValue = TotalElectricalCost \times (1 + ThermalComfortPenalty) \quad (26)$$

There are many ways of calculating thermal comfort as well as considering thermal comfort penalties. In this study, Fanger's thermal comfort model as implemented in EnergyPlus is chosen and the penalty is calculated as follows: At hour *t*, the Fanger PMV value of the building is the PMV value of the most uncomfortable zone, i.e.

$$PMV_t = \max(|PMV_j|) \text{ for j = 1, … K number of zones}$$

The hourly thermal comfort penalty coefficient at hour *t* is

$$R_t = \begin{cases} 0 & \text{if } PMV_t \le 0.5 \text{ or if the building is unoccupied} \\ 1 & \text{if } PMV_t > 2.0 \text{ or if the building is occupied} \\ \left|\frac{(PMV_t - 0.5)}{2.0 - 0.5}\right|^2 & \text{if } 0.5 < PMV_t \le 2.0 \text{ and if the building is occupied} \end{cases}$$

The total thermal comfort penalty coefficient is the sum of the hourly thermal comfort penalty coefficients over the optimization horizon, i.e.

$$ThermalComfortPenalty = \sum_t PMV_t$$

This method of penalty calculation considers all *PMV* in excess of 2.0 to be equally uncomfortable and unacceptable; the penalty for PMV larger than 2.0 is considered 100% which doubles the electrical costs. Within 0.5, it is considered equally comfortable and thus no penalty is added. Between 0.5 and 2.0, the penalty is calculated using a parabola which increases the gradient of the penalty as the *PMV* approaches 2.0.

Figure 33 a) and b) show the temperature profiles and the PMV of each of the 15 zones of the heavy-mass building after optimizing TES without or with thermal comfort penalty.

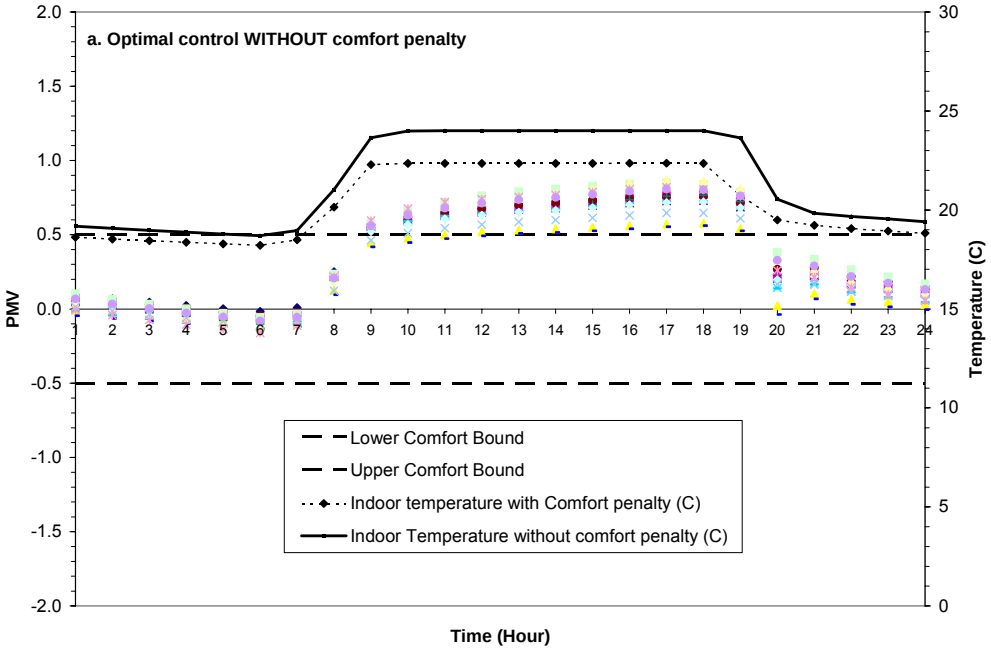

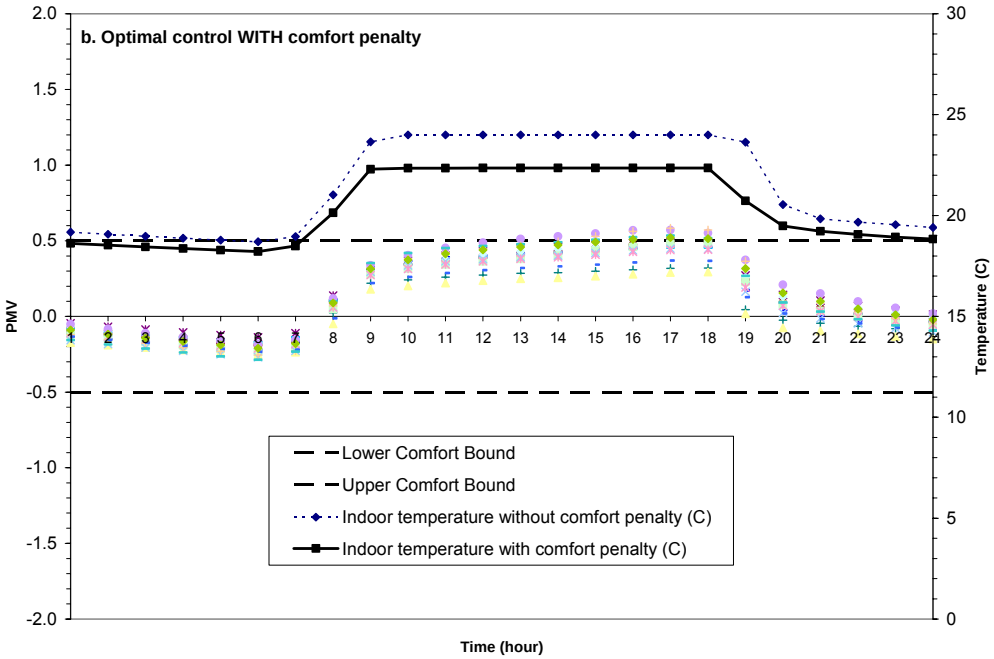

Figure 33: Zone PMV and temperature profiles a) without and b) with comfort penalty optimal control

It can be seen from the above figures that without thermal comfort penalty, indoor temperature during the occupied period (8:00-19:00) is kept at 24.0°C. After 10:00 most of the zones are too warm with PMV > 0.5. The thermal comfort penalty coefficient is 0.414. With the thermal comfort penalty, the indoor temperature during occupied period is kept at 22.4°C. Almost all of the zones are in the comfort area (-0.5 < PMV < 0.5). The thermal comfort penalty coefficient is reduced to 0.0089. Table 28 summarizes the comparison of optimal combined thermal storage control with and without thermal comfort penalty.

Table 28: Summary of savings of optimal control with and without thermal comfort penalty

	Base		Optimal w/o Comfort Penalty			Optimizing w/ Comfort Penalty		
	Total Cost ($)	Comfort Penalty	Total Cost ($)	Comfort Penalty	Savings	Total Cost ($)	Comfort Penalty	Savings
Heavy Mass, Strong Incentive, Summer	816	3.24	678	0.414	-16.9%	711	0.0089	-12.8%
Heavy Mass, Normal Incentive, Summer	908	3.24	824	0.699	-9.3%	859	0.0081	-5.3%
Heavy Mass, Strong Incentive, Spring	732	1.64	601	0.151	-17.9%	640	0.00124	-12.6%
Medium Mass, Strong Incentive, Summer	819	3.52	685	0.579	-16.4%	742	0.0346	-9.4%
Medium Mass, Normal Incentive, Summer	912	3.52	832	0.837	-8.9%	892	0.0374	-2.3%
Medium Mass, Strong Incentive, Spring	736	1.69	629	0.29	-14.6%	655	0.0112	-11.0%
Light Mass, Strong Incentive, Summer	820	3.63	692	0.765	-15.6%	758	0.0936	-7.6%
Light Mass, Normal Incentive, Summer	913	3.63	836	0.98	-8.5%	909	0.0952	-0.5%
Light Mass, Strong Incentive, Spring	737	1.75	632	0.54	-14.2%	676	0.0431	-8.3%

Without thermal comfort penalty, total electrical costs of optimal control are lower than with thermal comfort penalty. Thermal comfort penalty coefficients are high in the cases of nighttime setback control.

Inspecting the thermal comfort penalty coefficient in Table 28, it can be found that when conducting optimization without thermal comfort penalty, the light mass building has a higher penalty than the heavy mass building when both indoor air temperatures are about 24°C. This is because the mean radiant temperature of the heavy mass building is lower than that of the light mass building. Therefore, when thermal comfort penalty is introduced in optimization, the light-mass building tends to lose more savings than the heavy-mass building does.

4.12.4 Effect of Central Plant Capacities

Figure 34 shows the indoor air temperature, active storage inventory level, and the total electrical energy use of two central plants of different sizes. Plant 1 has base chiller capacity of 500 kW and an active TES tank size of 800 kWh. Plant 2 has base chiller capacity of 300 kW and an active TES tank size of 800 kWh. A summary of results from different plant sizes is included in Table 29.

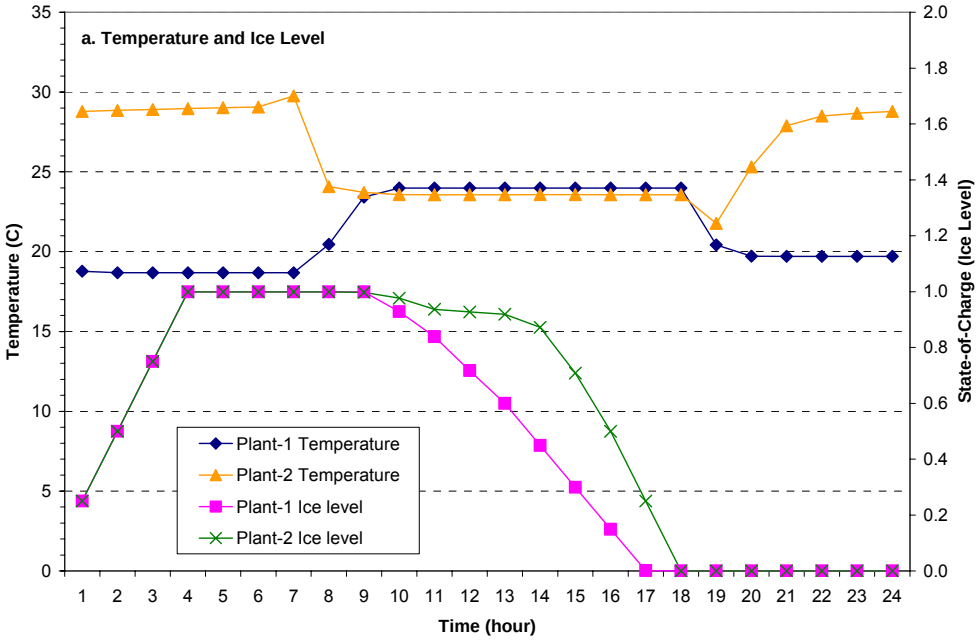

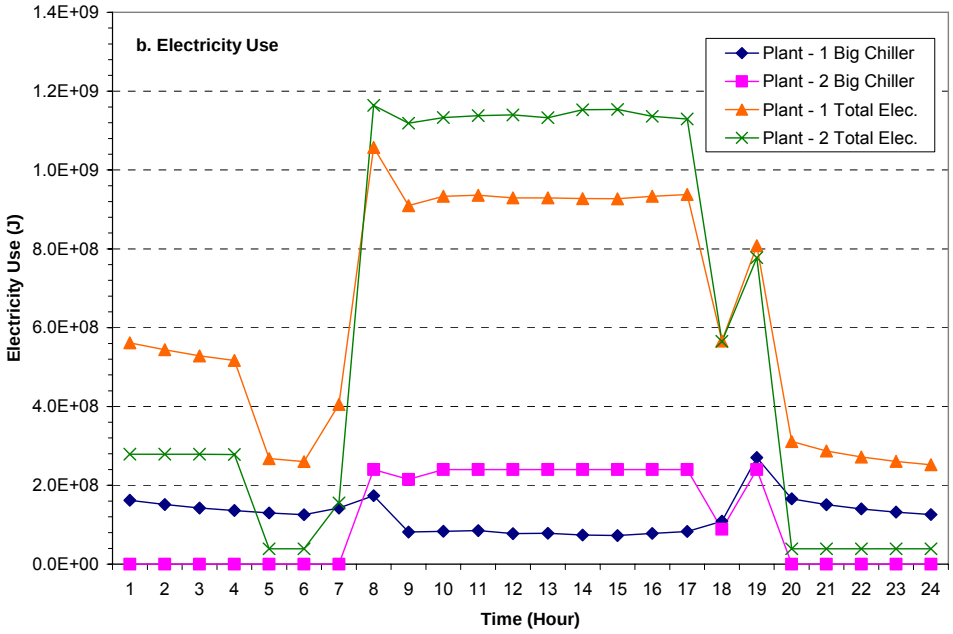

Figure 34: a) Control variables and b) electricity use profiles of optimal combined thermal storage for two central plant sizes

Table 29: Summary of optimal control savings for different central plant sizes

Central Plant Capacity	Cost	Savings
Nighttime Setback Control 500 kW 1500 kWh	777	
500 kW 1500 kWh Optimal Control	647	-16.7%
500 kW 800 kWh Optimal Control	671	-13.6%
300 kW 1500 kWh Optimal Control	733	-5.6%
300 kW 800 kWh Optimal Control	755	-2.7%

It can be observed that as the base chiller is downsized, the system has less capability to achieve effective precooling, i.e. to make use of the passive building thermal storage inventory. As the ice tank capacity is reduced, savings from active thermal storage inventory utilization is reduced.

4.12.5 Effect of Air-Side Economizer

Due to the existence of a temperature economizer, which adjusts fresh air flow rate by comparing the outdoor air temperature and return air temperature, nighttime ventilation can be used to increase the effect of passive thermal storage. Figure 35 a) and b) show the outdoor air flow rate compared with the total air flow rate and the chiller electrical consumptions under optimal control with and without economizer in the spring in Phoenix, AZ.

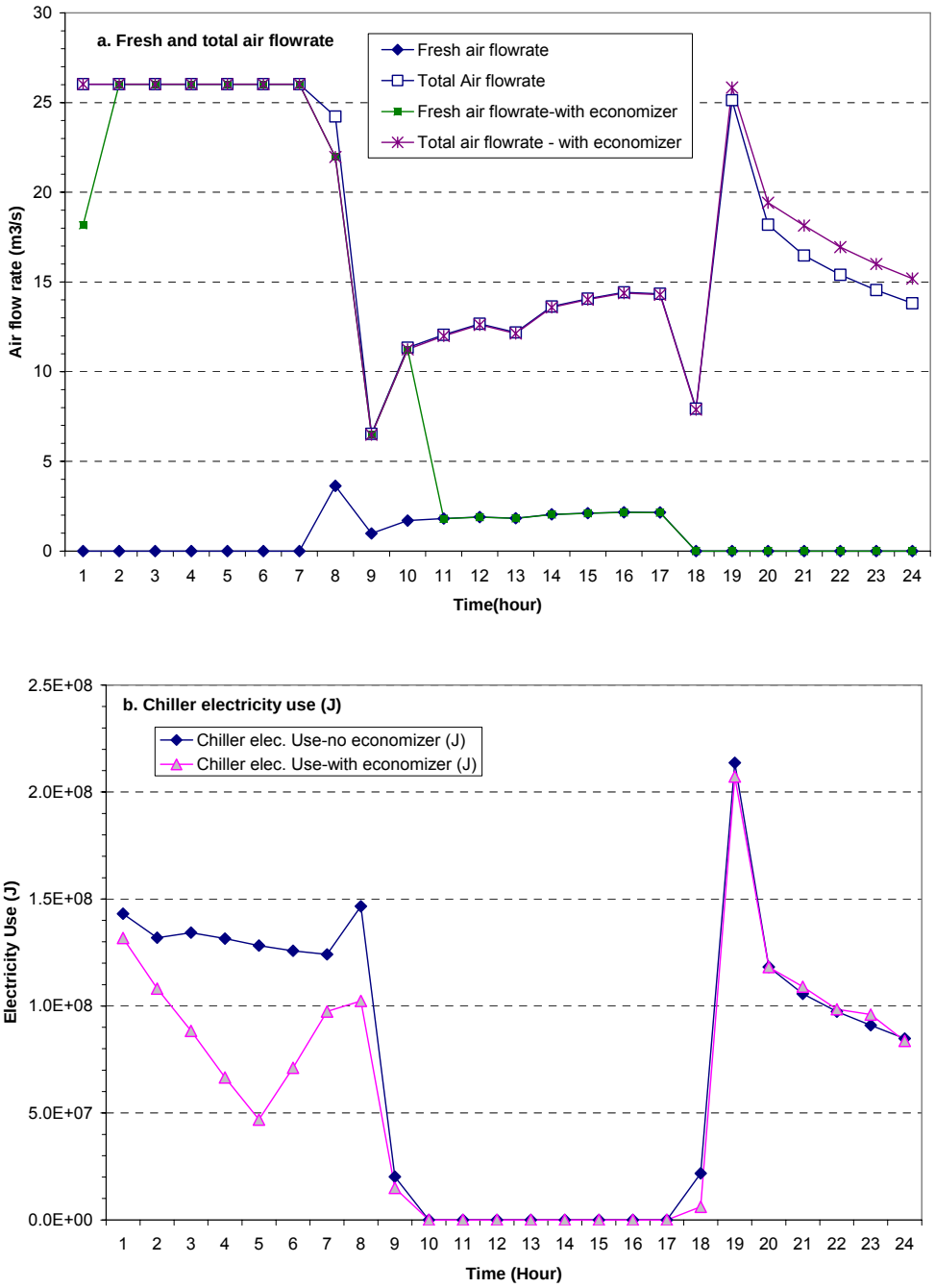

Figure 35: a) Air flow rate and b) electricity use profile of optimal combined thermal storage control with and without economizer

From Figure 35, it can be observed that in spring, since the night outdoor dry bulb temperature is lower than the returned air temperature, the economizer can take advantage of the cool ambient air to facilitate part of the precooling. Chiller cooling electricity use is saved. Table 30 summarizes the comparison of optimal combined thermal storage control with or without economizer.

Table 30: Summary of total costs of optimal combined thermal storage control with and without economizer for Phoenix, AZ

Economizer	Base	Optimization with Economizer		Optmization without Economizer	
	Total Cost ($)	Total Cost ($)	Savings	Total Cost ($)	Savings
Heavy Mass, Strong Incentive, Summer, Phoenix	815.6	677.93	-16.9%	678.09	-16.9%
Heavy Mass, Strong Incentive, Spring, Phoenix	732.28	601.14	-17.9%	623.52	-14.9%
Light Mass, Strong Incentive, Summer, Phoenix	819.88	692.14	-15.6%	692.14	-15.6%
Light Mass, Strong Incentive, Spring, Phoenix	736.96	631.99	-14.2%	639.79	-13.2%

From Table 30, it can be observed that in the summer, since the night outdoor dry bulb temperature is still high in Phoenix, the existence of economizer has no effect on reducing cooling costs; in spring, the night outdoor dry bulb temperature is lower than return air temperature, and optimal combined thermal storage control that takes advantage of cool nighttime air can therefore achieve higher savings.

4.13 Conclusions

A parametric analysis was conducted to assess the effects of building mass, utility rate, building location and season, thermal comfort, central plant capacities, and economizer on the cost saving performance of optimal control for active and passive building thermal storage inventory. The key findings are:

- Heavy-mass buildings, strong-incentive time-of-use electrical utility rates, and large on-peak cooling loads will likely lead to attractive savings resulting from optimal combined thermal storage control.
- By using an economizer to take advantage of the cool fresh air during the night, the building electrical cost can be reduced by using less mechanical cooling.
- Larger base chiller and active thermal storage capacities have the potential of shifting more cooling loads to off-peak hours and thus higher savings can be achieved.
- Optimal combined thermal storage control with a thermal comfort penalty included in the objective function can improve the thermal comfort levels of building occupants when compared to the non-optimized base case.

Field experimentation confirmed the influence of building mass on the passive storage performance and the benefits of using an air-side economizer as documented in Chapter 5. Future work is required to validate the findings with respect to thermal comfort.

4.14 References

[51] Zhou, G., M. Krarti, and G.P. Henze (2005) "Parametric Analysis of Active and Passive Building Thermal Storage Utilization." *Journal of Solar Energy Engineering,* Vol. 127, No. 1, pp. 37-46, American Society of Mechanical Engineers, New York, New York.

[52] EnergyPlus v1.1.1 (2003). EnergyPlus Documentation and Manuals, U.S. Department of Energy, also refer to http://www.eere.energy.gov/buildings/energy_tools/energyplus/

[53] P. Ihm, M. Krarti, and G.P. Henze (2003). "Integration of a Thermal Energy Storage Model within EnergyPlus", Proceedings of the *Eighth International IPBSA Conference Building Simulation 2003*, pp. 531-538, Eindhoven, Netherlands.

[54] ASHRAE Handbook of Fundamentals, (2001), Chapter 8 Thermal Comfort, American Society for Heating, Refrigerating and Air Conditioning Engineers, Atlanta, GA.

[55] Henze, G.P., D. Kalz, S. Liu, and C. Felsmann (2005) "Experimental Analysis of Model-Based Predictive Optimal Control for Active and Passive Building Thermal Storage Inventory." International Jour-

nal of HVAC&R Research, Vol. 11, No. 2, pp. 189-214, American Society of Heating, Refrigerating, and Air-Conditioning Engineers, Atlanta, Georgia.

Phase 2: Laboratory Testing at the Larson HVAC Lab

4.15 Description of the Larson HVAC Laboratory

The Larson Building System Laboratory at the University of Colorado at Boulder shown in Figure 36 is a unique facility in the HVAC industry in that it permits the study of entire HVAC systems in a controlled dynamic environment, providing repeatable test conditions that have been heretofore unavailable. It is used for educational and research purposes and is designed for dynamic testing of complete and full-scale commercial HVAC and building systems. The facility consists of a full-size commercial HVAC system, four representative commercial building zones, a system for producing repeatable and controllable loads on the HVAC system, and sophisticated data acquisition and control systems. Activities at the laboratory include evaluation and testing of control algorithms and hardware for HVAC components and systems, interactions between multiple control functions of HVAC systems, the dynamic interactions between building thermal response and HVAC system controls, ventilation control for indoor air quality, and HVAC system diagnostics.

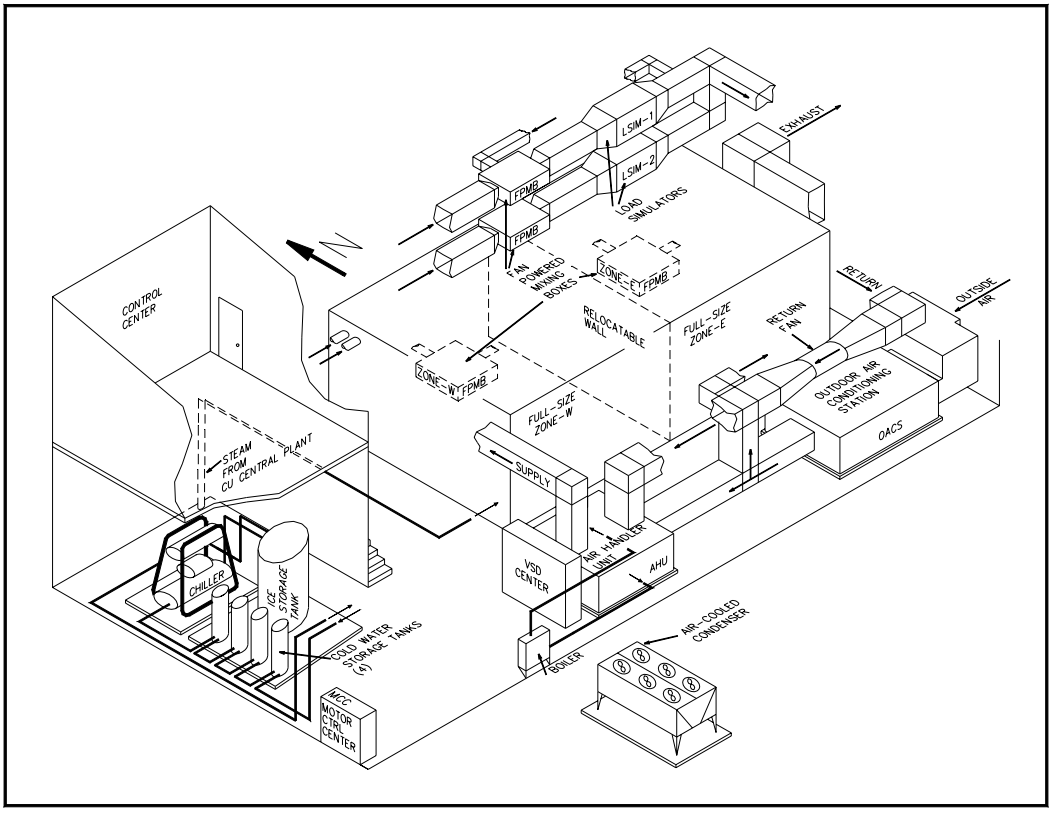

Figure 36: Isometric View of Larson Laboratory at the University of Colorado

The laboratory has been designed for maximum flexibility to encourage a wide variety of research and testing programs. In particular, both the HVAC and control systems in the laboratory are re-configurable in that components, subsystems or entire systems can be readily installed, tested, and modified.

The main HVAC system of the laboratory consists of a 12,000 cfm air-handling unit that is connected to four building zones by variable-air-volume (VAV) fan powered mixing boxes. To provide cooling to the four zones, a chiller, rated at 265 kW (75 tons) cooling capacity comprised of two screw-type compressors, is available within the lab. Continuous capacity control is provided down to 10% of rated capacity. This chiller, a 2.2 kW (3 hp) constant-volume pump, and a 668 kWh (190 ton-hour) ice storage tank are incorporated into a primary loop. A separate constant-volume 2.2 kW (3 hp) pump circulates water through a secondary loop to the zone simulators and the two air-handling units. The chilled water loop contains 25% glycol brine and allows

the primary loop to operate at temperatures as low as -5°C. The ice storage tank will be used to provide chilled water to the air-handling unit.

The entire lab is controlled using programmable direct digital control (DDC). The DDC system uses electronic actuators for damper and valve control, all of which accept standard analog control signals. The system employs laboratory-grade instrumentation for accurate control. All the control strategies to be tested in this project can be easily programmed using this DDC system. The data acquisition can accommodate up to 300 data channels. Data collected include temperature, humidity, pressure, flow rate, fan speed, and electric power consumption. The accuracy measurements meet or exceed all relevant ASHRAE/ASTM standards.

4.16 Description of the Experiments

The experiments focus on lab validation of optimal control of active and passive building thermal storage inventory in a light-mass building as represented by the Larson HVAC Laboratory at the University of Colorado at Boulder.

Experiments on passive-only, active-only and combined building thermal storage control were carried out and the results analyzed. Two electrical utility rates are studied: a strong incentive rate and a weak incentive rate. For the strong incentive rate, on-peak and off-peak energy charges are 0.20 $/kWh and 0.05 $/kWh respectively and demand charges are 20 $/kW and 5 $/kW respectively. In the weak incentive rate, on-peak and off-peak energy charges are 0.10 $/kWh and 0.05 $/kWh respectively and demand charges are 10 $/kW and 5 $/kW respectively. The results from experiment and simulation are discussed below.

4.17 Base Case

The building is occupied from 8:00-19:00, the on-peak period is 10:00-18:00 and the rest of the day is off-peak period. The two zone simulators (ZSIM1, ZSIM2) are conditioned to 75°F for 24 hours with internal loads schedules of 19 kW and 20 kW for 24 hours respectively. The two full size zones (FSZW, FSZE) are conditioned to 75°F during occupied period and allowed to float up to 105°F during unoccupied period. The peak internal loads of the two full size zones are 6 kW each zone. The internal loads are 30% peak load during 8:00-9:00, 12:00-13:00 and 18:00-19:00 and 50% peak load during 9:00-12:00 and 13:00-18:00. Simulated weather file of summer design day in Phoenix, AZ are successfully incorporated in the outside air conditioning station (OACS) as illustrated by Figure 37.

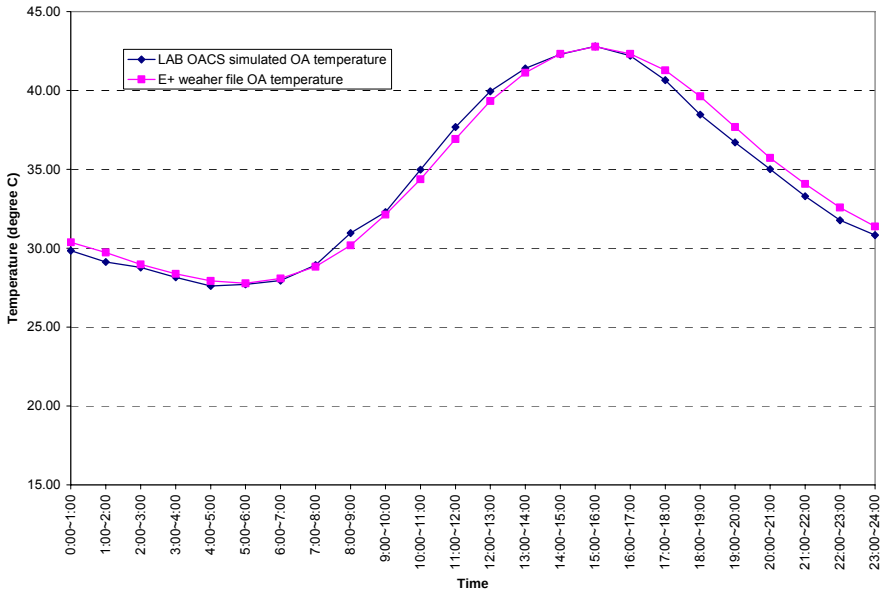

Figure 37: Simulation and measured outdoor air dry-bulb temperature profiles

Figure 38 shows the indoor air temperatures, and chiller power consumption profile comparison between experiment and simulation results. Excellent agreement between model and laboratory performance can be noted. The average error of simulation on chiller power consumption is 0.6%.

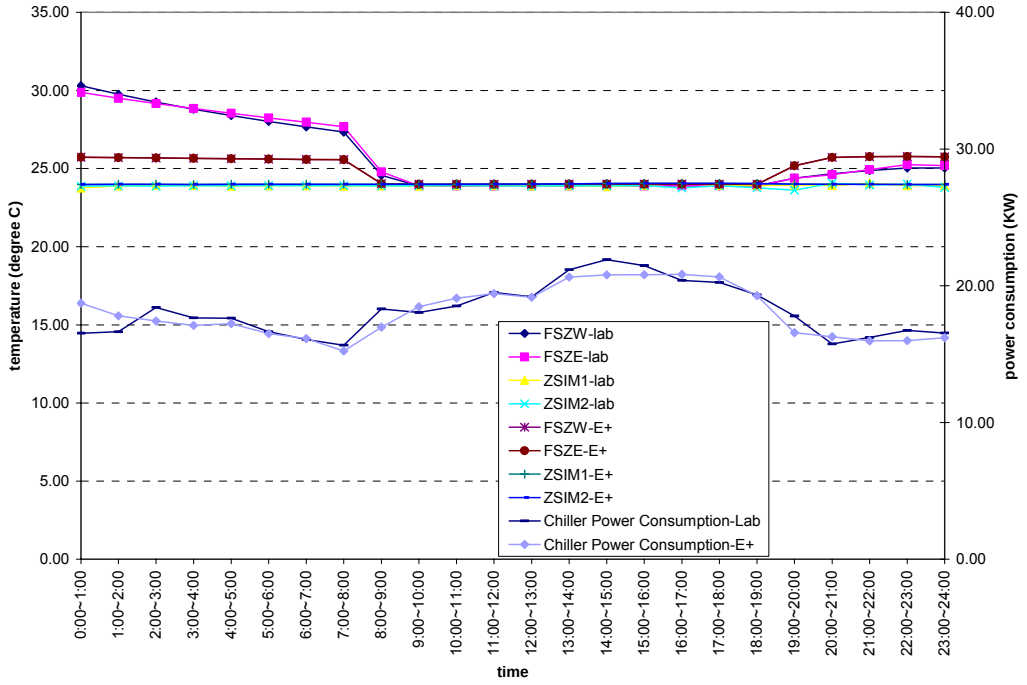

Figure 38: Simulated and measured zone air temperature and chiller power consumption profiles under base case control

4.18 Strong Incentive Utility Rate

4.18.1 Passive-Only (Nighttime Precooling)

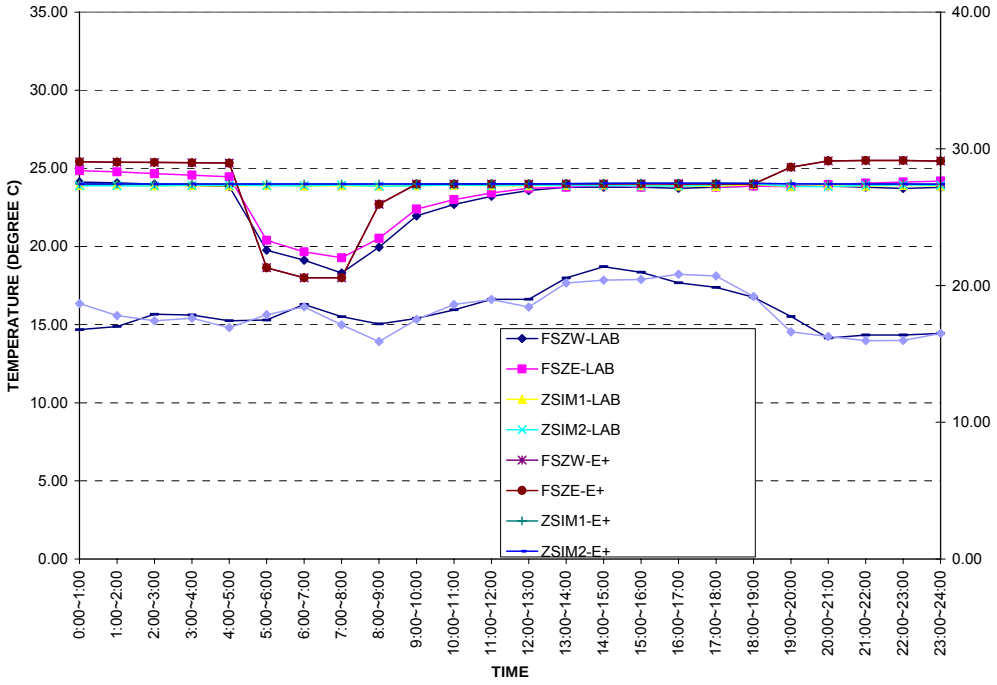

Figure 39: Simulated and measured zone air temperature and chiller power consumption profiles in passive-only optimal control under strong incentive utility rate

The optimal passive building thermal storage control suggests precooling the full-size zones to 18.3°C for 3 hours before occupancy then maintaining zone setpoint of 24°C. In the experiment and as expected, it is found that the zone temperature of the full-size zones does not drop to 18.3°C immediately. It takes about 2 hours to cool the zone to desired precooling temperature. Also, after precooling, the zone temperature rise more slowly than the simulation results. In general, the difference in chiller power consumption between experiment and simulation are within an acceptable range. The chiller consumes more power during 5:00-8:00 due to precooling and cooling energy costs are slightly lower than the base case.

4.18.2 Active-Only (Ice Storage)

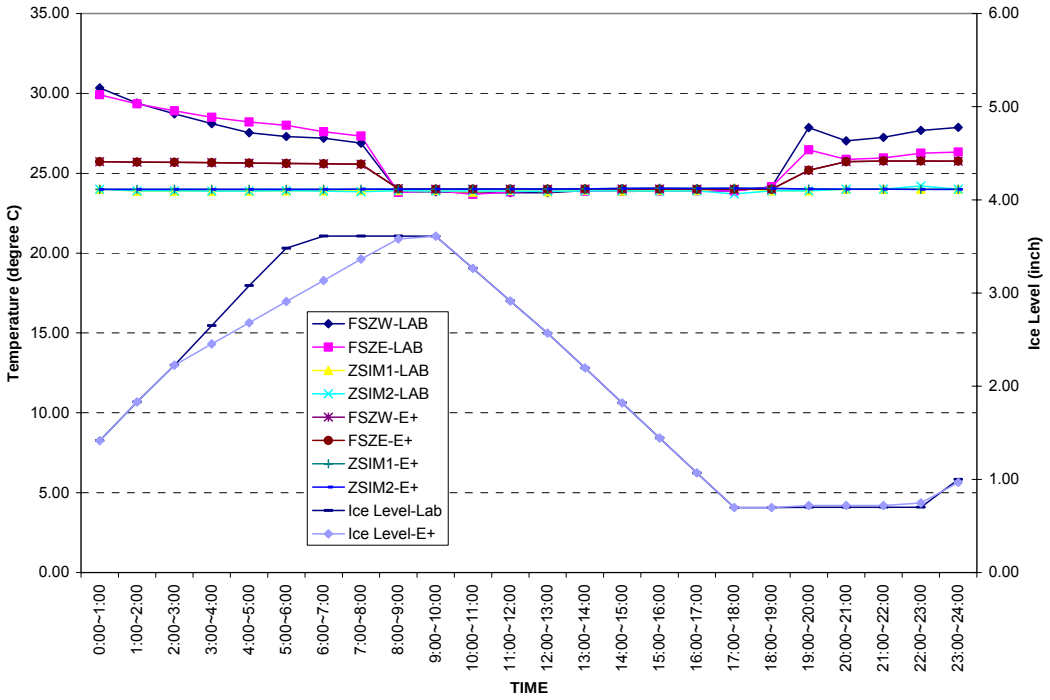

Figure 40: Simulated and measured zone air temperature and TES state-of-charge profiles of active-only optimal control under strong incentive utility rate.

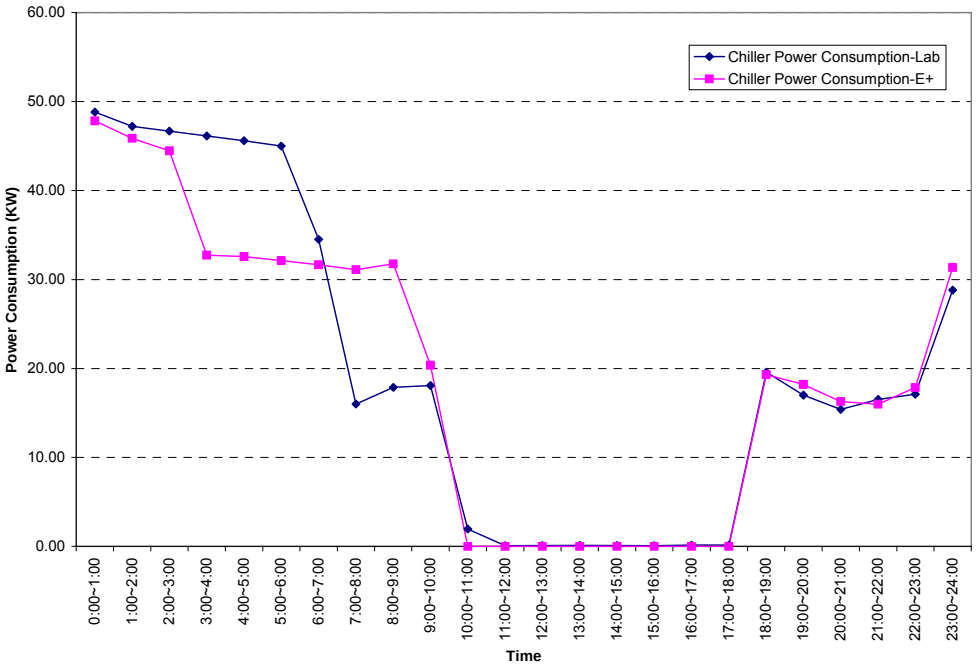

Figure 41: Simulated and measured chiller power consumption profiles in active-only optimal control under strong incentive utility rate

From Figure 40 and Figure 41, it can be observed that the simulated and measured TES state-of-charge profiles and chiller power consumption profiles display differences. This is due to the difficulty of controlling the TES charging process as accurately as the simulation because of the existence of constant speed pump and PID controlled valve as well as the nonlinear heat transfer characteristics of the active storage itself. In the experiment, only the initial and final ice level during charging and discharging process is controlled. Although the profiles reveal differences, the error of total power consumption and energy cost are 3% and 8%, respectively, and deemed as acceptable.

4.18.3 Combined Active and Passive Building Thermal Storage

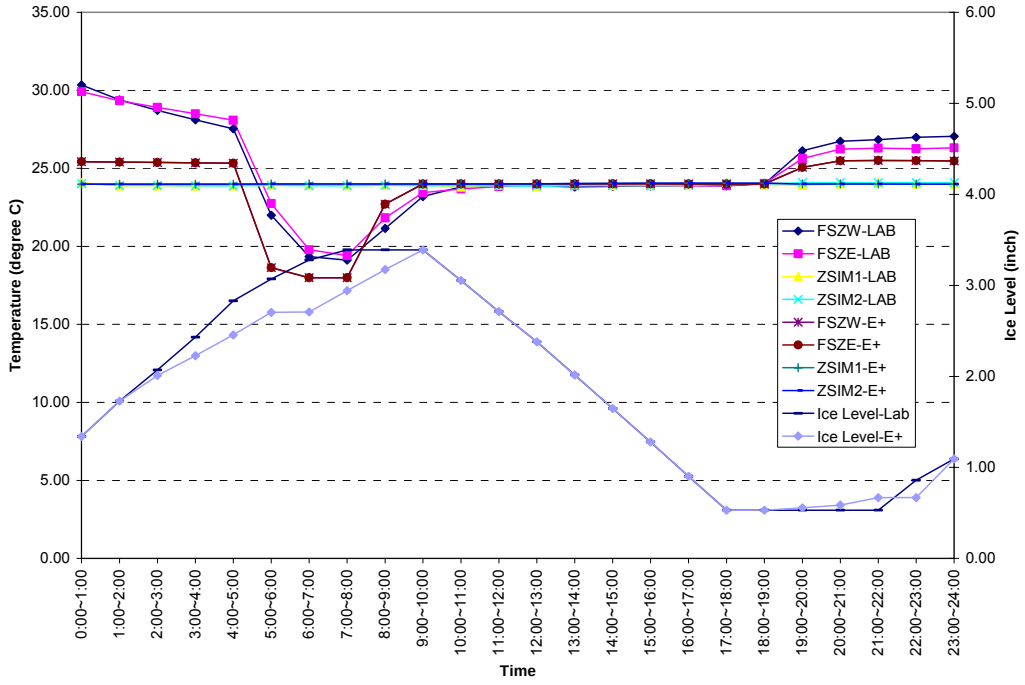

Figure 42: Simulated and measured zone air temperature and TES state-of-charge profiles in combined active and passive optimal control under strong incentive utility rate

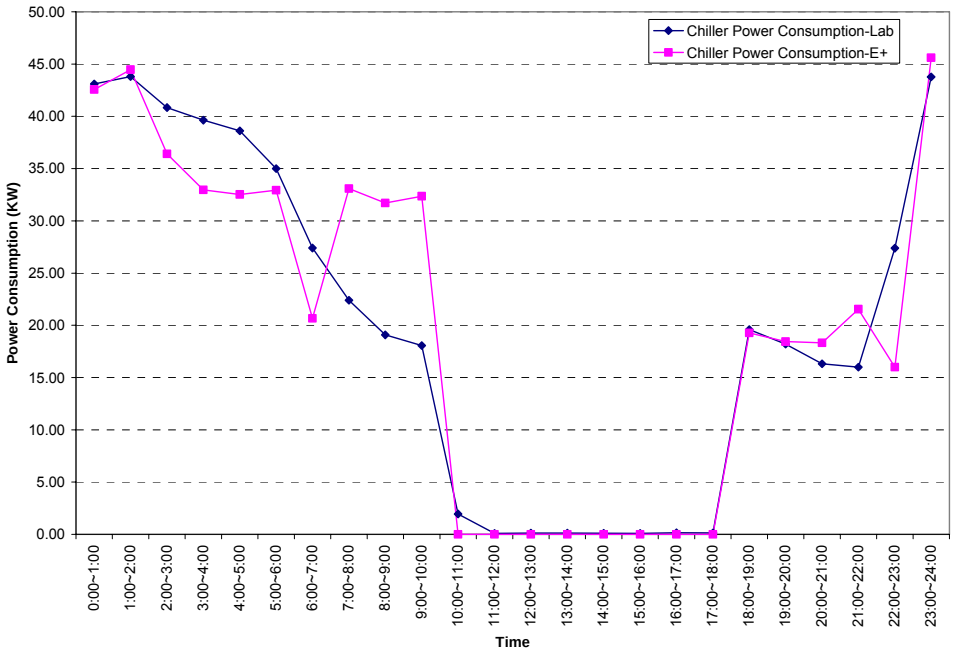

Figure 43: Simulated and measured chiller power consumption profiles in combined active and passive optimal control under strong incentive utility rate

The passive building thermal storage inventory is precooled to 18°C for 3 hours before occupancy and the ice tank is charged to from 1" to 3.4" inches of ice before the beginning of the on-peak period and discharged to 0.53" during the on-peak time and after that recharged to 1". The error of total chiller power consumption and energy costs are 1% and 3%, respectively.

4.19 Weak Incentive Utility Rate

4.19.1 Passive-Only (Nighttime Precooling)

The optimal control of passive building thermal storage under weak rate ratio is the same as that of intensive rate ratio in our case. Only the percentage of savings achieved is reduced. The error of total power consumption and energy costs are within 1%.

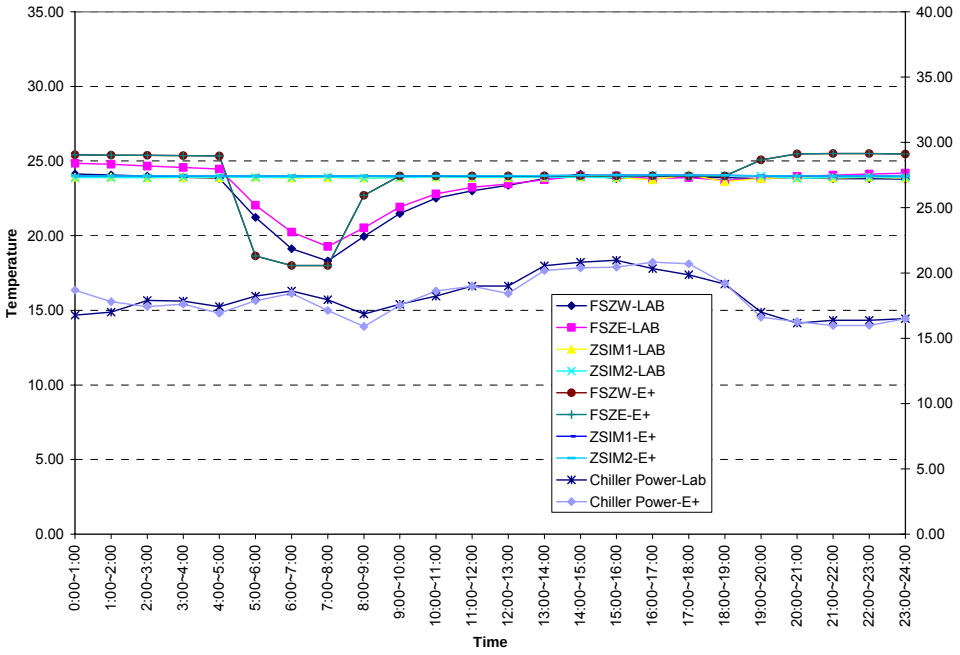

Figure 44: Simulated and measured zone air temperature profiles and chiller power consumption in passive-only optimal control under weak incentive utility rate

4.19.2 Active-Only (Ice Storage)

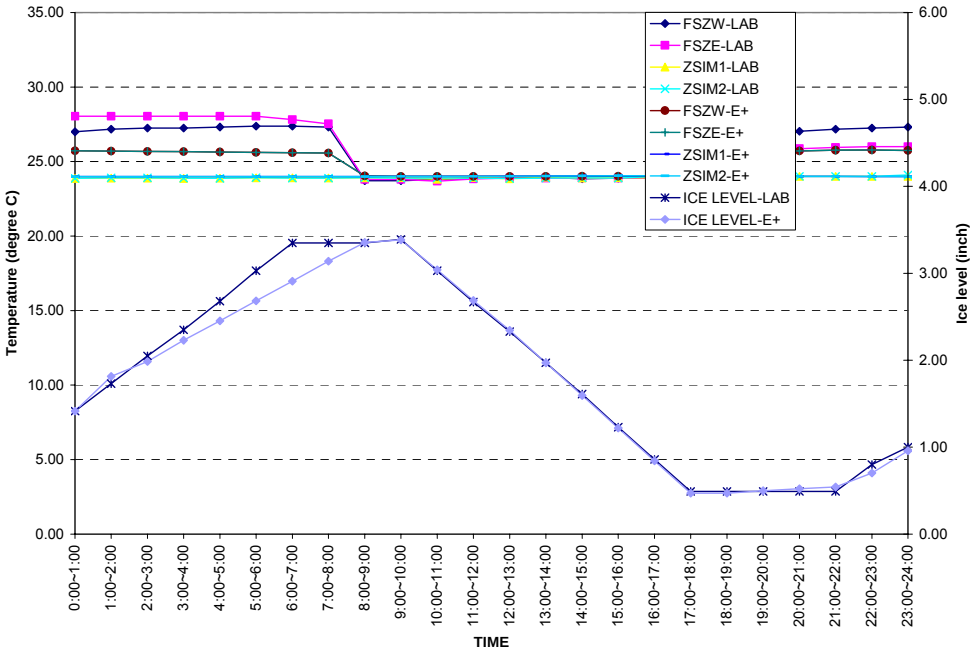

Figure 45: Simulated and measured zone air temperature and TES state-of-charge profiles in active-only optimal control under weak incentive utility rate

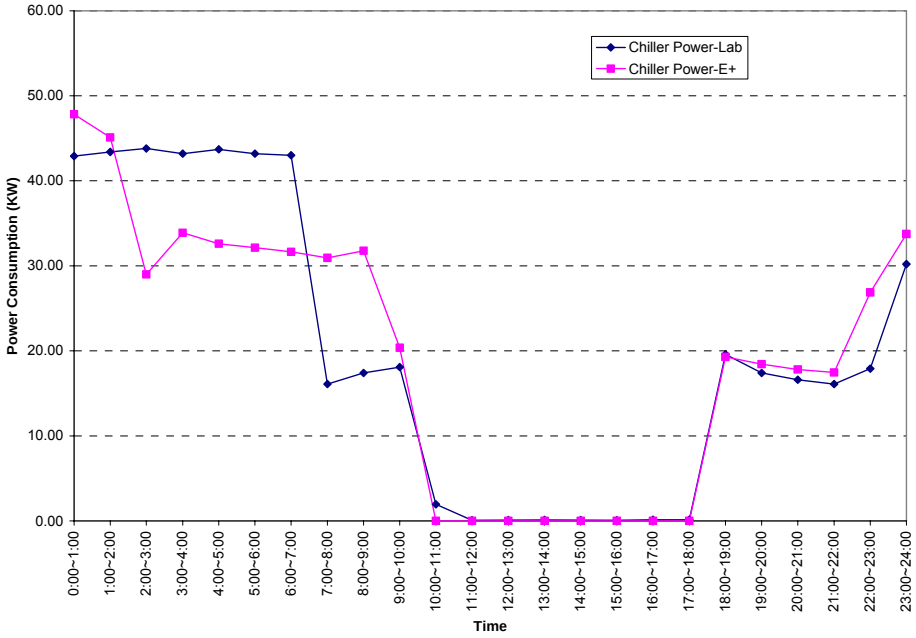

Figure 46: Simulated and measured chiller power consumption profiles in active-only optimal control under weak incentive utility rate

The ice tank is charged from 1" to 3.39" of ice level before occupancy and discharged to 0.5" of ice level during on-peak time and recharged to 1" in the night. The error of cost savings is within 1%.

4.19.3 Combined Active and Passive Building Thermal Storage

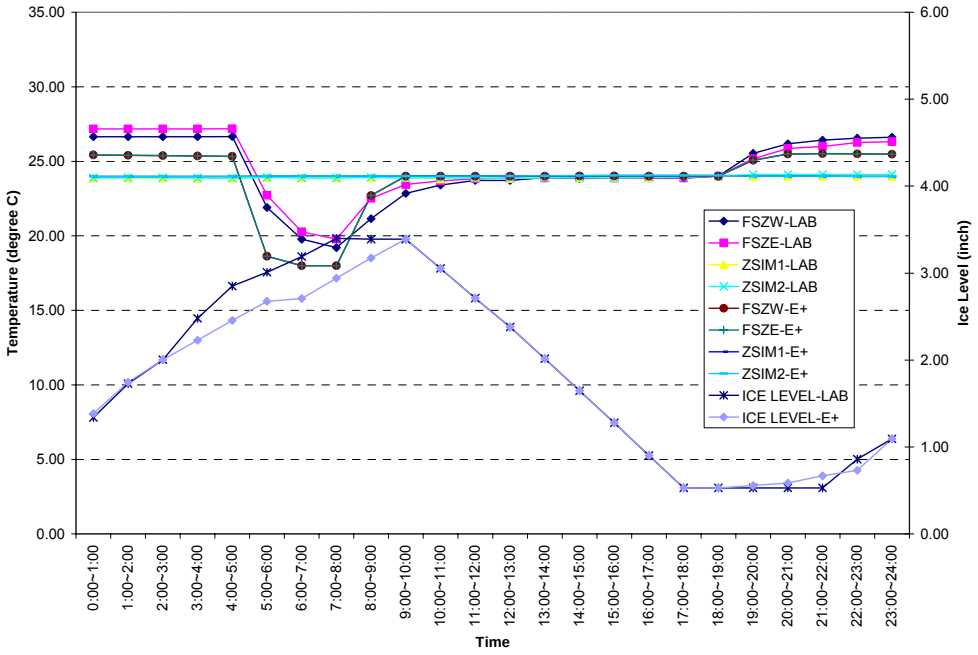

Figure 47: Simulated and measured zone air temperature and TES state-of-charge profiles in combined-TES optimal control under weak incentive utility rate

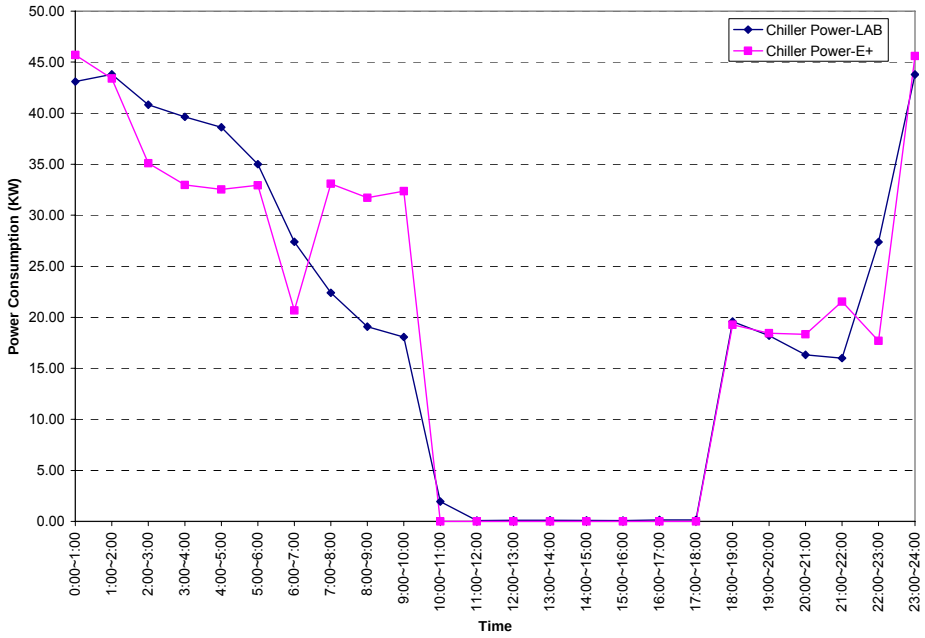

Figure 48: Simulated and measured chiller power consumption profiles in combined active and passive building thermal storage optimal control under weak incentive utility rate

4.20 Effect of night floating temperature

As can be seen from the previous figures, in some of the experiment, the nighttime floating temperature of the full size zones is different from that from simulation. This is mainly due to the fact that in some of the experiment, the lights in the full size zones are kept on during the night. In the morning, different zone temperature will affect the results of optimization.

Therefore, simulations were conducted to study the impact of nighttime zone floating temperature on optimization results. Figure 49 shows the zone temperature profiles and chiller power consumptions in two optimal controls with different initial zone temperatures. Table 31 shows the comparison of cost savings achieve under high and low initial temperatures.

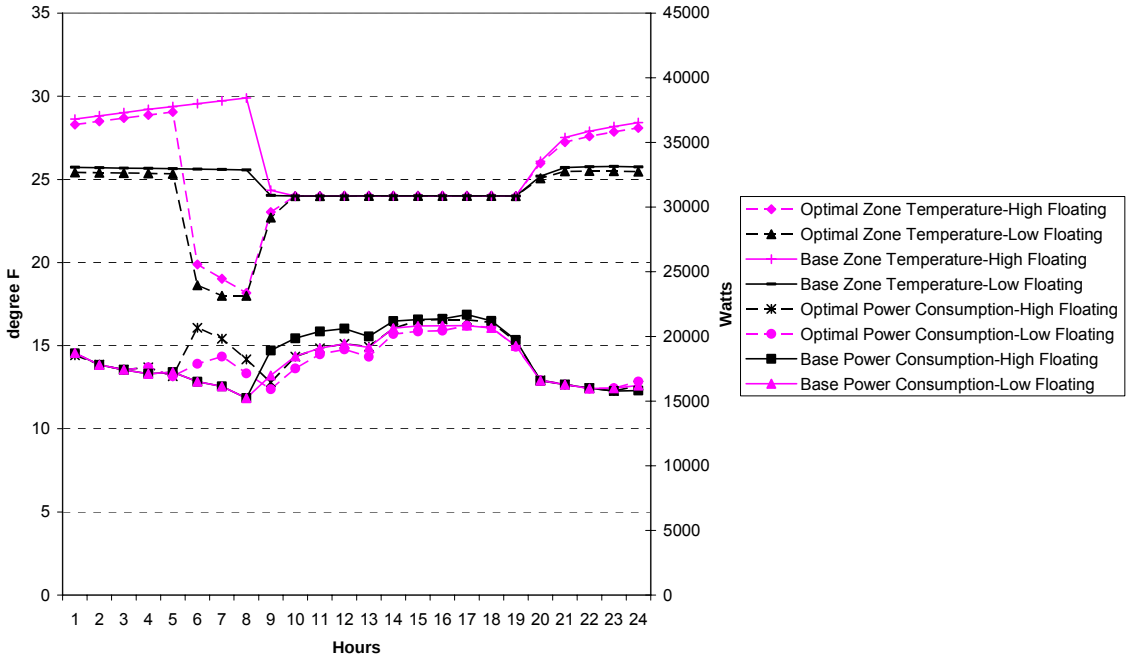

Figure 49: Zone temperature and chiller power consumption profiles under different nighttime floating temperatures for light mass with strong incentive utility rates.

Table 31: Comparison of Cost Saving Achieved by Optimal Control of Passive TES under High and Low Floating Temperature

		Hight Floating Temperature	Low Floating Temperature
Base Case	Power Consumption (KWH)	442.79	433.33
	Cooling Costs ($)	144.34	141.15
Optimal Passive TES Control	Power Consumption (KWH)	445.59	434.48
	Cooling Costs ($)	143.85	140.91
	Cost Savings	-0.34%	-0.17%

From Figure 49, it can be seen that, by leaving the lights in the full size zones on, the floating temperature in the morning before occupancy can be 5°F higher than leaving the lights off. With higher starting temperature in the morning, more cooling power is consumed in order to keep the zone at a comfort level. But since the building mass is very light, the impact of morning zone floating temperature does not affect the optimal control. In both cases, the optimal control of passive TES suggests to cool the zone to 18°C for 3 hours before occupancy. In terms of cost savings, both cases save within 0.5% due to the light mass.

4.21 Summary

The power consumption and cooling cost savings are summarized below.

Table 32: Comparison of Simulation and Measured Results

		Rate Ratio 4:1		Rate Ratio 2:1	
		Lab	E+	Lab	E+
Base Case	Cooling Energy Use (KWH)	436.41	433.33	436.41	433.33
	Cooling Cost ($)	64.01	62.98	40.47	39.89
Passive Only	Cooling Energy Use (KWH)	437.08	434.48	436.53	434.48
	Cooling Cost ($)	63.18	62.59	39.94	39.79
	Savings	**-1.31%**	**-0.62%**	**-1.29%**	**-0.25%**
Active Only	Cooling Energy Use (KWH)	483.07	469.41	475.33	468.82
	Cooling Cost ($)	34.00	31.44	31.85	31.41
	Savings	**-46.88%**	**-50.08%**	**-21.28%**	**-21.27%**
Combined	Cooling Energy Use (KWH)	471.97	478.89	471.97	481.33
	Cooling Cost ($)	32.61	31.55	31.69	31.68
	Savings	**-49.05%**	**-49.91%**	**-21.70%**	**-20.58%**

From Table 32 it can be observed that the EnergyPlus simulation is a surprisingly accurate prediction of the experiment. Therefore, actual savings of building energy costs can be expected by applying optimal controls from simulation results. However, it can also be concluded that the Larson HVAC Laboratory has only marginal passive building thermal storage inventory and is therefore not representative of a heavy-mass commercial building.

4.22 Uncertainty Analysis

An uncertainty analysis is performed for the active storage (ice-based TES) charging/discharging heat transfer rate. It is a function of the measured independent parameters, i.e. ice tank inlet/out let temperature and ice tank flow rate.

$$\dot{Q} = A\rho\dot{V}C_p(T_{outlet} - T_{inlet})$$

where,

A is a conversion factor, A=6.667e-4 (ft^3/gal)(min/hr)(ton-hr/Btu),

ρ_{brine} is the density of the brine, ρ_{brine}= 65 lbm/ft^3,

C_p is the specific heat of the brine, $C_{p,brine}$=0.85 Btu/lbm/°F,

$\dot{V}$ is the volumetric flow rate of the brine, $\dot{V}$ =105 gal/min,

T_{inlet} is the ice tank inlet temperature, T_{inlet} = 25°F,

T_{outlet} is the ice tank outlet temperature, T_{outlet} = 30°F.

Measurement errors for the density and specific heat properties of the brine are neglected.

The ice tank flow rate measurement has an absolute precision of 0.3 gal/min and an absolute bias of 0.9 gal/min. The temperature measurements have absolute precisions of 0.2°F and absolute biases of 0.3°F.

Since,

$$\theta_{\dot{V}} = \frac{\partial \dot{Q}}{\partial \dot{V}} = A\rho C_p(T_{outlet} - T_{inlet})$$

$$\theta_{T_{inlet}} = \frac{\partial \dot{Q}}{\partial T_{inlet}} = -A\rho C_p\dot{V}$$

$$\theta_{T_{outlet}} = \frac{\partial \dot{Q}}{\partial T_{outlet}} = A\rho C_p \dot{V}$$

$$B_{\dot{Q}} = [(\theta_{\dot{V}} \times B_{\dot{V}})^2 + (\theta_{T_{inlet}} \times B_{T_{inlet}})^2 + (\theta_{T_{outlet}} \times B_{T_{outlet}})^2]^{1/2}$$

$$S_{\dot{Q}} = [(\theta_{\dot{V}} \times S_{\dot{V}})^2 + (\theta_{T_{inlet}} \times S_{T_{inlet}})^2 + (\theta_{T_{outlet}} \times S_{T_{outlet}})^2]^{1/2}$$

The absolute bias, relative bias, absolute precision and relative precision of heat transfer rate can now be calculated.

The uncertainty is obtained by combining the absolute precision index and the absolute bias limit, using the additive (ADD) or the root-sum-square (RSS) models for 99% and 95% of coverage respectively.

$$U_{ADD} = (B_{\dot{Q}} + st \times S_{\dot{Q}})$$

$$U_{RSS} = [B_{\dot{Q}}^2 + (st \times S_{\dot{Q}})^2]^{1/2}$$

The student factor, *st*, is used calculate the precision uncertainty and is based on the number of observations per sample, also known as the degrees of freedom. For this case, the number of observation was obtained by dividing average time interval (5 minutes) by the time-step of the readings (10 seconds). The degree of freedom is calculated by:

$$v = \left(\frac{5\,\text{min}}{10\,\text{sec}} \times 60\,\text{sec/min}\right) - 1 = 29$$

Therefore, the measured reading is 19.98 ton ±1.7 ton with 95% coverage, with a 8.3% of relative uncertainty.

5 Phase 3: Field Testing at the ERS in Ankeny, IA

5.1 Review of Past Work

Cooling of commercial buildings contributes significantly to the peak demand placed on an electrical utility grid. Time-of-use electricity rates encourage shifting of electrical loads to off-peak periods at night and weekends. Buildings can respond to these pricing signals by shifting cooling-related electrical loads either by precooling the building's massive structure, by the use of an active energy storage system only, or by a combination of both thermal reservoirs. Henze et al. (1997) [58] developed a predictive optimal controller for active thermal energy storage (TES) systems and investigated the potential benefits of optimal control for ice storage systems under real-time pricing in order to minimize the cost of operating a central cooling plant. It was found that in the presence of complex rate structures, i.e., real-time pricing rates that change on an hourly basis, the proposed optimal controller has a significant performance advantage over conventional control strategies while requiring only simple predictors.

Braun (2003) [57] surveyed research on passive building thermal storage utilization, i.e., the precooling of a building's thermal mass during nighttime in order to shift and reduce peak cooling loads in commercial buildings. He identified considerable saving potential for operational costs, even through the total zone loads may increase. Opportunities for reducing operating expenses are due to four effects: reduction in demand costs, use of low cost off-peak electrical energy, reduced mechanical cooling resulting from the use of cool nighttime air for ventilation precooling, and improved mechanical cooling efficiency due to increased operation at more favorable part-load and ambient conditions. However, these benefits must be balanced with the increase in the total cooling requirement that occurs with the precooling of the thermal mass. Therefore, the savings associated with load shifting and demand reduction are very sensitive to utility rates, building and plant characteristics, weather conditions, occupancy schedules, operation condition, the method of control, and the specific application. In general, better opportunities for effective precooling exist for higher ratios of on-peak to off-peak rates, longer on-peak periods, heavy-mass building construction with a small ratio of the external area to the thermal mass, and for cooling plants that have a good part-load characteristics for which the best performance occurs at about 30% of the design load.

The *combined* usage of both active and passive building thermal storage inventory under optimal control has recently been investigated by Henze et al. (2004a) [59] and documented in Chapter 2 for the reduction of electrical utility cost in the context of common time-of-use rate differentials. The objective function used in the optimization is the total utility bill including the cost of heating and a time-of-use electricity rate without demand charges. The analysis showed that when an optimal controller for combined utilization is given perfect weather forecasts and when the building model used in the model-based predictive control perfectly matches the actual building, the utility cost savings are significantly greater than either storage, but less than the sum of the individual savings and the cooling-on-peak electrical demand can be drastically reduced.

While Chapter 2 established the theoretical maximum performance of this novel control strategy, subsequent research by Henze et al. (2004b) [60] as documented in Chapter 3 explored how strongly prediction uncertainty in the required short-term weather forecasts affects the controller's cost saving performance. The best prediction accuracy was found for a bin model that develops a characteristic daily profile from observations collected over the past 30 or 60 days. Assuming that the building thermal response is perfectly represented by the building model, i.e., there is no mismatch between the modeled and actual building behavior, the predictive optimal control of active and passive building thermal storage inventory involving weather predictions lead to utility cost savings that are only marginally inferior compared to a hypothetical perfect predictor that exactly anticipates the weather during the next planning horizon. The primary finding is that it takes only very simple short-term prediction models to realize almost all of the theoretical potential of this storage control technology.

Liu and Henze (2004) [61] as documented in Chapter 4 investigated the impact of five categories of building modeling mismatch on the performance of model-based predictive optimal control of combined thermal storage using perfect prediction. It was found that for an internal heat gain dominated commercial building, the deviation of building geometry and zoning from the reference building only marginally affects the optimal control strategy; reasonable simplifications are acceptable without loss of cost saving potential. In fact,

zoning simplification may be an efficient way to improve the optimizer performance and save computation time. The mass of the internal structure did not strongly affect the optimal results; however, it did change the building cooling load profile, which in turn will affect the operation of the active storage (TES) system. Exterior building construction characteristics were found to impact building passive thermal storage capacity. Thus, it is recommended to make sure the construction material is well modeled. Furthermore, zone temperature setpoint profiles and TES performance are strongly affected by mismatches in internal heat gains, thus efforts should be made to keep the internal gain mismatch as small as possible. Efficiency of the building energy system has no direct impact on the building cooling load, but it affects both, zone temperature setpoints and active TES operation because of the coupling to the cooling equipment. Mismatch in this category may be significant.

On the background of these findings, a predictive optimal controller for the combined usage of active and passive thermal storage that accounts for uncertainty in predictive variables and model mismatch was developed and verified in the context of the presented work. Once the supervisory controller was implemented in the laboratory setting, the test facility was controlled by the optimizer in real-time, which to the authors' knowledge has not been done before. This topical report describes the implementation of the real-time control strategy and evaluates its benefits with respect to HVAC energy consumption and cost reduction. In addition, model accuracy and constraint compliance will be examined. The report concludes with a recreation of the experiment in a simulation environment during which previously experienced problems such as the interruption of the communication to the building automation system were avoided.

5.2 Description of Test Facility

5.2.1 General Background on the ERS

The building used in this study to investigate the potential of the optimal controller is the Energy Resource Station (ERS); operated by the Iowa Energy Center (IEC). The ERS is a unique demonstration and test facility wherein laboratory-testing capabilities are combined with real building characteristics. The ERS is capable of simultaneously testing two full-scale commercial building systems side-by-side with identical thermal loading. Located on the campus of the Des Moines Area Community College (DMACC) in Ankeny, Iowa; it has a latitude of 41.7° North, a longitude of 93.6° West, and an elevation of 286 m above sea level. The facility is orientated for a true north/south solar alignment and no surrounding objects and no trees block solar radiation on the ERS, except for the north side of the building that has a fenced in mechanical yard with a concrete floor.

The ERS building, a single story structure with a concrete slab-on-grade, has a height of 4.6 m and a total floor area of 855 m^2, divided into a general area (office space, service rooms, media center, two classrooms, etc.), and two sets of identical test rooms, labeled '*A*' and '*B*'; adjacent to the general area. The eight test rooms are organized in pairs with three sets of zones having one exterior wall (east, south, and west) and one set that is internal. Figure 50 presents a layout or the ERS including the four sets of identical test rooms used for the experiment.

The opaque exterior envelope of the ERS is composed of several layers of construction materials with a thermal mass outside of the insulation. The percentage of the window area to exterior wall area is 15% on the east side, 16% on the west side, 32% on the south, and no windows on the north (Price and Smith, 2000) [63].

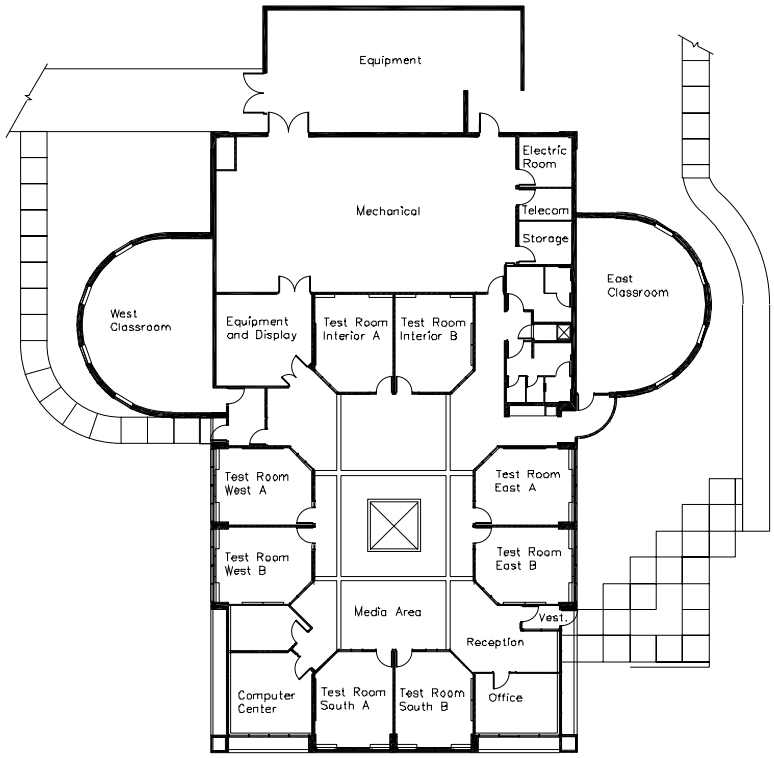

Figure 50: Layout of the test facility, the Energy Resource Station (ERS), Ankeny Iowa.

5.2.2 Primary and Secondary HVAC Systems

The ERS is equipped with a central heating plant consisting of a natural gas-fired boiler and a cooling plant comprising three nominal 35 kW air-cooled chillers for both chilled-water and ice-making modes. The chilled-water loop is filled with 22% propylene glycol water solution. In addition, the building includes a 440 kWh internal melt ice-on-tube thermal energy storage tank as well as pumps and auxiliary equipment needed to provide cooling. District cooling can be provided by the DMACC campus chilled water plant but was not used in this experiment. Hence, several modes of operation between these sources of cooling are possible in order to supply chilled water to the air handling units (AHU). The chilled water loop is a primary-secondary flow arrangement with dedicated constant-volume chiller pumps and secondary variable-flow distribution pumps in the AHU loop under VFD control.

The secondary HVAC system consists of three AHUs that condition the building: Test rooms A and B are served by two similar single-duct VAV with reheat AHU systems A and B, and the general area is served by a similar but larger AHU-1. An overhead air distribution system utilizing pressure-independent VAV boxes supplies air to each test room using hydronic or 3-stage electrical resistance reheat.

Finally, there is an on-site weather station with measurements of outdoor air dry-bulb temperature, relative humidity, wind speed and direction, atmospheric pressure, total normal incidence solar flux, and global horizontal solar flux.

5.2.3 Investigated Test Rooms

The experiment was executed in the test rooms A and B, each with a net floor area of 24.8 m^2 and carpeted floor. The ceiling height is 2.6 m and there is a plenum above the suspended ceiling with a height of 1.7 m. Having the same geometry and construction specifications, but being thermally isolated from each other; the identical pairs A and B experience the same heating and cooling load. The window area of the exterior zones consists of double-pane 6.4 mm clear insulating glass and measures 6.9 m^2. During the test, these windows were covered with fully open external blinds. Furthermore, to reduce thermal coupling to the general area,

the interior windows between the test rooms and the general area were covered with 12.7 mm dry wall paper. Following the suggestion of Braun et al. (2002) at the ERS, additional mass was added to the interior test rooms A and B in the form of two rows of standard concrete cinder block, 3.05 m long and each stacked three layers high. The walls were located near the middle of each interior room.

The rooms are unoccupied; however, false internal heat gains can be introduced using baseboard heaters and lights to simulate the occupancy schedule of a typical building. Test rooms A are equipped with 2-stage lighting whereas test rooms B are fitted with dimming electronic ballasts, both with a maximum wattage of 585 W. The baseboard heater at each zone can operate at two stages with a maximum output of 1.8 kW (900 W per stage).

A comfort sensor measuring the air temperature, humidity, and wind speed was placed in the middle of the rooms. Conditioned air at a temperature of 13°C was supplied to the test rooms by two ceiling mounted diffusers in order to maintain the room temperature within a range of 20°C and 24°C during time of occupancy. The interior flow rate throughout the occupied period was characterized by a minimum flow of 94 L/s and a maximum flow of 189 L/s. Finally, all test rooms were kept locked throughout the period of the experiment in order to avoid disturbance and interruptions. These conditions were applied to all eight test rooms.

The ERS is not a particular good candidate for the use of building thermal mass as documented by Braun (2003) due to two reasons: (i) it is a light-weight single-story structure with a high exterior surface area to volume ratio and (ii) significant thermal coupling with the ground, the ambient and the zones adjacent to the test rooms is present. Furthermore, the test zones are not equipped with a representative amount of furniture and the floor is carpeted, which reduces thermal coupling to the massive structure.

5.2.4 Assumptions for Predictive Optimal Control

The simulated occupied period extends from 8 a.m. to 5 p.m. each day including weekends. During this time, baseboard heaters are applied at one stage (0.9 W) and they are turned off during the remaining hours. Furthermore, one stage of lighting (360 W) is employed from 7 a.m. to 6 p.m. The applied utility rate structure assumes an on-peak electricity rate of $0.20/kWh from 9 a.m. to 7 p.m. and an off-peak electricity rate of $0.05/kWh the remaining hours. Demand charges are not levied.

Of the available equipment, the HVAC system during the test consists of two chillers, namely a main and a dedicated precooling chiller, and the ice-based TES system. The main chiller that is responsible for charging the TES tank and meeting on-peak cooling loads operates in the chilled-water mode with a coefficient-of-performance (COP) of 2.1 and in the ice-making mode (charging the TES) with a COP of 2.4. The COPs were validated through repeated tests at the ERS. Consequently, meeting cooling loads through the usage of ice storage is more attractive from an energy consumption perspective than standard chilled-water operation.

Initial tests investigating conventional control strategies revealed that charging of the TES system takes noticeably more time than estimated by the controller, which was traced back to a significantly reduced chiller capacity to only 50% in the ice-making mode. Further, it was determined that the ice storage system behaves very nonlinearly below 20% and above 90% state-of-charge (SOC). Since the model employed in the predictive optimal control assumes a linear change in SOC with the charging and discharging rates, the SOC was limited to an available range of 25% to 75%, effectively cutting the storage capacity in half to 220 kWh.

The dedicated precooling chiller with a measured COP of 3.4 is assigned to flush the building with cool air during nighttime and, consequently, to precool the building's massive structure and furniture. Both chillers cannot simultaneously supply chilled water to the AHU.

The outdoor air ventilation is governed by a return air temperature economizer that allows for free cooling when the ambient air conditions are favorable. The minimum outdoor intake damper is restricted to a position of 45% open for AHU A and 37.5% open for AHU B to ensure 20% of ventilation air at design air flow conditions.

Simulations and experiments in the same facility conducted by Braun et al. (2002) revealed that there exists significant thermal coupling between the test rooms and the adjacent general area. As a result, there would be significant energy transfer between zones when utilizing different zone temperature strategies. Therefore, the decision was made to control the entire facility with a uniform schedule for occupancy and a similar con-

trol strategy. As a result, the evaluation of optimal and conventional control strategies is accomplished by comparing measured results under optimal control and simulated results using conventional control and not by comparing measured results from test rooms A under optimal and test rooms B under conventional control.

The general area was conditioned with 13°C supply air from 7 a.m. to 5 p.m. with a zone temperature set-point of 22°C. During unoccupied periods, temperatures were allowed to flow. Outside air intake was controlled by an economizer, restricting the minimum damper position to 10%.

It was verified by ERS personnel that all sensors were sufficiently calibrated and over 750 monitoring points at minute-by-minute intervals were recorded during the experiments.

5.3 Description of Implemented Predictive Control Strategy

5.3.1 Overview

In this study we employed a sequential approach to model-based control: 1) short-term forecasting, 2) optimization, and 3) post-processing and control command implementation as shown in Figure 51. A real-time weather station provides the current weather data to the short-term weather predictor. This predictor provides an improved forecast for the next planning horizon to the optimal controller, which adjusts the control variables in the model according to Figure 53 until convergence is reached. The optimal solution is passed to a post-processor that interprets the optimal results and turns them into commands understood by the building automation system of the facility under control. The building is modeled in TRNSYS (2003) [64], while the general purpose technical computing environment Matlab (2000) [62] including the optimization toolbox was used to interface with the building simulation program.

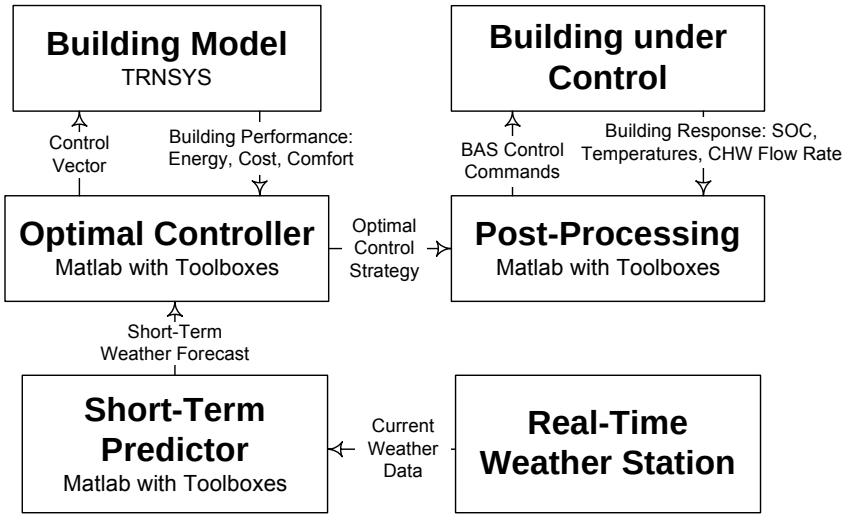

Figure 51: Real-time predictive optimal control schematic.

5.3.2 Prediction

A 30-day bin predictor model was found to provide the most accurate weather forecasts for a range of models tested in Chapter 3. The predicted variables include ambient air dry-bulb temperature, relative humidity, global solar radiation, and direct normal solar radiation. The assumption underlying the prediction procedure is that the actual time series will exhibit a behavior similar to a reference pattern, developed by rendering bin estimates. For a planning horizon of L = 24 hours, the bin model develops the characteristic profile on the basis of observations collected over the past 30 days. The forecast is made by shifting the L-hour profile such that the predicted value for the current hour k^* coincides with the actual measured value by the weather station at the ERS. Hence, the forecast bin values are computed from

$$\left\{\hat{X}_t\right\} = \frac{1}{d}\sum_{n=1}^{d} X_{t-24n}, \quad t \in [k^*, k^* + L], \tag{27}$$

where d is the number of past days used to compute the bins, and X_t is the observed variable. The 24-hour forecast is handed over to the optimal controller that uses these values among others to estimate the building cooling load profile for the next L hours.

5.3.3 Real-Time Model-Based Predictive Optimal Control

The optimal controller governing the two sources of thermal energy storage can minimize an objective function of choice including total energy consumption, energy cost, occupant discomfort, or a combination of these. In this study, the real-time controller was charged to minimize operating cost for time-of-use differentiated electricity and fixed-cost natural gas by adjusting global zone temperature setpoints $T_{Z,SP}$ for the passive storage and a dimensionless charge/discharge rate u for the active storage.

Optimal control is defined as that control trajectory that minimizes the total monthly utility bill C_m for electricity and heating:

$$\begin{aligned} J_m &= \min C_m = \min\left\{C_{elec,m} + C_{heat,m}\right\}, \text{ where} \\ C_{elec,m} &= \sum_{k=1}^{K_m} r_{e,k} P_k \Delta t_h; \qquad C_{heat,m} = \sum_{k=1}^{K_m} r_h \dot{Q}_{heat,k} \Delta t_h \end{aligned} \tag{28}$$

where $r_{e,k}$ is the energy rate for electricity according to the utility tariff in effect for time k, K_m is the number of hours in the current month, Δt_h is a time increment of one hour, r_h is the unit cost of heat delivered, and $\dot{Q}_{heat,k}$ is the heating demand from zone reheat in hour k.

To apply fixed-horizon optimal control to an infinite-horizon problem such as the given real-time control (it could go on indefinitely), closed-loop optimization (CLO) is employed, i.e., the predictive optimal controller carries out an optimization over a predefined planning horizon L and of the generated optimal strategy only the first action is executed. At the next time step the process is repeated. The final control strategy of this near-optimal controller over a total horizon of K steps is thus composed of K initial control actions of K optimal strategies of horizon L, where $L < K$. Figure 52 illustrates the procedure involved in determining the predictive optimal control policy. By moving the time window of L time steps forward and updating the control strategy after each time step, a new forecast is introduced at each time step and yields a policy (thick dotted line), which is different from the policy found without taking new forecasts into account (thin dashed line). Since we optimize over a planning horizon of L hours, we can only minimize an approximate cost function C_L, which allows for the determination of a near-optimal strategy, whose cumulative utility cost approaches the desired J_m at the end of the billing period.

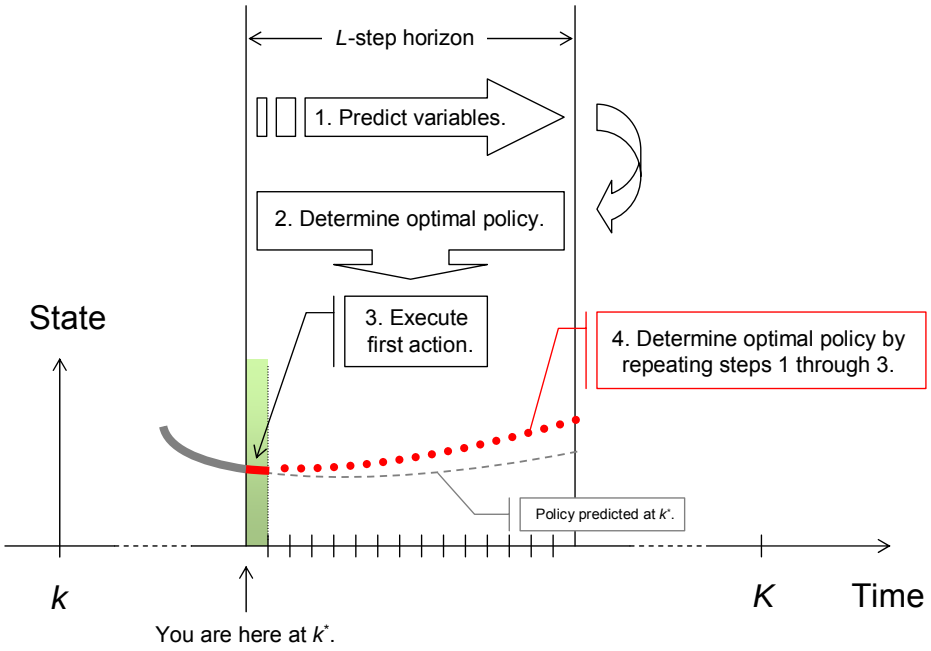

Figure 52: Closed-Loop Predictive Optimal Control

Figure 53 illustrates how the minimal utility cost J_L over time horizon L is determined. At time zero and starting with initial zone temperature setpoints $\{T_{Z,SP}\}_{init}$ halfway between the upper and lower bounds and no active storage utilization $\{u\}_{init} = 0$, the passive storage inventory is optimized to minimize C_L. As a result, the optimal building cooling load profile is computed and handed over to the active storage optimization, which calculates an optimal TES charge/discharge strategy. In a second pass, the optimal active storage utilization strategy and the previously found optimal zone temperature setpoint profile are employed to determine the new optimal zone temperature setpoint profile and optimal utility cost J_L. This cycle is repeated until the optimal cost J_L converges. Typically, convergence is attained after 2 to 3 iterations. Previously optimal solutions are stored as starting values for subsequent optimizations to reduce execution time. We refer to Henze et al. (2004a) for a detailed description of the model-based predictive optimal controller for building thermal storage inventory.

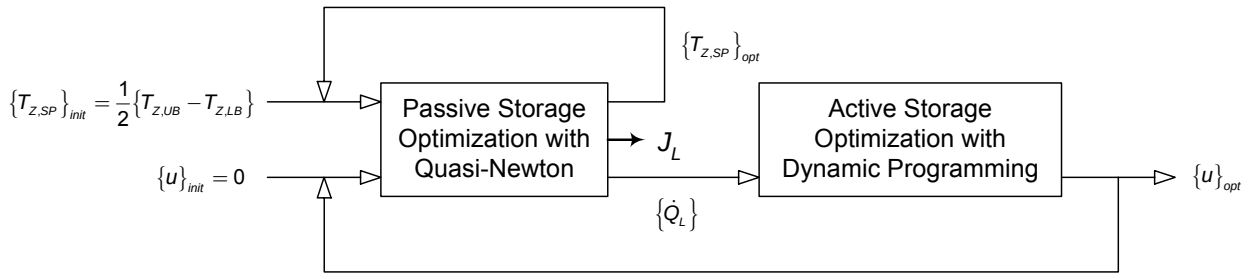

Figure 53: Iterative sequential optimization of utility cost C_L

At each time step k^*, the model-based controller derives the following four operational parameters for the active TES system from the optimal charge/discharge rate u_{k^*}: charging load for the main chiller (Q_{charge}), discharging load for the active TES system ($Q_{discharge}$), remaining cooling load for the main chiller (Q_{main}), and cooling load met by the precooling chiller ($Q_{precool}$). Rules incorporated in the building model ensure that a) charging and discharging cannot occur simultaneously; b) when the main chiller charges the active TES tank, any

building cooling load has to be met by the precooling chiller; and c) when the TES system is discharged, any remaining building cooling load has to be met by the main chiller.

5.3.4 Post-Processing

A post-processing computer program was developed for the ERS test facility to translate the optimal results produced by the model-based controller into commands, which can be understood by the building automation system and executed by the ERS HVAC system. The post-processing program sketched in Figure 54 sequentially executes the following operations every hour: (a) setup of a communication channel between the optimal controller environment and the BAS using a proprietary general-purpose communication software, (b) reading the optimal results from the optimal control and the required values from the BAS, (c) conversion of optimal results into control commands, and (d) sending the new control commands to the BAS.

The following post-processing procedure is executed: First, the room air temperature setpoint is sent directly to the BAS. Next, the cooling discharge rate of the TES is accomplished by sending the TES leaving water temperature as a setpoint for the TES mixing valve local loop control. The leaving water temperature $T_{LW,TES}$ is calculated from $\dot{Q}_{\text{discharge}} = \dot{m} c_p \left(T_{EW,TES} - T_{LW,TES} \right)$, where flow rate ($\dot{m}$) and entering water temperature ($T_{EW,TES}$) are read from the BAS.

During occupancy, the cooling output of the main chiller, operating with a constant cooling output in one of two stages, is accomplished by pulse width modulation (PWM). The PWM algorithm translates the optimal control result Q_{main} into a chiller stage and minutes of operating time during the next hour. The PWM time period was 20 min. Thus, the total chiller operating time is distributed over three PWM periods per hour. Operational constraints have also been taken into account. For example, there are at least five minutes between two periods of chiller operation in order to avoid the chiller cycling too frequently. Moreover, if the calculated main chiller load results in an operating time less than 5 minutes, than the chiller will operate 5 min. The precooling chiller is operated by the existing on-off control algorithm without PWM to maintain the global zone temperature setpoint $T_{Z,SP}$ in the building.

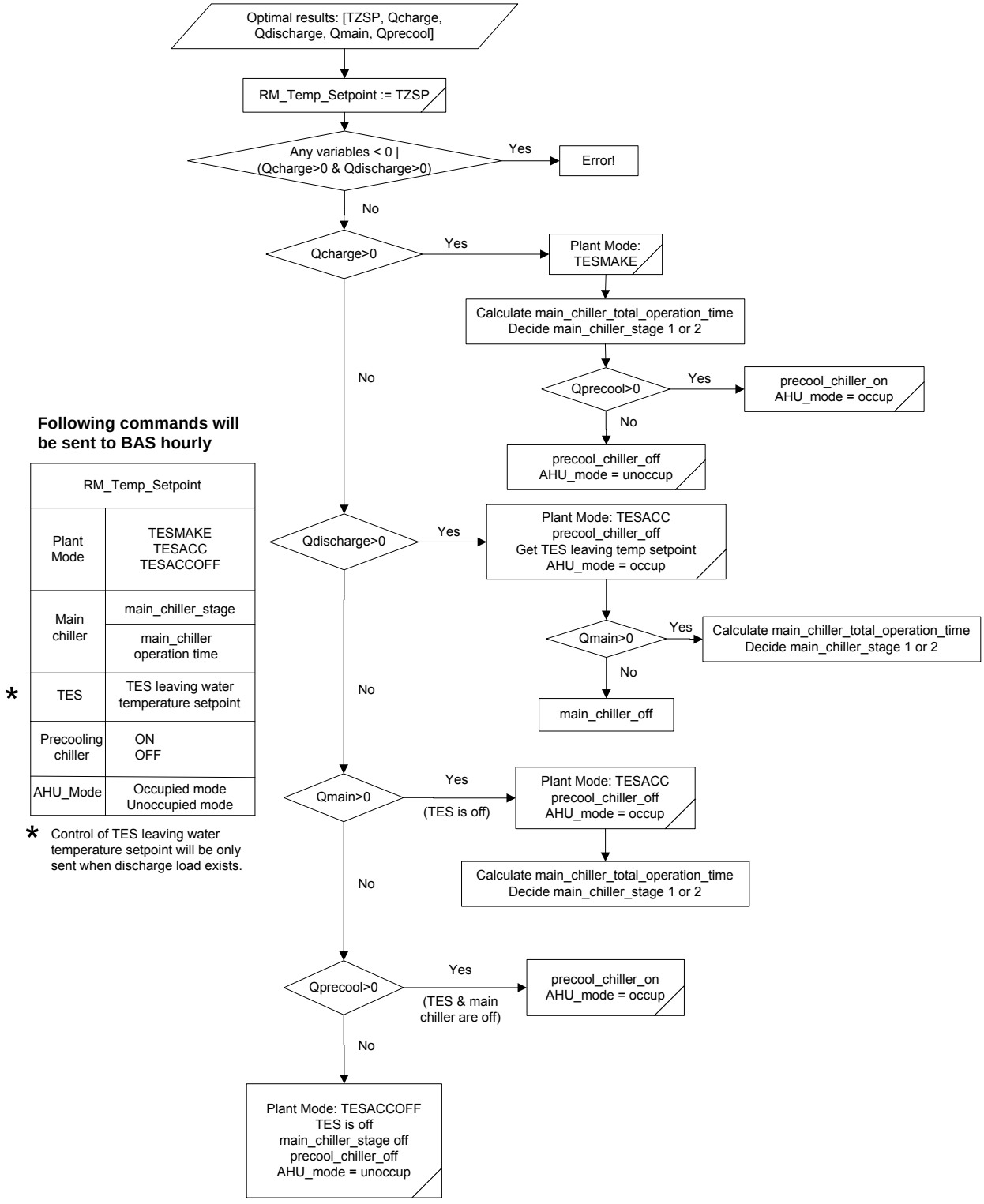

Figure 54: Post-processing program flow chart.

5.3.5 Control Command Execution

The building automation system requires five plant modes, which had previously been defined for the ERS test facility and had been modified to accommodate the predictive optimal control. A plant mode has to be selected before a command from the post-processing program can be sent to the HVAC system. The three of the available plant modes used in the context of our experiment were: TESMAKE plant mode which represents charging of the active TES system, TESACC plant mode in which the test rooms are conditioned by the main chiller and/or the active TES system, and TESACCOFF where the entire HVAC system is turned off. In addition, the BAS enables the air-handling unit fans based on the existence of a cooling load on the AHU cooling coils. In summary, the post-processing program obtains the optimal results from the controller, converts the values into comprehensible commands, selects a plant mode and forwards the commands using the communication channel to the BAS.

5.4 Description of Conventional Control Strategies

Before the real-time control experiments were conducted, two additional tests, a reference case and a base case test, were carried out. Both tests were required to calibrate the simulation model with respect to the building thermal response, the mechanical systems, and the operational schedules. Figure 55 shows the system configuration for the reference case and the base case. The active TES system is bypassed in the reference case.

5.4.1 Reference Case

The reference case represents the standard case of a cooling system with one sufficiently sized chiller (35 kW) which serves the air-handling units (AHU) A and B during occupancy, with nighttime setback during unoccupied periods and with neither active nor passive building thermal storage utilization. The test was run under the same schedule of occupancy and temperature setpoints: During occupied hours the zone temperature cooling setpoint was 24°C and the heating setpoint was 20°C, while the space temperature was allowed to float within the range of 15-30°C during unoccupied periods.

5.4.2 Base Case

In the base case test, the zone temperature setpoints were identical to the reference case test, however, the main chiller is downsized to only 25% of its nominal capacity (8.8 kW). During those periods when the cooling load exceeds the reduced chiller capacity, the remaining cooling is taken from the active TES system. At night the active TES system is recharged with full capacity of 35 kW to the upper inventory level of 75% state-of-charge. As in the reference case, the passive building thermal storage inventory is not utilized.

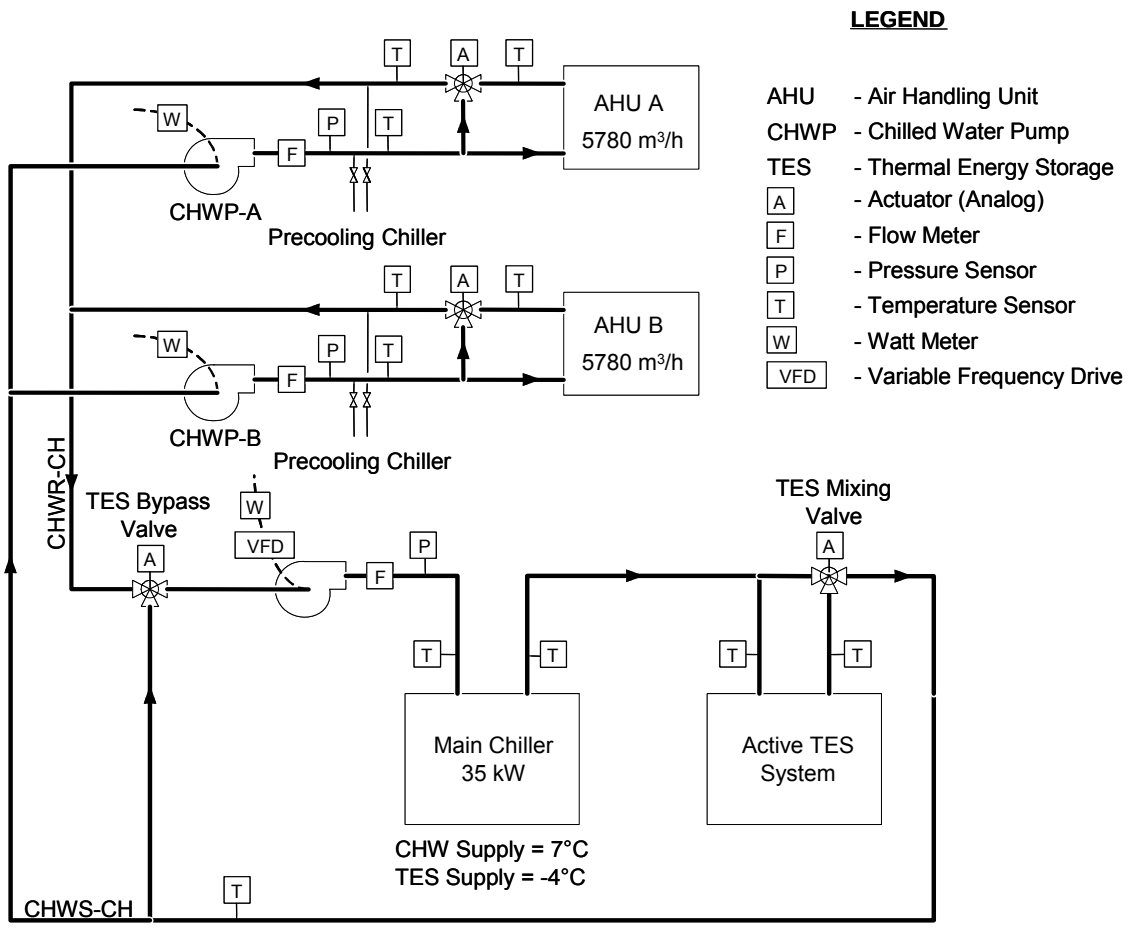

Figure 55: System schematic of ERS HVAC equipment

5.5 Results

5.5.1 Modeling Accuracy

The real-time optimal control experiment was executed over a period of 5 days (128 hours) from midnight on September 13 until 8 a.m. on September 18. In order to verify the experimental results, the accuracy of the building model must be evaluated. Minute-by-minute measurements taken at the test facility from September 14 to September 17, 2003 (subscript *ERS)* are compared to the optimal results determined by the controller during the real-time control experiment (subscript *ActPredOpt*, actual predictive optimal results). Preliminary tests conducted during June and July of 2003 facilitated the calibration the simulation model. As supported by evidence provided below, the accuracy of the building model was sufficiently high. Moreover, the post-processing program correctly translated and transferred the optimal control results and the HVAC systems and components were successfully orchestrated.

The experiment experienced two interruptions due to server crashes that made the communication channel to the building automation system unavailable on September 16 at 18:00 and on September 17 at 12:00 noon. During these interruptions the BAS returned zero values for all properties and deviations between model and measured data necessarily occurred.

Figure 56 compares the total simulated and measured AHU cooling loads of system B. It can be seen that the measured and modeled values are in good agreement. However, there are some peak cooling loads which are not represented well by the model-based controller. The AHU loads are due to internal heat gains from

baseboard heaters and lighting, which were chosen to be constant throughout the test days, solar gains, and the required intake of ventilation air.

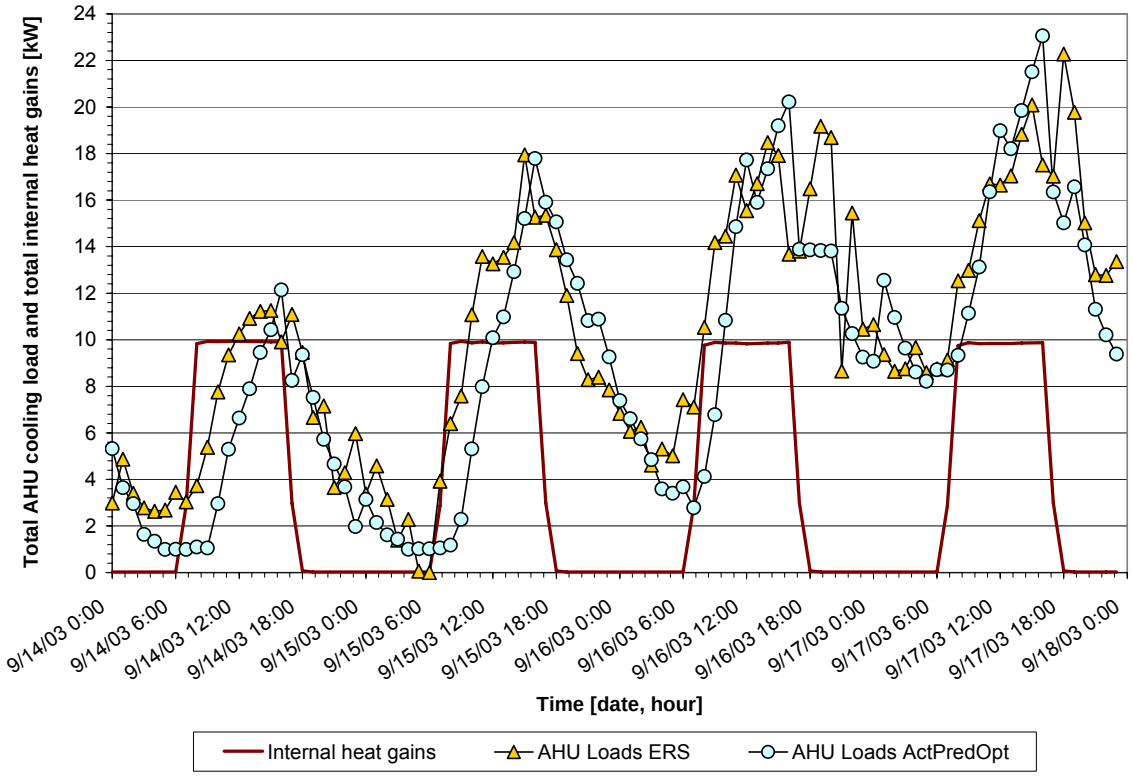

Figure 56: Measured and modeled total AHU cooling loads as well as measured internal heat gains [kW].

Figure 57 illustrates the measured and modeled charging and discharging performance of the active TES system for the September 15. It can be observed that the charging performance is accurately modeled; however, the discharge performance is modeled less precisely. Still, the discharge trend is captured well by the model used in the predictive optimal controller. While the charge/discharge performance appears to be adequately modeled, the profiles of the state-of-charge do not match well. Differences of up to 12% of active inventory can be observed and are attributed to a) the compounded differences in the charge/discharge performance and b) the poor accuracy of the inventory sensor (claimed to be ±5%). To eliminate the discrepancy between the simulated and measured values of state-of-charge, the SOC was measured throughout the testing period and updated seven times in the simulation environment. This procedure implies that the SOC sensor reads inventory levels accurately, which is not the case. Thus, the compounded effect of modeling mismatch in the charge/discharge process is eliminated, yet at the time the low SOC sensor accuracy is introduced to the optimization environment.

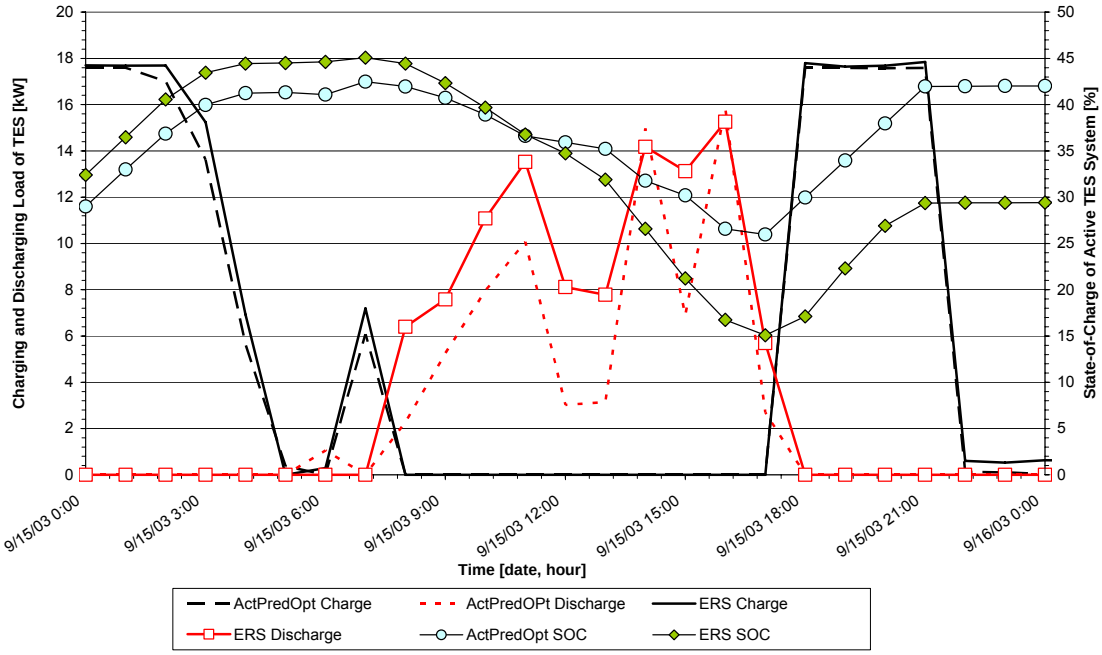

Figure 57: Measured and simulated charging and discharging load [kW] and state-of-charge [%].

Figure 58 illustrates the measured and simulated performance of the precooling chiller. Compared to the main chiller cooling profiles (not shown), the modeling accuracy for the precooling chiller is inferior. Unlike the active TES system and the main chiller, the precooling chiller was not controlled to maintain a particular value of $Q_{precool}$, but to maintain a global zone temperature setpoint $T_{Z,SP}$.

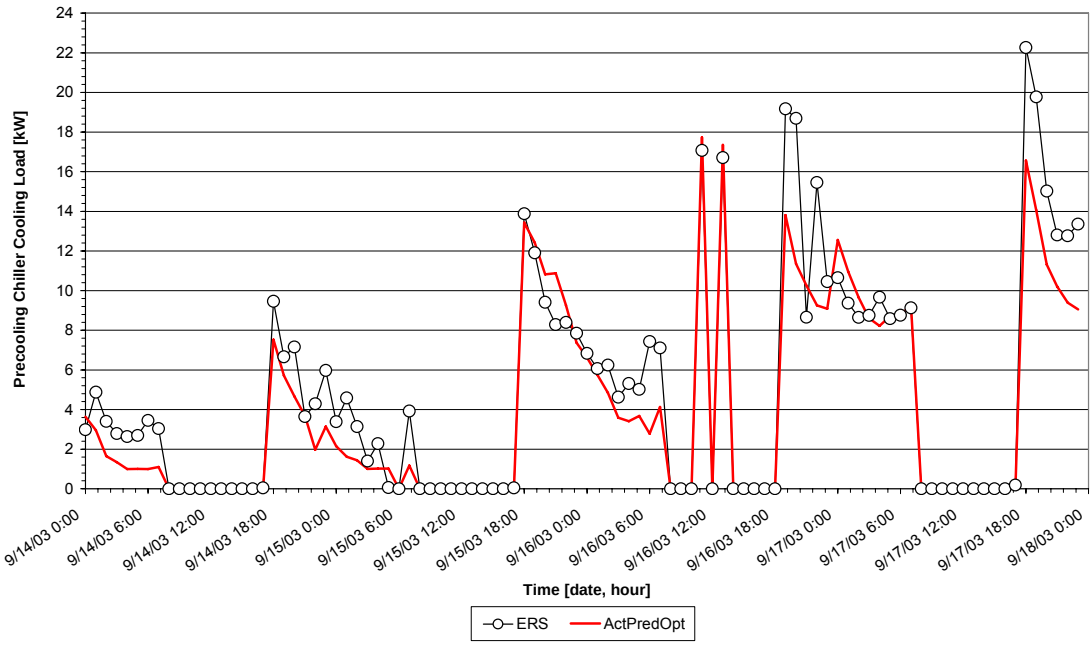

Figure 58: Measured and simulated precooling chiller cooling load [kW].

Does the model-based predictive optimal control comply with the operational constraints imposed in the model? Figure 59 shows the ambient air temperature, the average room air temperature, and the upper and lower temperature bounds selected for the operation of the ERS, represented by thick lines. During the real-

time control experiment, the optimal controller decided on substantial nighttime precooling down to 20°C averaged over all test rooms. Had the controller decided to precool the building even lower, a need for heating would have occurred at the onset of the occupied period. When the temperatures were allowed to float as in the reference and base cases, the average test room temperature rises above 26°C during unoccupied periods. During occupied periods, the room temperature stayed within the required comfort range for all three control strategies investigated in this study.

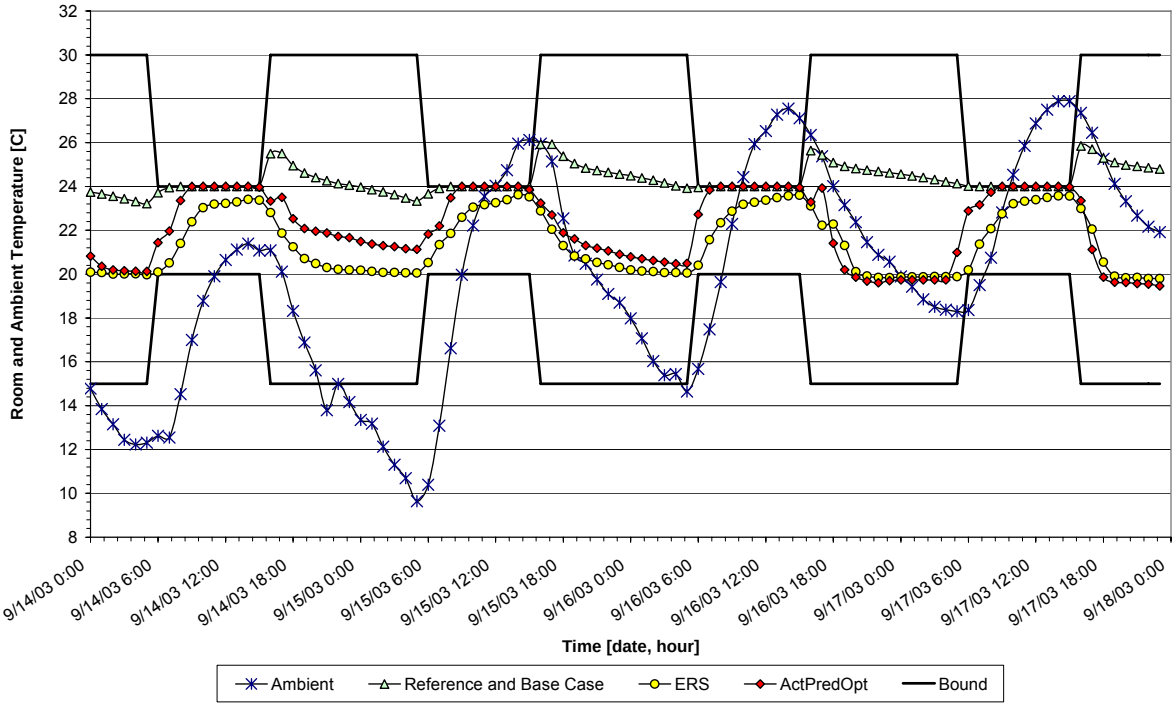

Figure 59: Average test room air temperature and ambient air temperature [°C].

The investigation of the active TES system state-of-charge data revealed that the simulated values remained consistently within the lower and upper bounds of 25% and 75%, respectively, while the measured TES inventory falls below the 25% mark due to a nonlinear discharging performance.

The average COPs of the main and precooling chillers were recalculated based on the data collected during the real-time control test in September of 2003. It was confirmed that the measured COPs deviated from the values in the building model by no more than ±0.1.

The schedules for occupancy and the HVAC system as implemented in the building model and the building automation system proved to match identically.

5.5.2 Energy and Cost Savings Performance

As mentioned above, changes in energy consumption and utility cost will be expressed relative to a simulated reference case or base case using the same building model and the same weather data as occurred during the real-time control tests. The performance metric for all cases is the utility cost for operating the entire HVAC system over a selected time horizon of four days from September 14-17, 2003. The data for September 13 were not considered to account for the transition from the uncontrolled to the controlled condition.

5.5.2.1 Energy and Cost Savings Performance based on Raw Data

The electrical utility rate structure includes a time-of-use differentiated energy charges ($/kWh) of $0.20/kWh on-peak and $0.05/kWh off-peak; no demand charge is levied. The on-peak period is daily from 9 a.m. to 6 p.m. with off-peak encompassing all remaining hours. The building is occupied from 8 a.m. to 5 p.m. While

the optimizer accounted reheat energy, no reheat was required in any of the test periods. The discussion therefore focuses on electrical energy consumption and costs.

The viewgraphs in this section are shown measurements at the ERS during the real-time-control test and simulation results for the reference and base cases for four days. In this time period, the outdoor air temperature ranges from 10°C early in the morning to 27°C at 6 p.m. Figure 59 reveals the increasing trend of daily average ambient air temperature over the course of the real-time control experiment.

In order to evaluate the results of the optimal control strategy with respect to cost and energy changes, the following tables and figures provide measured and calculated data for the following cases: a) reference case under nighttime setback, b) base case under chiller-priority control (labeled *Base Case 87%*), c) the data measured at the facility (labeled *ERS*), and d) the simulated data calculated during real-time control (labeled *ActPredOpt*). Both cases utilizing the active TES system, i.e., base and real-time control cases, started with an initial TES state-of-charge of 30%.

The original building model assumed a perfect, i.e., loss-free active TES system. This implies that 100% of the charging cooling load, Q_{charge}, is deposited in the storage tank. From measurements it was concluded that only about 87% of the cooling produced by the main chiller during the charging process contributes to changes of the active inventory storage, 13% are lost due to heat gains in the chilled-water distribution system and thermal transmission through the tank skin. For each charging period (5-7 hours per night) during the experiment, the change of the ice storage inventory was divided by the cumulative charging load that occurred over the same time period. The efficiency value of η = 87% was arrived at by averaging these five ratios.

$$\eta = \frac{1}{5}\sum_{p=1}^{5}\frac{\left(SOC_{final,p} - SOC_{inital,p}\right)}{\sum_{h=1}^{H_p} Q_{\text{charge},h,p}}, \tag{29}$$

where p denotes the charging period and H_p is the number of hours in charging period p. While the building model used for the ActPredOpt case assumed a perfect charging efficiency, the effect of heat gains and transmission losses on the state-of-charge was accounted for by periodically updating the SOC used in the simulation with measured SOC values at the test facility.

For an electrical utility rate structure without demand charges, we can plot daily profiles of HVAC utility costs for the main chiller, the precooling chiller, and chilled water pumps. The HVAC electrical energy consumption for September 17 is shown in Figure 60. The area under each curve represents the total daily operating consumption. It can be seen that the reference case incurs the highest on-peak demand, but as a result of nighttime setback does not consume any energy during the unoccupied period. The base case created the second highest energy demand during the on-peak period. Although the on-peak energy consumption for the base case is significantly less than that for the reference case, the on-peak consumption is greater than that under optimal control. During the day shown in Figure 60, the building cooling load was moderate and only a small contribution from the active TES system was required in the base case. Consequently only four hours of recharging were needed.

The model-based predictive optimal controller successfully shifted building cooling loads to off-peak periods and an excellent match between calculated (ActPredOpt) and measured (ERS) cooling load data can be observed.

The simultaneous utilization of active and passive building thermal storage inventory led to near-zero cooling-related electrical energy consumption during the on-peak period. The remaining energy consumption during the on-peak period is caused by the chilled water pump operating continuously. During the off-peak period high values of energy consumption can be observed which are due to precooling of the building structure (passive) and charging of the active TES system. It is obvious that on-peak energy consumption is reduced at the expense of increased off-peak energy consumption driven by the energy rate ratio of 4:1. Reducing on-peak electrical demand is a side effect of shifting expensive on-peak cooling loads to off-peak periods for an optimal controller minimizing electrical energy cost without a demand charge.

Although the building model was extensively calibrated, the seemingly small differences between measured and modeled hourly HVAC electrical energy consumption compounded to significant differences on a daily basis.

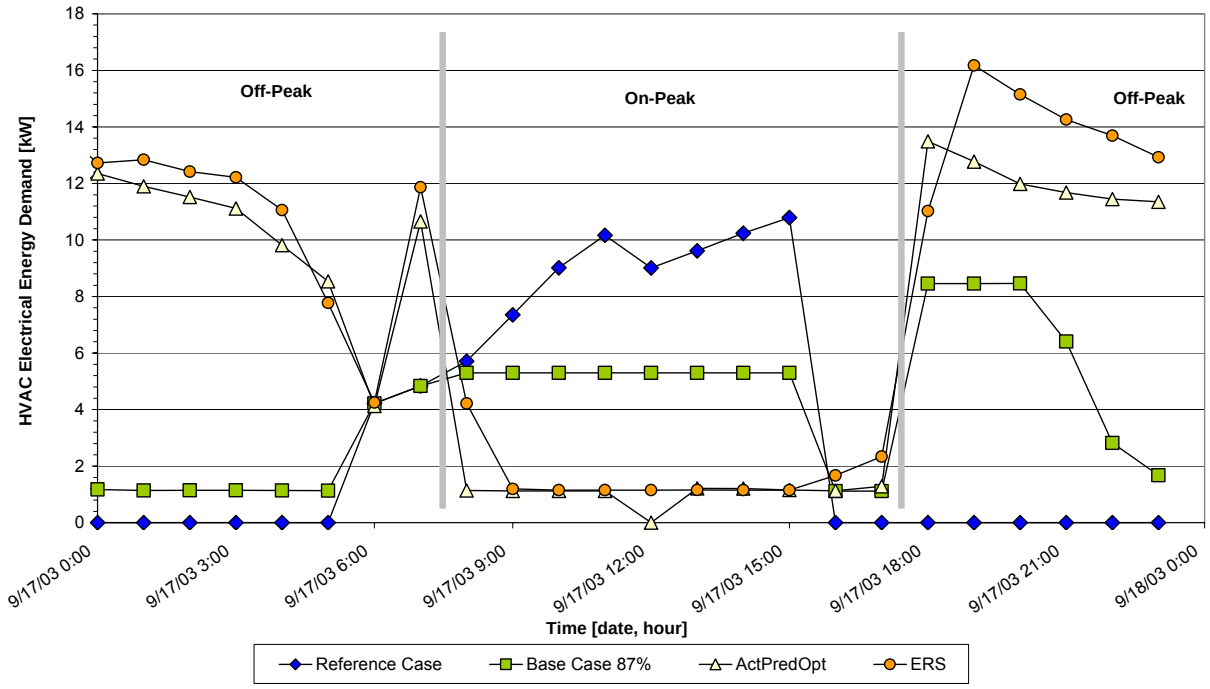

Figure 60: HVAC electrical energy consumption [kWh].

Table 33 provides the daily utility cost savings achieved during the experimental period. Relative to the reference case, measured savings of about 5% in total HVAC utility costs were achieved in the ERS, and about 10% of modeled savings (ActPredOpt). Compared to the base case with 87% charging efficiency, cost increases of about 7% and 1.4% were achieved for the ERS and the simulation, respectively. As shown, there are significant variations in the cost changes from one day to another relative to the reference and the base cases. This inconsistent pattern was caused by a number of reasons discussed in the next section.

Table 33: Changes of daily HVAC electrical utility cost of the optimal control strategy compared to the Reference Case and the Base Case 87% [%].

	14-Sep	15-Sep	16-Sep	17-Sep	Cumulative
Cost changes relative to Reference Case [%]					
ERS	-19.7	+11.5	+9.1	-21.2	-5.0
ActPredOpt	-32.2	+20.4	+7.1	-34.4	-9.9
Cost changes relative to Base Case 87% [%]					
ERS	-30.3	+17.3	+32.1	+1.3	+7.0
ActPredOpt	-41.1	+26.6	+29.7	-15.6	+1.4

5.5.2.2 Corrected Energy and Cost Saving Performance

Motivation for Correcting the Measured Results – Previous research (Henze et al., 2004a and 2004b) revealed that given strong load-shifting incentives, the benefits of the investigated predictive optimal control may be substantial. Therefore, we expected moderate daily savings, less fluctuation from day to day, and substantial cumulative savings. The promising potential of the optimal control strategy revealed in previous simulations may be obtained by the removal of erroneous data that occurred during the experiment. The corrected data discussed will be denoted by 'ERS*cor*' and 'ActPredOpt*cor*'.

Description of Experimental Problems – There were two experimental problems encountered during the tests: First, invalid data were produced by the building model during two hours of the experiment caused by the interruptions of the communication channel. These erroneous data were eliminated by interpolating between the valid adjacent data points.

Second, during three hours suboptimal solutions were found by the optimizer. As a result, main and precooling chiller activity occurred for three hours during the on-peak period of September 16 and drastically increased the electrical energy costs for that day. The precooling chiller activity can be observed for September 16 at 12 noon and 2 p.m. in Figure 58. The controller requested the main chiller to charge the TES with a very small charging load (not shown). As a result, the precooling chiller had to meet the daytime AHU cooling loads. Why did this happen? At any point in time, meeting a cooling load is least expensive by discharging the active TES system (only pump energy is incurred), next by using the precooling chiller (COP = 3.4), and finally by using the main chiller in chilled-water mode (COP = 2.1). Since both chillers cannot operate at the same time, the optimizer decided to charge an insignificant amount in order to be able to use the precooling chiller to meet the on-peak cooling loads. We believe that the optimal controller was caught in a local minimum during these hours, thus it selected a suboptimal control strategy. These experimental defects affected both the measured and the simulated raw cost data as shown in Table 33.

Elimination of Experimental Defects – In order to fairly assess the potential of the model-based predictive optimal controller, we manually modified the measured and simulated raw data to account for the interruptions and spurious precooling chiller activity. In addition, we repeated the experiment in a simulation environment using the same building model, weather data, and initial state-of-charge (labeled *RecPredOpt*), and compared it with the manually modified simulated data (labeled *ActPredOptcor*). The expectation was that after removing the experimental defects from the raw data and repeating the simulation without the problem of local minima, the results should match closely. Indeed, a repeated simulation run did not produce the same idiosyncrasies with respect to the precooling chiller operation as can be seen in Figure 62.

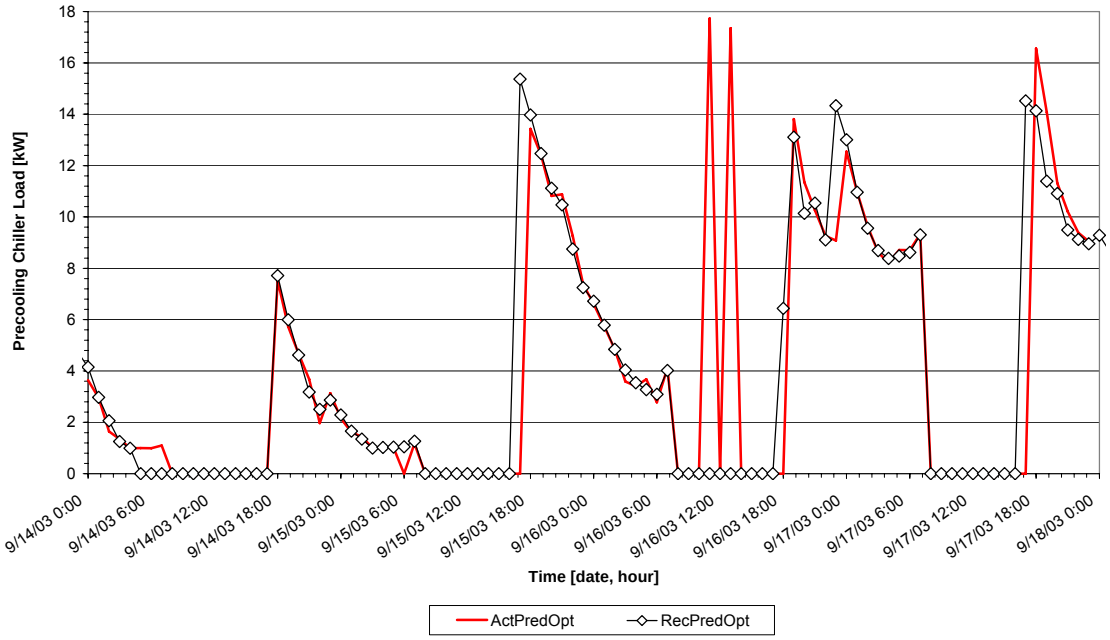

Figure 61: Simulated precooling chiller load as determined during the real-time experiment (ActPredOpt) and during recreated experiment (RecPredOpt) [kW].

The recreated experiment determines the cost savings we may have had obtained without interruptions and local minima. Interestingly, there are minor differences between the results collected for the real-time optimization ActPredOpt*cor* and the recreated optimization RecPredOpt. Obviously, the controller does not find exactly the same optimal solutions, which can be attributed to the convergence criterion of the optimizer.

Cost Comparison using the Modified Measured Results and the Recreated Simulation – Table 34 compares the daily savings of the corrected measurements at the ERS and of the corrected real-time simulation with the reference and base cases. It can be seen that the values for September 16 and 17 differ greatly from the cost calculation involving the raw data as shown in Table 33. After the removal of the erroneous data we obtain cost savings of 13% for the ERS data compared to the reference case and savings of 2% relative to the base case. The corrected real-time optimal results reveal higher cost savings as well. Cumulative savings of 18% are obtained when compared to the reference case and 7% are obtained relative to the base case. When comparing the recreated optimal results without local minima complications against the reference case, we obtain the same 18% savings as for corrected simulation results.

The recreated simulation did not require any updates of the SOC values since it did not occur in real-time and actual SOC data was not available. In order for the comparison of the recreated optimal and simulated base case to be valid, both have to use the same active TES model. We decided to assume a perfectly efficient charging process in the TES system for this comparison. The comparison yielded cost savings of about 7%.

Table 34: Changes of daily corrected HVAC electrical utility cost of the optimal control strategy compared to the Reference Case and the Base Case [%].

	14-Sep	15-Sep	16-Sep	17-Sep	Cumulative
Cost changes relative to Reference Case [%]					
ERS*cor*	-19.7	+11.6	-19.0	-22.4	-13.6
ActPredOpt*cor*	-32.8	+19.8	-19.6	-34.3	-18.0
RecPredOpt	-35.3	+13.2	-18.2	-30.5	-18.2
Cost changes relative to Base Case 87% [%]					
ERS*cor*	-30.2	+17.4	-1.9	+1.2	-2.2
ActPredOpt*cor*	-41.7	+26.0	-2.6	-14.2	-7.2
Cost changes relative to Base Case 100% [%]					
RecPredOpt	-42.9	+19.0	0	-8.3	-6.6

5.5.2.3 Consideration of AHU Fan Power Consumption

Motivation for Neglecting AHU Fan Operation – Preliminary tests had revealed that the global optimization of both active and passive building thermal storage inventory led to prohibitively long calculation times and inferior, i.e., often suboptimal solutions. In response, we adopted the iterative sequential optimization approach depicted in Figure 53. This decision required the plant models of the passive and active optimization steps are identical. To allow for easy plant model calibration, we decided to include a simplified HVAC plant model characterized by constant COPs in each mode of operation excluding the operation and energy consumption of the fans.

The measured data revealed that the fan energy consumption cannot be neglected and that fan operation has a significant impact on the decisions of the model-based predictive optimal controller. Therefore, the discussion of energy consumption and cost performance is now extended to take into account the fan power consumption and to highlight the differences in the optimal control decisions with and without fans.

Results with AHU Fan Power Consumption – On the basis of measured data, we approximated the supply and return fan electrical power consumption for AHU A and B with second-order polynomials and integrated those in the building model. The simulated results, shown in Figure 62 below, present the hourly HVAC electrical demand on September 17 for the reference case, the base case, the corrected measured data ERS*cor*, and the repeated optimal results RecPredOpt. The energy required by the reference case and the base case increased by the energy consumption of the fans during the occupied period.

Using the new plant model, the optimizer in a recreated experiment decides to make less use of the passive building thermal storage inventory, i.e., less precooling during the night and as a result saves an impressive 27% and 17% of electrical utility costs relative to the reference and base cases, respectively.

The actual experiment was conducted governed by a model-based predictive optimal controller that did not account for AHU fan power consumption. If we compare the measured total HVAC electrical energy consumption ERS*cor* with the fan consumption added to the reference and base cases using the modified plant model, the savings are reduced from 13.6% to 5.6% for the reference case and from 2.2% savings to cost increases of 8.3%. This investigation emphasizes that the inclusion of fan power consumption is mandatory for a successful implementation of passive thermal storage utilization. The optimal active TES system control strategy was not materially affected by the inclusion of the AHU fans in the plant model.

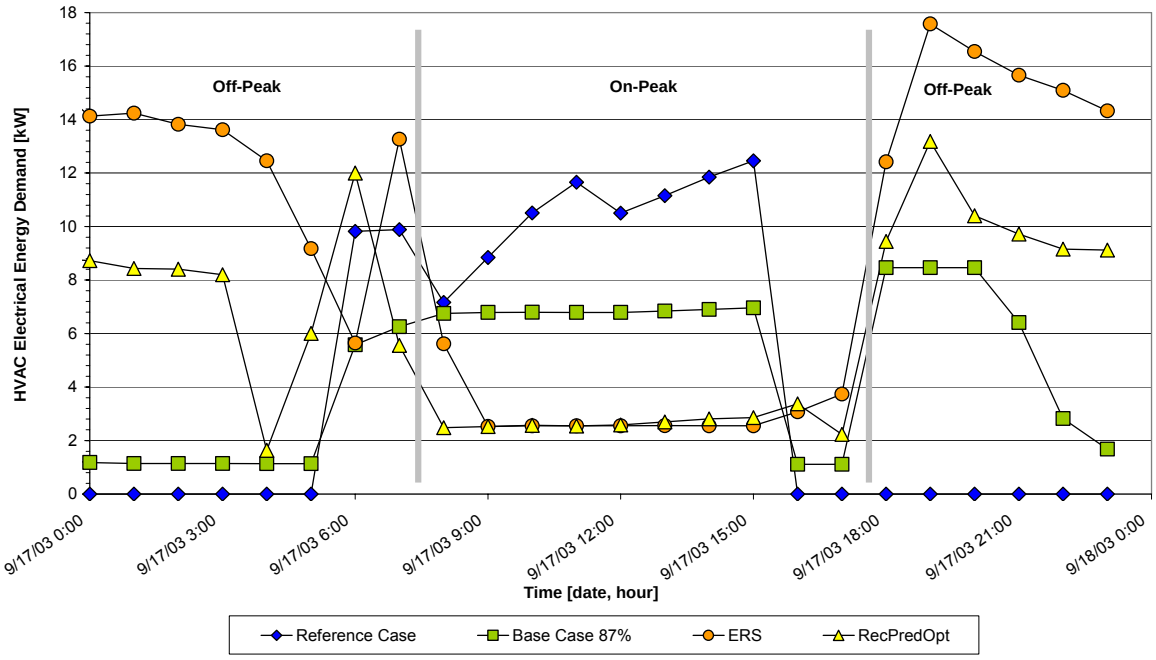

Figure 62: HVAC electrical demand including fan operation [kW].

Table 35: Changes of daily corrected HVAC electrical utility cost of the optimal control strategy compared to the Reference Case and the Base Case including the fan power consumption [%].

	14-Sep	15-Sep	16-Sep	17-Sep	Cumulative
Cost changes compared to the Reference Case [%]					
ERS*cor*	-7.9	+13.5	-11.4	-13.2	-5.6
RecPredOpt	-30.0	-13.9	-26.4	-36.4	-27.3
Cost changes compared to Base Case 87% [%]					
ERS*cor*	-11.6	+25.4	+7.5	+9.6	+8.3
Cost changes compared to Base Case 100% [%]					
RecPredOpt	-32.9	-4.9	-10.7	-19.8	-16.7

5.6 Conclusions and Future Work

This topical report investigates the demonstration of model-based predictive optimal control for active and passive building thermal storage inventory in a test facility in real-time using time-of-use differentiated electricity prices without demand charges. The novel supervisory controller successfully executed a three-step procedure consisting of 1) short-term weather prediction, 2) optimization of control strategy over the next

planning horizon using a calibrated building model, and 3) post-processing of the optimal strategy to yield a control command for the current time step that can be executed in the test facility.

The primary and secondary building mechanical systems consisting of two air cooled chillers, an ice-based thermal energy storage system, two identical air handling units and auxiliary equipment were effectively orchestrated by the model-based predictive optimal controller in real-time while observing comfort and operational constraints. The authors believe that this has not been accomplished before.

The findings reveal that even when the optimal controller is given imperfect weather forecasts and when the building model used for planning control strategies does not match the actual building perfectly, measured utility costs savings relative to conventional building operation can be substantial. This requires that the facility under control lends itself to passive storage utilization and the building model includes a realistic plant model.

The savings associated with passive building thermal storage inventory proved to be small because the test facility is not an ideal candidate for the investigated control technology: The building structure is of lightweight construction, the test rooms are unfurnished, and significant thermal coupling exists between controlled test rooms and an uncontrolled adjacent area. Moreover, the facility's central plant revealed the idiosyncratic behavior that the chiller operation in the ice-making mode was more energy efficient (COP=2.4) than in the chilled-water mode (COP=2.1).

To aid model calibration, the model used for real-time control employed a constant COP approach for each chiller and mode of operation and ignored VAV fan operation. The measured results show that the plant model must include AHU fan operation and should include part-load performance and correction for off-design conditions.

Field experimentation is now required in a suitable commercial building with sufficient thermal mass, an active TES system, and a climate conducive to passive storage utilization over a longer testing period to support the laboratory findings presented in this study.

Currently underway is research that attempts to create an optimal controller for the same control application that does not rely on a model description but learns to carry out the best control decisions based on reinforcement it received in response to past actions.

5.7 References

[56] Braun J.E., T.M. Lawrence, C.J. Klaassen, and J.M. House (2002) "Demonstration of Load Shifting and Peak Load Reduction with Control of Building Thermal Mass," Proceedings of the 2002 ACEEE Conference on Energy Efficiency in Buildings, Monterey, CA.

[57] Braun, J.E. (2003) "Load Control Using Building Thermal Mass", Journal of Solar Energy Engineering, Vol. 125, No. 3, pp. 292-301, American Society of Mechanical Engineers, New York, New York.

[58] Henze, G.P., R.H. Dodier, and M. Krarti (1997) "Development of a Predictive Optimal Controller for Thermal Energy Storage Systems." International Journal of HVAC&R Research, Vol. 3, No. 3, pp. 233-264.

[59] Henze, G.P., C. Felsmann, and G. Knabe (2004a) "Evaluation of Optimal Control for Active and Passive Building Thermal Storage." International Journal of Thermal Sciences, Vol. 43, No. 2, pp. 173-183, Elsevier Science, New York, New York.

[60] Henze, G.P., D. Kalz, C. Felsmann, and G. Knabe (2004b) "Impact of Forecasting Accuracy on Predictive Optimal Control of Active and Passive Building Thermal Storage Inventory." International Journal of HVAC&R Research, Vol. 10, No. 2, pp. 153-178, American Society of Heating, Refrigerating, and Air-Conditioning Engineers, Atlanta, Georgia.

[61] Liu, S. and G.P. Henze (2004) "Impact of Modeling Accuracy on Predictive Optimal Control of Active and Passive Building Thermal Storage Inventory." ASHRAE Transactions, Technical Paper No. 4683, Vol. 110, Part 1, pp. 151-163, American Society of Heating, Refrigerating, and Air-Conditioning Engineers, Atlanta, Georgia.

[62] Matlab (2000) Using Matlab v6. The MathWorks, Inc.

[63] Price, A.B. and T. F. Smith (2000) "Description of the Iowa Energy Center Resource Station: Facility Update III", Technical Report ME-TFS-00-001, Department of Mechanical Engineering, The University of Iowa, Iowa City.

[64] TRNSYS (2003) TRNSYS – A transient simulation program. SEL University of Wisconsin – Madison, http://sel.me.wisc.edu/trnsys/Default.htm.

5.8 Nomenclature

AHU	Air handling unit
ActPredOpt	Raw actual predictive optimal results during real-time simulation
ActPredOptcor	Corrected predictive optimal results during real-time simulation
BAS	Building automation system
Base Case 87%	Base case under chiller priority with 87% charging efficiency
Base Case 100%	Base case under chiller priority with 100% charging efficiency
CHWP	Chilled water pump
CLO	Closed-loop optimization
COP	Coefficient-of-performance
ERS	Energy Resource Station; raw measured data at ERS
ERScor	Corrected measured data at ERS
IEC	Iowa Energy Center
HVAC	Heating, ventilating, and air-conditioning
PWM	Pulse width modulation
RecPredOpt	Repeated predictive optimal results
SOC	State-of-charge for the inventory in the active thermal storage system [%]
TES	Active thermal energy storage system
TESACC	Plant mode: Condition the test rooms
TESACCOFF	Plant mode: Turn off HVAC system
TESMAKE	Plant mode: Charge active TES system
VFD	Variable-flow distribution
C_L	Cost function for horizon L [$]
C_m	Total monthly utility bill [$]
H_p	Number of hours in charging period p [-]
J_m	Optimal total monthly utility bill [$]
J_L	Optimal utility cost for horizon L [$]
K_m	Number of hours in current month [-]
L	Planning horizon for optimal control [h]
Q_{charge}	Charging load for the main chiller [kW]
$Q_{discharge}$	Discharging load for TES system [kW]
Q_{heat}	Heating demand from zone reheat [kW]
Q_{main}	Cooling load for main chiller [kW]
$Q_{precool}$	Cooling load for precooling chiller [kW]
$T_{EW,TES}$	Entering water temperature of TES [°C]
$T_{LW,TES}$	Leaving water temperature of TES [°C]

$T_{z,SP}$	Global zone temperature setpoint [°C]
$\{\hat{X}_t\}$	Forecasted time series
$\{X_t\}$	Observed time series
c_p	Specific heat capacitance [kJ/kgK]
d	Number of days [-]
k^*	Current hour [-]
$\dot{m}$	Mass flow rate [kg/s]
n	Day index [-]
$r_{e,k}$	Energy rate for electricity [$/kWh]
r_h	Cost of heat delivered [$/kWh]
t	Time [-]
u	Charge/Discharge rate [-]
Δt_h	Time increment for one hour [-]
η	Efficiency value for charging TES [%]

6 Phase 3: Field Testing at the Energy Plaza in Omaha, NE

6.1 Abstract

As the third and final phase of the project on predictive optimal control of active and passive building thermal storage inventory, field experimentation has been carried out in Omaha, NE during the summer of 2005. This chapter summarizes the efforts that had been made to implement a model-based predictive optimal controller in a commercial building in order to 1) explore the merits of harnessing the active and passive thermal storage inventories simultaneously by means of predictive optimal control, 2) validate the previous findings in the first (modeling and analysis) and second (laboratory testing) phases, and 3) provide the experience and guidance for future application in real buildings. This chapter will first describe the tested commercial building and its facilities. The methodology of implementation of model-based predictive optimal controller will then be introduced, followed by data analysis.

6.2 Description of Experiment Facility

6.2.1 General Background on Energy Plaza

The target building is selected as Energy Plaza, which is a commercial office building located at the 16th Street of Omaha, Nebraska. This building premise consists of the separate office blocks East, West, and Garage. The exterior atrium connects these blocks and has glazing roof-construction to illuminate the space area with the daylight. In this field experimentation, only the east office block will be under the control of predictive optimal controller. The total conditioned area is about 14,000 square meter including the basement, arcade, interior atrium, open space offices (2nd to 10th floor), and mechanical floor. The estimated occupancy is about 480.

The following photographs capture the main features of the Energy Plaza building.

6.2.2 Primary and Secondary HVAC Systems

There are five air-handling units (AHU-1, 2, 3, 4 and 5) serving the east office block of Energy Plaza. AHU-1, 2, 3 and 4 are single-duct VAV systems that serve office areas, and AHU-5 is a single-zone unit that serves the atrium. Two AHUs, AHU-1 and 2, are located at the basement and the other three are located at the penthouse. The main AHUs (AHU-1, 2, 3 and 4) are interconnected as a single duct ladder loop as shown in Figure 63.

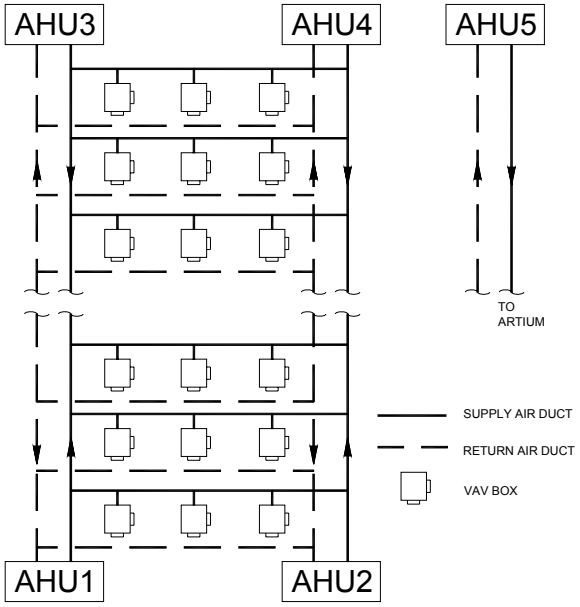

Figure 63: Air distribution for the entire building

The chilled water system consists of three chillers (CH-1, CH-1A and CH-1B), three ice storages (TSU-1A, 1B and 1C), a heat exchanger between ice water loop and chilled water loop, two brine pumps (P-1A and 1B), two ice water pumps (P-2A and 2B) and three brine pumps (P-3A, 3B and 3C). Figure 64 shows the detailed schematic of chilled water, ice water and brine loops.

Until the summer of 2004, the plant was running under storage-priority control; this was changed to chiller-priority control as one of the outcomes of the continuous commissioning activities. The existing two chillers charge the ice storage units during unoccupied hours (initiation time: midnight). The high temperature (new) chiller operates on demand while the existing chiller is operating. During occupied hours, the ice storages are discharged to provide cooling for peak demand and no chiller shall operate. If the load exceeds the ice storage capacity during the discharging period, the high temperature chiller shall operate to support the ice storage system. One of the ice water pumps and one of the chilled water pumps can be modulated by variable frequency drives. The ice water pump is modulated to maintain the chilled water supply temperature at 38ºF. The chilled water pump is modulated to maintain the pressure differential at the remote loop. There are two-way valves for the cooling coils in AHUs.

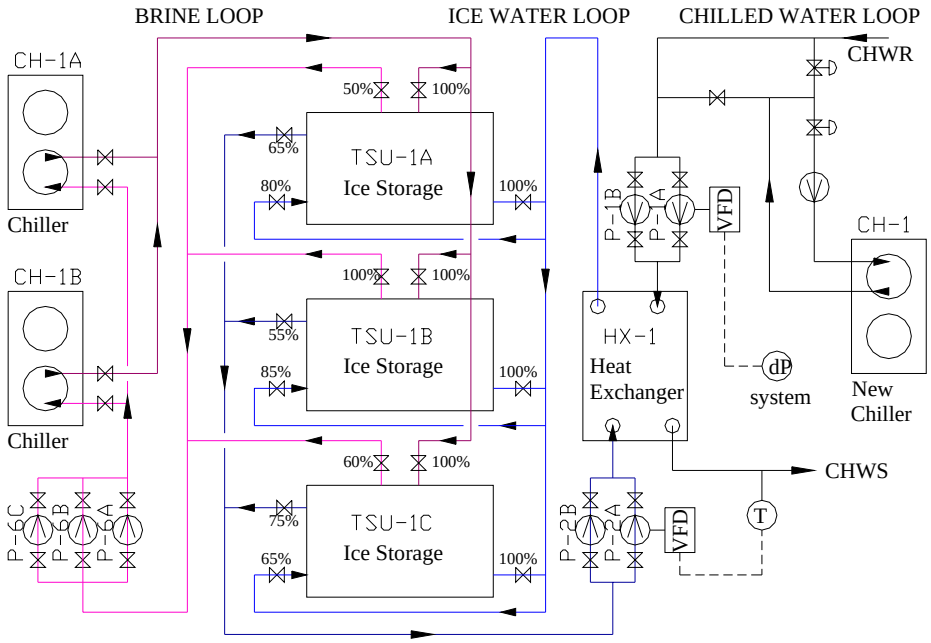

Figure 64: Schematic of the chilled water system

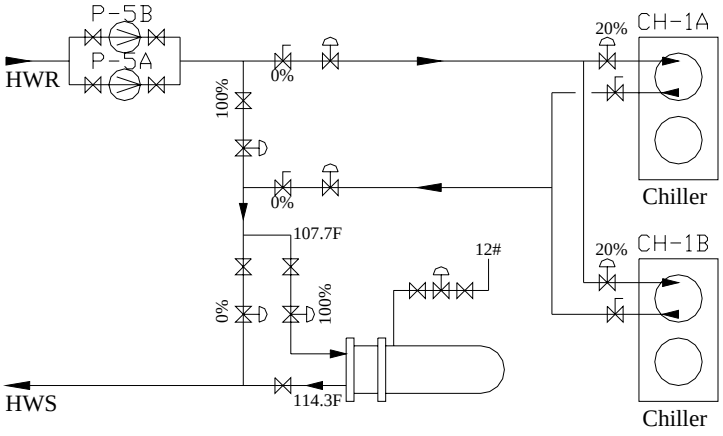

Figure 65: Schematic of the hot water system

Figure 65 shows schematic of the hot water system. The hot water pump operates at constant speed. The returning hot water can be heated in the condensers of ice making chiller while the chillers are operating. Otherwise, a steam-hot water heat exchanger heats up hot water. The capacity of the main chiller (labeled as New Chiller in Figure 64) is 200 Ton (703.4kW). The system has its primary constant speed pump and constructs a primary-secondary chilled water system with the secondary chilled water pumps. The capacity of each ice-making heat pump is 160 Ton (562.7kW). The total capacity of the ice-storage system is 2850 ton-hours (9975kWh).

6.3 Development of the Building Model for Energy Plaza

6.3.1 Modeling Assumptions

In the study, we only consider the office spaces including the arcade and interior atrium level, which are served by the four single duct air handling units (AHU) (described in Section 6.2.2). The arcade level and the interior atrium level are connected by the opening stairs and the air floats freely, therefore, we assume the two levels have the same zone air temperature and consider them as one zone. Furthermore, from the 2nd floor on, there are open space offices in the core and small offices at the exterior walls. Since the air movement between them is unlimited and they are controlled by the same sensors, we model each floor as one thermal zone. The building model is developed in TRNSYS [36].

6.3.2 Modeling of Interior Gains

From site visits, we assume that the time of use or occupancy, respectively, is daily 6 AM to 7 PM and from Monday to Friday for all offices except the first and the tenth floor, which have to be served (conditioned) around the clock. Otherwise, the offices are unoccupied. The interior gains of the occupants as well as of the lighting during the occupied periods are modeled as shown in Figure 66.

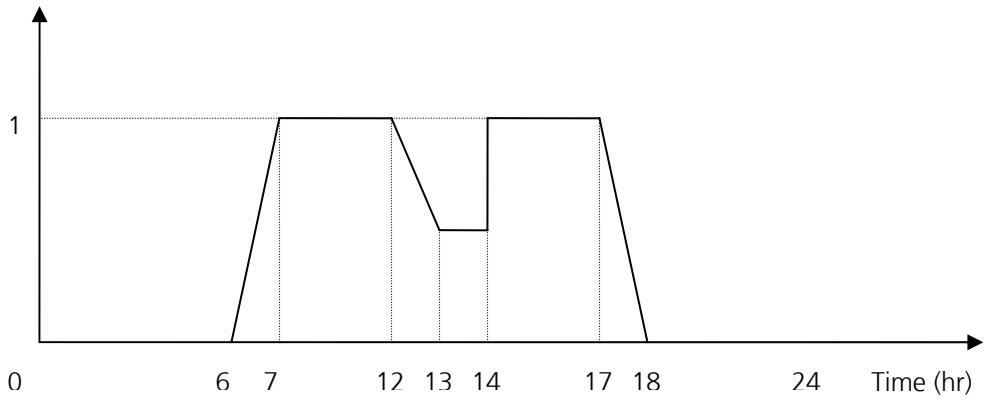

Figure 66: Internal gain schedule for Energy Plaza

6.3.3 Calibration of Building Model

The Energy Plaza building has undergone a retrofit of lighting fixtures starting last winter, which requires our building model to be updated accordingly. Figure 67 compares the hourly electricity load of a typical office floor before and after the change of lighting fixture.

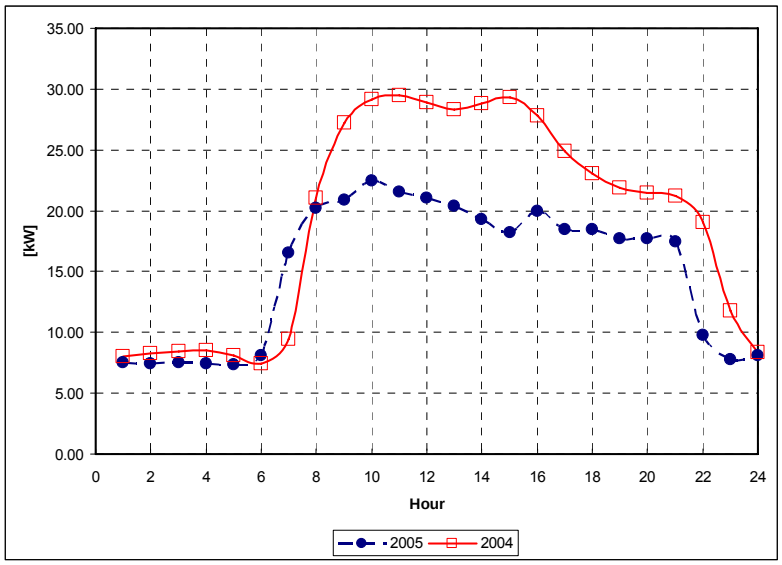

Figure 67: Comparison of electrical load before and after retrofit

Based on measurements, the building model has been changed correspondingly.

Another important parameter is the utility rate structure for the program. Energy Plaza is subject to a special utility rate, which does not include a time-of-use (TOU) feature as our program expected. An investigation has been carried out in order to create an artificial time-of-use rate that has a suitable structure with our program and that approximates the actual electricity bill of the building as close as possible. It is assumed that the on-peak period as 10:00 AM – 18:00 PM, and the rest is the off-peak hours. By comparing different rate structures, it was decided that using off peak rate as $0.03/kWh and on-peak $0.09/kWh can provide a total deviation of only 2.4% for the months of June – September and strong load-shifting incentive ratio of 3:1. Figure 68 provides the comparison of electricity bill of June – September of 2004 between the actual value and the projected ones using the artificial utility rate structure.

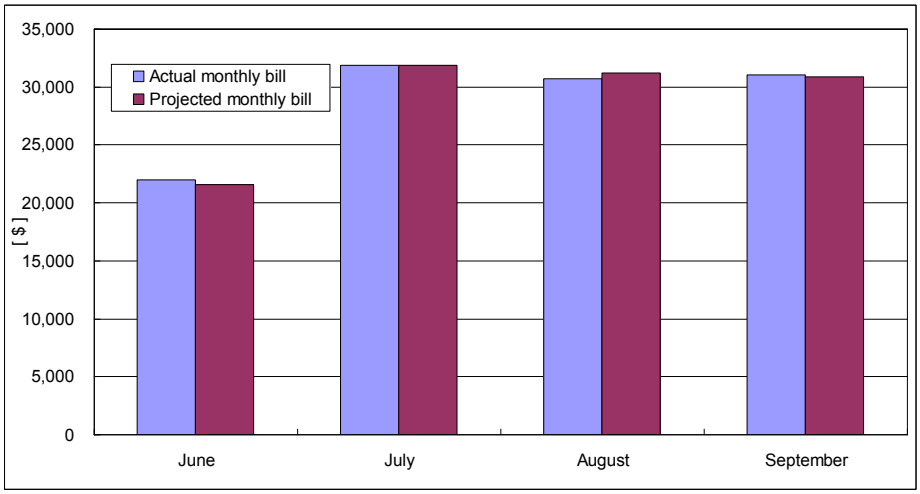

Figure 68: Actual and projected values of monthly electricity bill for the Energy Plaza

6.4 Implementation of predictive optimal controller

The implementation of model-based predictive optimal control program was carried out by sequentially executing the following three programs at each time step: 1) short-term weather prediction, 2) optimization of control strategy over the next planning horizon using a calibrated building model, and 3) post-processing of the optimal strategy to yield a control command for the current time step that can be executed in the test facility. This structure had proved successful in the laboratory experimentation.

6.4.1 Implementation of Weather Predictor

A 30-day bin predictor model was implemented to cooperate with the predictive optimal controller. The predicted variables included ambient air dry-bulb temperature, relative humidity, global solar radiation, and direct normal solar radiation. The implementation of the weather predictor required two sets of data available:

6.4.1.1 Last 30 day's bin data.

During the laboratory experimentation in the ERS 2003, a weather station provided all the data we needed. Since there was no weather station available in Energy Plaza, we had to find historical weather data for Omaha, NE to build up the bin data. Unfortunately, even though there are many weather stations available locally and nationally, and the temperature and relative humidity are easy to get, solar radiation data, especially historical solar data is almost unavailable. Because of this fact, instead of using monitored data in Omaha of 2004, TMY2 weather data is used to build up the initial weather bin data. It is worth pointing out that the bin data will be updated every hour. During the experiment, the real-time weather data was used to update this bin data. As the dry-run tests proceeded, the bin data became more and more realistic.

6.4.1.2 Real-time weather data

As mentioned earlier, without the local weather station, the real-time actual ambient condition was hard to acquire directly. Installation of a weather station and setting up the corresponding communication system is a straight forward solution, but it also could be very time consuming. Meanwhile, there are many local weather stations in Omaha, which provide sufficiently accurate information to meet our requirement. Since all these information is available on the internet, a program was developed to acquire this information remotely. The following three weather stations were inquired hourly to provide the following specific weather information:

- Creighton University weather station provided the ambient air dry-bulb temperature and relative humidity.
- Gretna weather station provided the hourly global solar radiation data
- Omaha.com weather prediction provided the current sky condition, which will be used to estimate the direct normal solar radiation.

6.4.2 Implementation of Post-processing Program

A post-processing computer program was developed for the Energy Plaza facility to translate the optimal results produced by the model-based controller into commands, which can be understood by the building automation system and executed by the HVAC system.

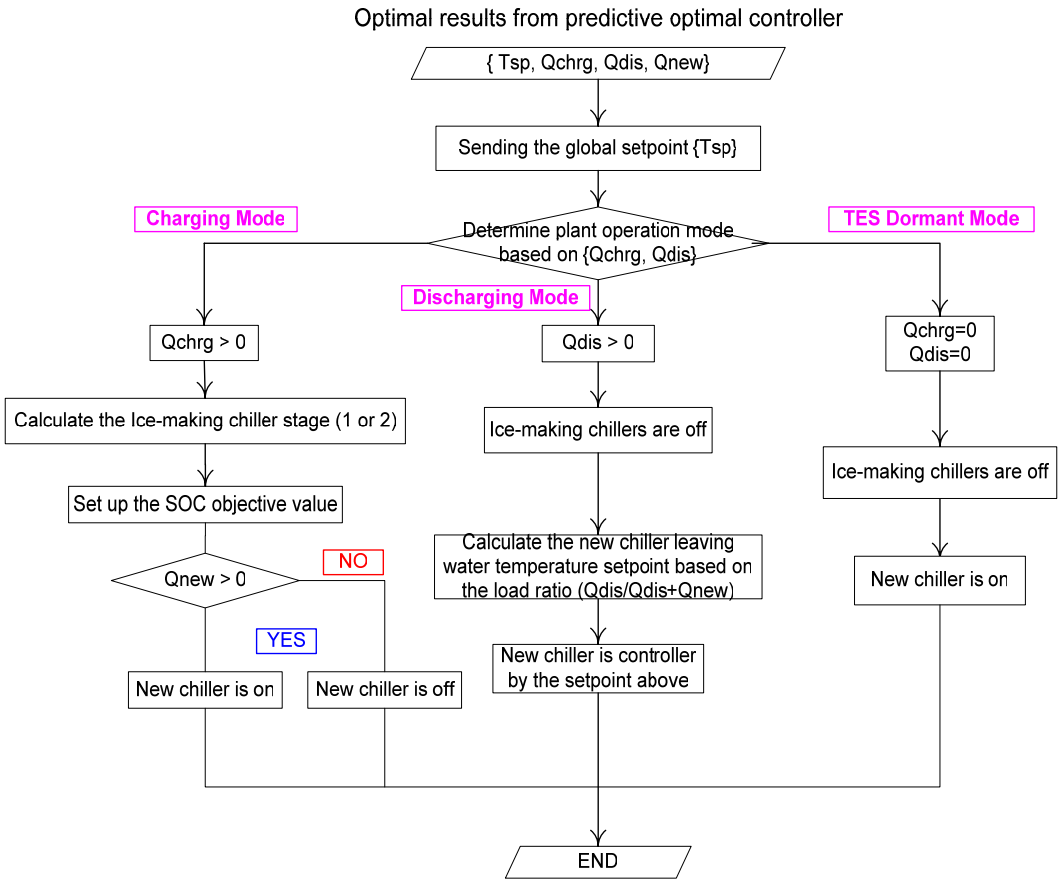

Figure 69: Flowchart of the post-processing program

Figure 69 shows the flowchart of the post-processing program. As shown above, based on the optimal result from the predictive optimal controller, the post-processing program will generate a set of commands hourly, which mainly include:

1) Turn on/off chillers, including base load chiller and ice-making chiller.
2) Reset the cooling temperature setpoint for all of the terminal boxes universally.
3) Setting the leaving water temperature setpoint when the plant is in the discharging mode.
4) Setting the charging limit when the plant is in the charging mode.

6.4.3 Communication with the BAS of Energy Plaza

During the laboratory experimentation described in Chapter 0, communication between predictive optimal controller and the BAS of the building was not a very difficult problem. By using the NDDE (Network Dynamic Data Exchange) application programs, which are built-in functions in Matlab, the commands interpreted by the post-processing program can be immediately executed by the BAS. We attempted to use the same methodology in the Energy Plaza facility, but it turned out that the NDDE is reliable when it is working in the context of a virtual private network (VPN). The final solution was to let the DDE work locally on our computer, in which the predictive optimal control program resides, and the data between the program and the BAS of the EnergyPlaza is exchanged through a shared Excel file, which is opened in the control server of Energy Plaza. The Excel file works as an interface between our computer and the control server in Energy Plaza.

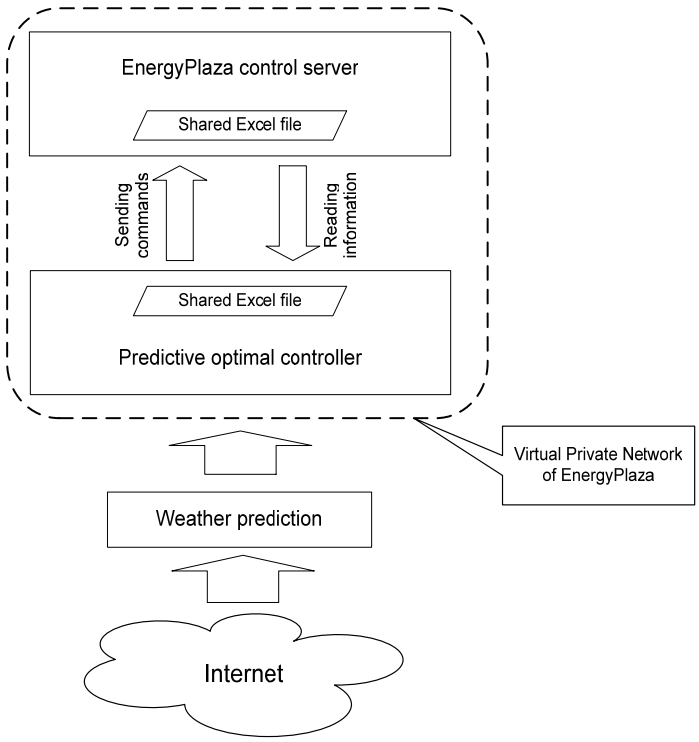

Figure 70: Communication architecture of the programs

Figure 70 depicts the communications of the programs with each other. Another computer has to be set up to run the weather prediction program because once the computer that carries out the predictive optimal control program logs on the Virtual Private Network of the Energy Plaza, it will lose connectivity with internet, which will be needed to make weather prediction.

6.5 Data Analysis

This final report presents an analysis based on the available data. Although such a short period including a couple of interruptions cannot provide a full evaluation of the predictive optimal control program as we expected, it still provides an opportunity to analyze the performance of the optimal controller. Table 36 presents a brief test log during the test period, which is helpful to interpret the results in the following discussion.

Table 36: Test period log

Case	Date	Note
Base Case	June 22 0:00 to July 16 9:00	Normal operation
	July 16 9:00 to July 20 15:00	Normal operation, flow meter down
	July 20 15:00 to July 25 10:00	Normal operation
Optimal Case	July 25 10:00 to July 28 7:00	Optimal operation, server crash at 7:15AM, but program is continued
	July 28 8:00 to July 29 13:00	Optimal operation, server crash at 7:45AM, but program is terminated including main Matlab run file at 13:00
	July 29 13:00 to Aug 1 8:00	Normal operation (optimal test suspended)
	Aug 1 8:00 to Aug 3 12:00	Optimal operation
	Aug 3 12:00	Server crash, and test is terminated

The two cases mentioned in Table 36 stand for two different operating schemes described in the following data analysis. The base case refers to the normal operation without using the predictive optimal control program, which is chiller-priority TES control with constant zone air temperature setpoint during occupancy and nighttime setup. Optimal case is the test period when our predictive optimal control program is applied. The normal operation has been monitored since the middle of June of 2005. Data from July 11 to 17 are selected to represent the base case, which is one week before the optimal case started. It should be noted that the flow meter had malfunctioned for about 5 days since July 16. Another finding is that the state-of-charge SOC sensor is not reliable; sometimes the data indicates that the SOC could jump from an empty to 80% inventory in one hour, which of course is not possible.

6.5.1 Base case

July of 2005 was the hottest month for Omaha this year, especially the last two weeks of July. As earlier mentioned, the plant has been modified from storage-priority to chiller-priority control as a result of the continuous commissioning efforts. The selected data are supposed to represent the normal plant operation. Figure 71 and Figure 72 presents the weather data and room temperature of the Energy Plaza building from July 11 to July 17.

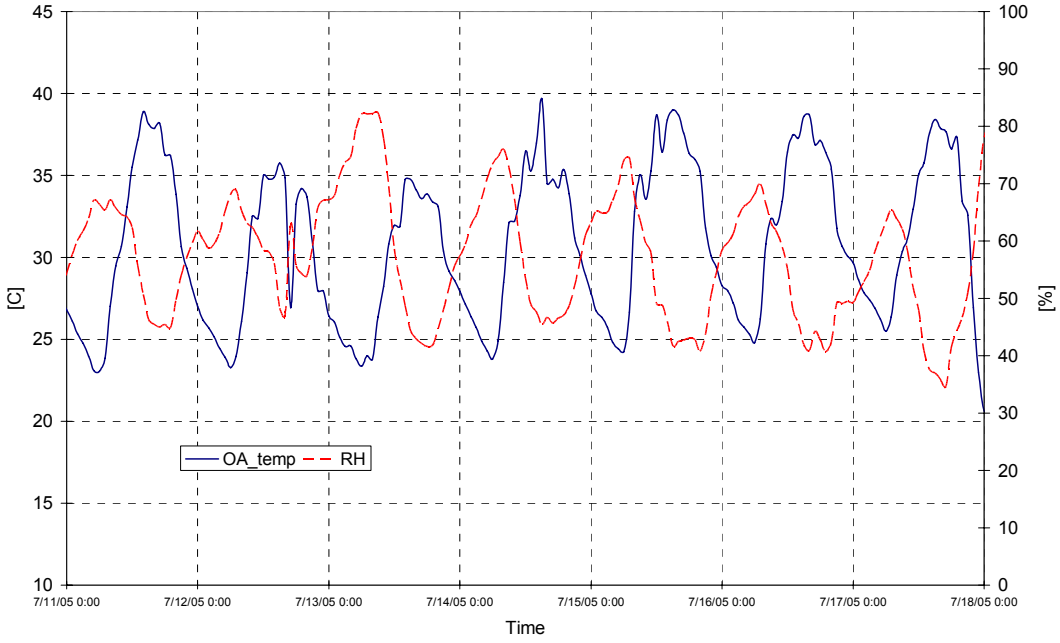

Figure 71: Ambient condition from July 11 to July 17, 2005

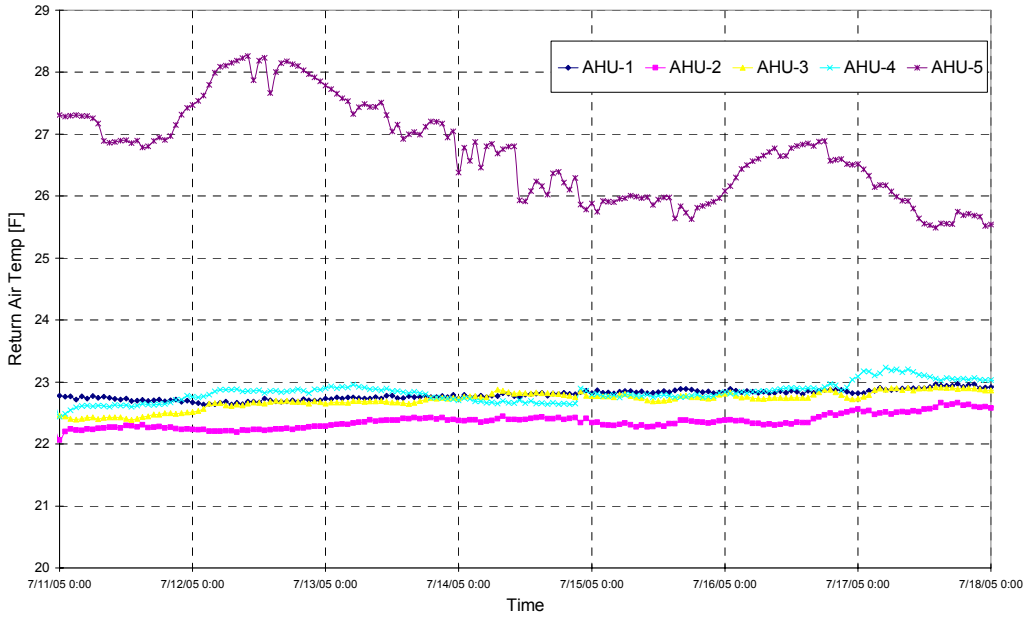

Figure 72: Room temperature of Energy Plaza from July 11 to July 17, 2005

The room air temperature is approximated by the return air temperature of air handling units (AHU). It can be seen from Figure 72 that the zone temperature has been maintained around 22-23°C except for AHU 5, which serves the atrium. It is not surprising to see that AHU 1-4 have almost constant return air temperature because there are two AHUs running during the unoccupied period to maintain the same setpoint of building as the occupied period.

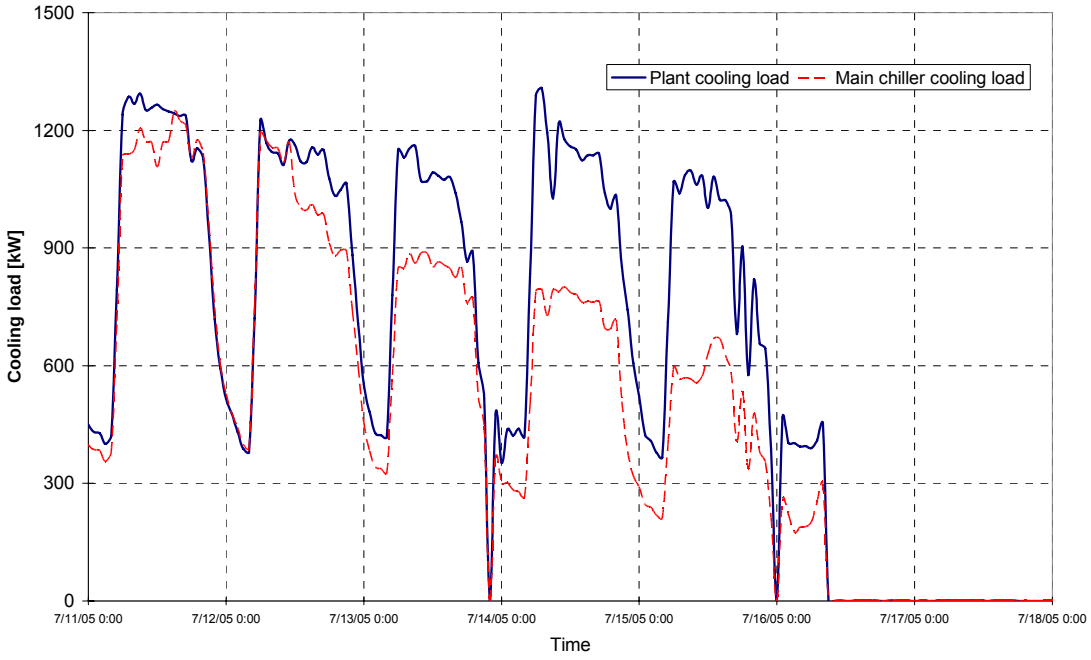

Figure 73: Cooling load profiles from July 11 to July 17, 2005

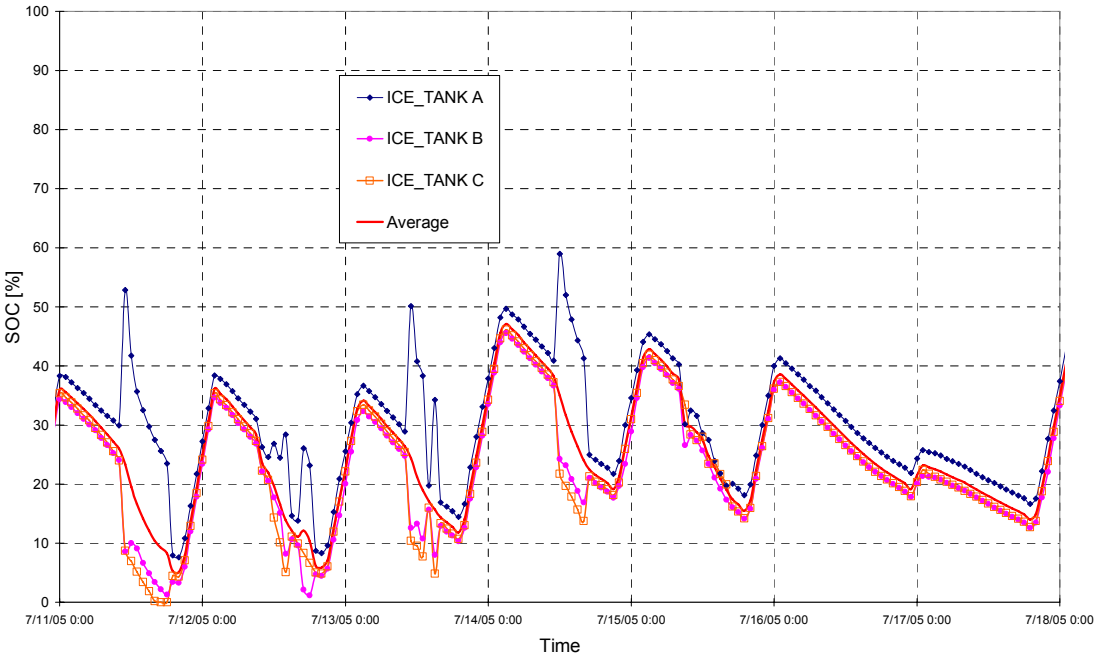

Figure 74: SOC profiles of TES tanks from July 11 to July 17, 2005

Figure 73 presents the cooling load profiles from July 11 to July 17. Since the flow meter mounted at main chilled water piping system was down from July 16, the cooling load of July 17 and 18 cannot be calculated. It can be seen that the majority of the cooling loads were met by the main chiller, and the TES has been utilized to assist the main chiller to meet the building cooling load. State-of-charge SOC profiles of the TES sys-

tem in Figure 74 also reveal that all of the TES tanks have been cyclically charged and discharged in the investigated week. There are some points that had been identified as unreliable data because it is impossible that the inventory of TES varies from 30 to 50 percent or more in one hour.

6.5.2 Optimal Control Case

As mentioned earlier, the real-time optimal control started on July 25, and lasted until August 3, but there has been two of interruptions due to the server crash and loss of communication between the building automation server and the server running the predictive optimal control program. By interpreting the data, three days data are identified to represent the optimal control case, and one particular day has found load shifting effect as we expected. Figure 75 shows the weather condition from July 25 to August 3. There was a severe thunder storm from July 25 to 26, which dramatically cooled down the temperature.

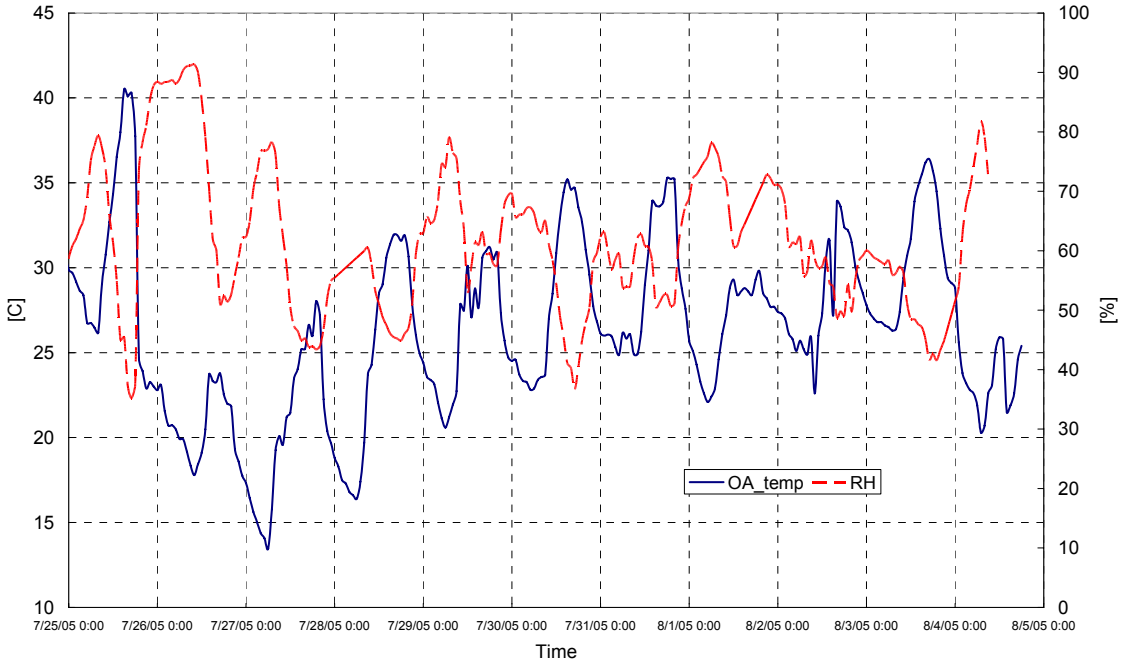

Figure 75: Ambient conditions from July 11 to July 17, 2005

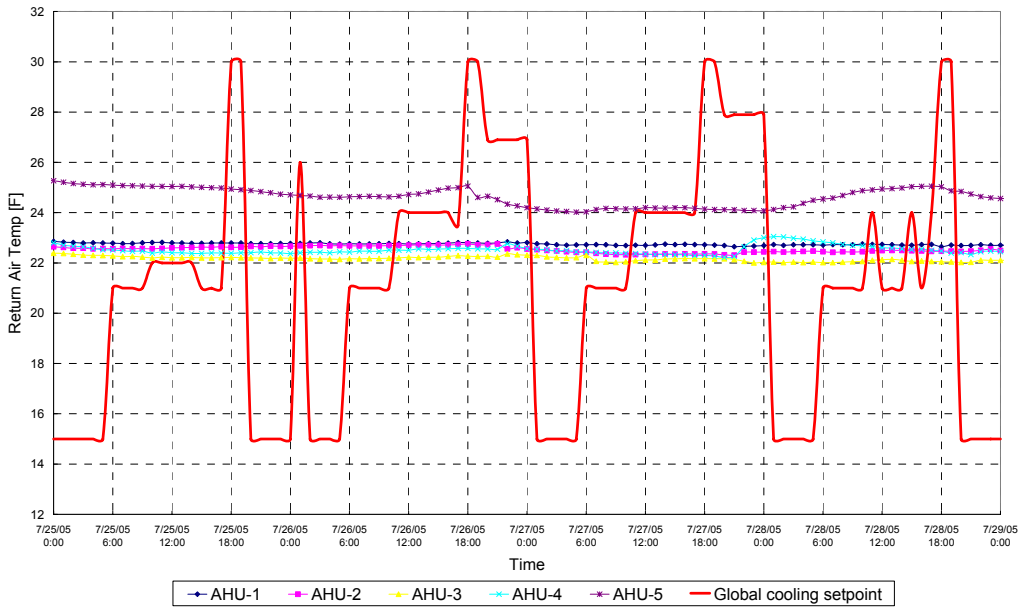

Figure 76: Room temperature of Energy Plaza from July 11 to July 17, 2005

Figure 76 shows the global cooling setpoint selected by the optimal control program and the actual room temperature of the building. As can be seen from the figure above, the global setpoint has the similar pattern in the selected three days. The setpoint from midnight to 5:00 AM is usually set to 15°C in order to precool the building. Then, the setpoint was increased to 21°C from 6:00 AM to 9:00 AM because the earliest occupancy started at 6:00 AM, and on-peak rate began at 10:00 AM. For the thermal comfort of occupants, the lower bound of cooling setpoint was set as 21°C. The optimal controller still decided to cool down the building as much as possible to shift the coming cooling load from the on-peak period. For the on-peak period, the setpoint usually was chosen as the upper bound of the thermal comfort region, i.e. 24°C. From the end of occupancy to the midnight, the controller tended to let the temperature of the building float by setting a high value for the cooling setpoint, i.e. 30°C. However, the actual room temperature did not follow the setpoint very closely. Comparing with the base case shown in Figure 72, the room temperature is only slightly reduced. One of reasons might be that the capacity of the system is insufficient to cool the building down any further.

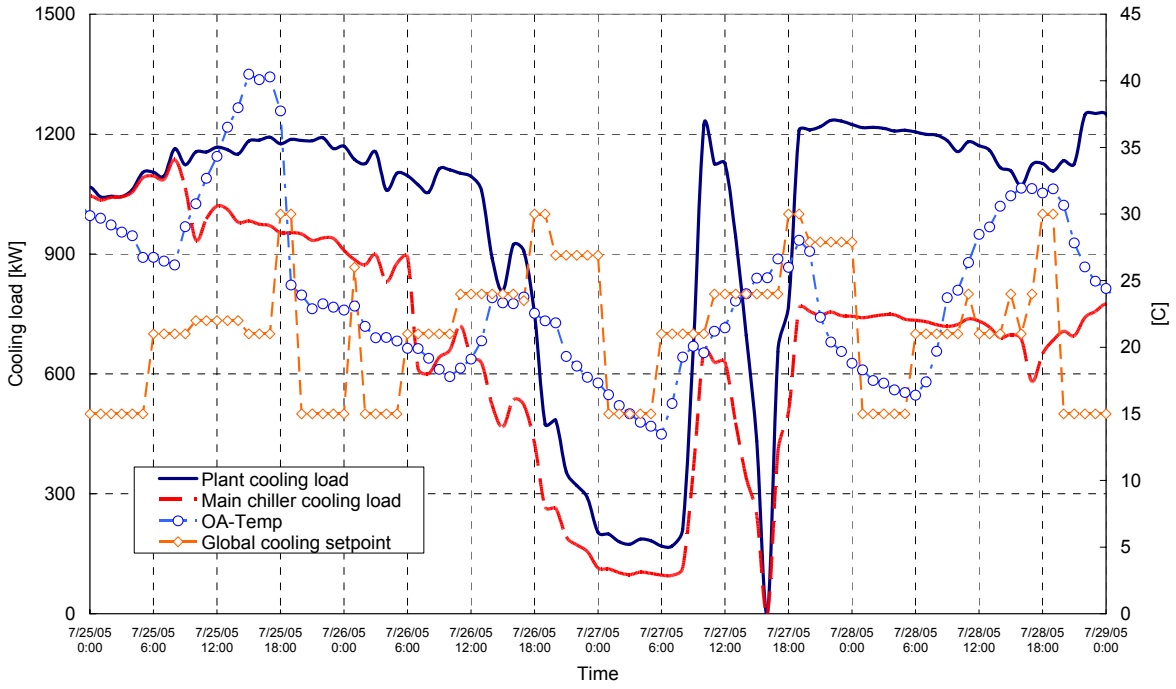

Figure 77: Cooling load profiles from July 25 to July 28, 2005

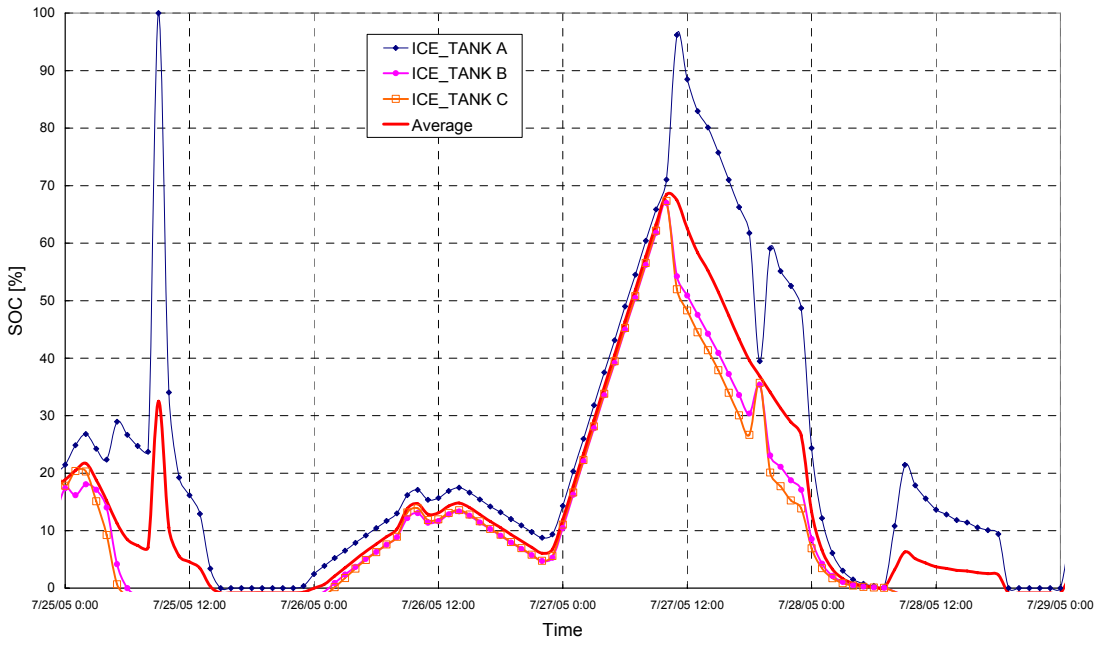

Figure 78: SOC profiles of TES tanks from July 25 to July 28, 2005

Figure 77 depicts the cooling load profiles during the optimal control test, and Figure 78 depicts the SOC profiles of the plant. It is difficult to detect the load shifting effect from the chart above at first sight. The global setpoint started to be handed over to the BAS from 8:00 AM of July 25, which is a very hot and humid day before the thunder storm coming. As we can see from the figure above, the cooling load during night of July 25 to 26 is still high because the setpoint of the building had been lowered to 15°C. The cooling load

during the occupied period of July 26 is lower than the normal value (1100 – 1200 kW) shown in Figure 73, but it might also be caused by the ambient temperature decrease. Low ambient temperatures on July 27 led to the lowest cooling loads from midnight because of the availability of free cooling by using the economizer. Cooling loads of July 27 were also low due to the combination of cool weather and the effect of precooling, and most cooling loads were met by the TES, thus the main chiller had only been running for several hours. It is surprising to see that the cooling load of July 28 is still relatively high even though there had been a pre-cooling period from midnight of July 27 to 28. The SOC profiles also show that the TES had been utilized as expected.

6.6 Energy and Cost Analysis

An energy and cost analysis has been carried out based on the hourly cooling load profiles. The measured data from Energy Plaza only had very limited information on the energy consumption. There is no power consumption measurement for the fans and pumps, and the power consumption data of the plant could not provide a meaningful interpretation due to limited availability of "good quality" data. Therefore, the analysis below focuses on the energy consumption of the cooling plant only, and is calculated based on constant COP (coefficient-of-performance) value of the chillers, which were obtained during the previous calibration. The COP of the main chiller was determined to be 4.5 and the COP of the icemaking chiller was identified as 2.1.

Table 37: Hourly energy consumption and cost for base case

Date	Hour	Electricity Consumption [kWh]			$/kWh	$	Date	Hour	Electricity Consumption [kWh]			$/kWh	$	Date	Hour	Electricity Consumption [kWh]			$/kWh	$
		Main Chiller	Icemaking	Total					Main Chiller	Icemaking	Total					Main Chiller	Icemaking	Total		
11-Jul	0:00	88.06	268.69	356.75	0.03	10.70	13-Jul	0:00	101.11	48.15	149.26	0.03	4.48	15-Jul	0:00	64.56	239.40	303.96	0.03	9.12
	1:00	85.70	0.00	85.70	0.03	2.57		1:00	85.09	40.52	125.61	0.03	3.77		1:00	54.45	233.86	288.31	0.03	8.65
	2:00	85.04	0.00	85.04	0.03	2.55		2:00	75.84	36.11	111.95	0.03	3.36		2:00	53.04	237.03	290.07	0.03	8.70
	3:00	78.90	0.00	78.90	0.03	2.37		3:00	75.03	35.73	110.75	0.03	3.32		3:00	48.45	68.56	117.01	0.03	3.51
	4:00	84.13	0.00	84.13	0.03	2.52		4:00	72.12	34.34	106.46	0.03	3.19		4:00	46.78	0.00	46.78	0.03	1.40
	5:00	158.71	0.00	158.71	0.03	4.76		5:00	128.13	61.01	189.14	0.03	5.67		5:00	88.75	0.00	88.75	0.03	2.66
	6:00	252.29	0.00	252.29	0.03	7.57		6:00	188.71	89.86	278.58	0.03	8.36		6:00	132.33	0.00	132.33	0.03	3.97
	7:00	253.18	0.00	253.18	0.03	7.60		7:00	188.32	89.68	278.00	0.03	8.34		7:00	125.76	0.00	125.76	0.03	3.77
	8:00	255.51	0.00	255.51	0.03	7.67		8:00	196.79	93.71	290.50	0.03	8.71		8:00	126.54	0.00	126.54	0.03	3.80
	9:00	267.98	0.00	267.98	0.03	8.04		9:00	191.45	91.17	282.62	0.03	8.48		9:00	125.83	0.00	125.83	0.03	3.77
	10:00	260.18	0.00	260.18	0.09	23.42		10:00	197.07	93.84	290.91	0.09	26.18		10:00	123.64	0.00	123.64	0.09	11.13
	11:00	259.80	0.00	259.80	0.09	23.38		11:00	197.04	93.83	290.87	0.09	26.18		11:00	127.24	0.00	127.24	0.09	11.45
	12:00	245.89	0.00	245.89	0.09	22.13		12:00	189.36	90.17	279.53	0.09	25.16		12:00	139.84	0.00	139.84	0.09	12.59
	13:00	259.89	0.00	259.89	0.09	23.39		13:00	192.29	91.57	283.86	0.09	25.55		13:00	148.40	0.00	148.40	0.09	13.36
	14:00	260.47	0.00	260.47	0.09	23.44		14:00	190.36	90.65	281.01	0.09	25.29		14:00	148.68	0.00	148.68	0.09	13.38
	15:00	277.33	0.00	277.33	0.09	24.96		15:00	188.27	89.65	277.93	0.09	25.01		15:00	139.14	0.00	139.14	0.09	12.52
	16:00	271.98	0.00	271.98	0.09	24.48		16:00	183.19	87.23	270.42	0.09	24.34		16:00	129.50	0.00	129.50	0.09	11.66
	17:00	269.49	0.00	269.49	0.09	24.25		17:00	189.19	90.09	279.28	0.09	25.13		17:00	90.09	0.00	90.09	0.09	8.11
	18:00	250.78	0.00	250.78	0.09	22.57		18:00	168.60	80.29	248.89	0.09	22.40		18:00	118.69	0.00	118.69	0.09	10.68
	19:00	261.31	0.00	261.31	0.03	7.84		19:00	172.04	81.93	253.97	0.03	7.62		19:00	75.01	0.00	75.01	0.03	2.25
	20:00	253.67	0.00	253.67	0.03	7.61		20:00	115.23	54.87	170.10	0.03	5.10		20:00	106.27	81.70	187.97	0.03	5.64
	21:00	213.30	137.12	350.42	0.03	10.51		21:00	98.69	46.99	145.68	0.03	4.37		21:00	84.56	245.89	330.46	0.03	9.91
	22:00	166.39	273.60	439.99	0.03	13.20		22:00	0.00	0.00	0.00	0.03	0.00		22:00	78.36	242.88	321.24	0.03	9.64
	23:00	133.83	267.27	401.10	0.03	12.03		23:00	81.55	38.83	120.38	0.03	3.61		23:00	47.24	232.12	279.35	0.03	8.38
	Total			5940.47		319.56		Total			5115.69		303.63		Total			4004.60		190.05
12-Jul	0:00	117.34	264.42	381.76	0.03	11.45	14-Jul	0:00	66.45	246.05	312.50	0.03	9.38							
	1:00	106.27	270.12	376.39	0.03	11.29		1:00	67.17	247.63	314.81	0.03	9.44							
	2:00	98.30	261.09	359.39	0.03	10.78		2:00	62.85	244.94	307.80	0.03	9.23							
	3:00	88.37	0.00	88.37	0.03	2.65		3:00	61.85	71.88	133.74	0.03	4.01							
	4:00	86.20	0.00	86.20	0.03	2.59		4:00	58.60	0.00	58.60	0.03	1.76							
	5:00	167.40	0.00	167.40	0.03	5.02		5:00	112.06	0.00	112.06	0.03	3.36							
	6:00	265.00	0.00	265.00	0.03	7.95		6:00	175.53	0.00	175.53	0.03	5.27							
	7:00	261.07	0.00	261.07	0.03	7.83		7:00	176.73	0.00	176.73	0.03	5.30							
	8:00	256.93	0.00	256.93	0.03	7.71		8:00	161.60	0.00	161.60	0.03	4.85							
	9:00	256.33	0.00	256.33	0.03	7.69		9:00	176.28	0.00	176.28	0.03	5.29							
	10:00	248.24	0.00	248.24	0.09	22.34		10:00	175.19	0.00	175.19	0.09	15.77							
	11:00	259.96	0.00	259.96	0.09	23.40		11:00	178.12	0.00	178.12	0.09	16.03							
	12:00	230.58	0.00	230.58	0.09	20.75		12:00	174.46	0.00	174.46	0.09	15.70							
	13:00	222.64	0.00	222.64	0.09	20.04		13:00	173.72	0.00	173.72	0.09	15.63							
	14:00	221.48	0.00	221.48	0.09	19.93		14:00	169.12	0.00	169.12	0.09	15.22							
	15:00	224.69	0.00	224.69	0.09	20.22		15:00	169.72	0.00	169.72	0.09	15.28							
	16:00	218.60	0.00	218.60	0.09	19.67		16:00	169.18	0.00	169.18	0.09	15.23							
	17:00	219.20	48.87	268.08	0.09	24.13		17:00	169.70	0.00	169.70	0.09	15.27							
	18:00	202.83	0.00	202.83	0.09	18.25		18:00	154.60	0.00	154.60	0.09	13.91							
	19:00	195.82	0.00	195.82	0.03	5.87		19:00	154.07	0.00	154.07	0.03	4.62							
	20:00	198.69	0.00	198.69	0.03	5.96		20:00	159.27	0.00	159.27	0.03	4.78							
	21:00	198.61	59.37	257.99	0.03	7.74		21:00	112.93	0.00	112.93	0.03	3.39							
	22:00	164.50	259.51	424.01	0.03	12.72		22:00	84.59	100.54	185.13	0.03	5.55							
	23:00	132.68	235.28	367.97	0.03	11.04		23:00	70.92	246.05	316.97	0.03	9.51							
	Total			6040.42		307.04		Total			4391.83		223.78							

Table 38: Hourly energy consumption and cost of optimal case

Date	Hour	Electricity Consumption [kWh]			$/kWh	$	Date	Hour	Electricity Consumption [kWh]			$/kWh	$
		Main Chiller	Icemaking	Total					Main Chiller	Icemaking	Total		
25-Jul	0:00	232.07	0.00	232.07	0.03	6.96	27-Jul	0:00	25.38	260.30	285.68	0.03	8.57
	1:00	229.96	122.55	352.51	0.03	10.58		1:00	24.91	265.05	289.96	0.03	8.70
	2:00	231.47	0.00	231.47	0.03	6.94		2:00	22.78	268.37	291.16	0.03	8.73
	3:00	231.80	0.00	231.80	0.03	6.95		3:00	21.64	277.88	299.52	0.03	8.99
	4:00	234.47	0.00	234.47	0.03	7.03		4:00	23.15	269.32	292.48	0.03	8.77
	5:00	242.42	0.00	242.42	0.03	7.27		5:00	22.37	268.85	291.22	0.03	8.74
	6:00	243.40	0.00	243.40	0.03	7.30		6:00	21.42	274.55	295.97	0.03	8.88
	7:00	241.47	0.48	241.94	0.03	7.26		7:00	21.34	262.68	284.02	0.03	8.52
	8:00	252.51	0.00	252.51	0.03	7.58		8:00	25.28	273.13	298.40	0.03	8.95
	9:00	236.67	0.00	236.67	0.03	7.10		9:00	79.50	267.43	346.93	0.03	10.41
	10:00	207.69	0.00	207.69	0.09	18.69		10:00	146.44	246.05	392.49	0.09	35.32
	11:00	219.51	0.00	219.51	0.09	19.76		11:00	139.54	0.00	139.54	0.09	12.56
	12:00	226.67	0.00	226.67	0.09	20.40		12:00	139.83	0.00	139.83	0.09	12.58
	13:00	224.80	0.00	224.80	0.09	20.23		13:00	106.18	0.00	106.18	0.09	9.56
	14:00	217.61	0.00	217.61	0.09	19.59		14:00	75.53	0.00	75.53	0.09	6.80
	15:00	218.39	0.00	218.39	0.09	19.65		15:00	54.60	0.00	54.60	0.09	4.91
	16:00	216.53	0.00	216.53	0.09	19.49		16:00	0.00	0.00	0.00	0.09	0.00
	17:00	215.73	0.00	215.73	0.09	19.42		17:00	89.84	0.00	89.84	0.09	8.09
	18:00	211.83	0.00	211.83	0.09	19.06		18:00	112.19	0.00	112.19	0.09	10.10
	19:00	211.93	1.43	213.35	0.03	6.40		19:00	170.02	0.00	170.02	0.03	5.10
	20:00	211.11	0.00	211.11	0.03	6.33		20:00	168.04	0.00	168.04	0.03	5.04
	21:00	207.55	0.48	208.02	0.03	6.24		21:00	165.88	0.00	165.88	0.03	4.98
	22:00	208.84	0.00	208.84	0.03	6.27		22:00	167.74	0.00	167.74	0.03	5.03
	23:00	208.68	0.00	208.68	0.03	6.26		23:00	165.66	0.00	165.66	0.03	4.97
	Total			5508.02		282.77		Total			4922.87		214.30
26-Jul	0:00	202.03	0.48	202.50	0.03	6.08	28-Jul	0:00	165.38	0.00	165.38	0.03	4.96
	1:00	196.83	0.48	197.30	0.03	5.92		1:00	164.55	0.00	164.55	0.03	4.94
	2:00	193.98	67.93	261.91	0.03	7.86		2:00	165.38	0.00	165.38	0.03	4.96
	3:00	199.64	76.00	275.64	0.03	8.27		3:00	166.21	0.00	166.21	0.03	4.99
	4:00	184.74	77.42	262.17	0.03	7.87		4:00	166.21	0.00	166.21	0.03	4.99
	5:00	194.74	71.73	266.47	0.03	7.99		5:00	163.71	0.00	163.71	0.03	4.91
	6:00	198.52	64.12	262.64	0.03	7.88		6:00	163.16	0.00	163.16	0.03	4.89
	7:00	136.11	63.17	199.29	0.03	5.98		7:00	162.33	0.00	162.33	0.03	4.87
	8:00	133.39	64.13	197.51	0.03	5.93		8:00	160.66	0.00	160.66	0.03	4.82
	9:00	142.60	199.98	342.58	0.03	10.28		9:00	159.71	0.00	159.71	0.03	4.79
	10:00	146.57	35.15	181.72	0.09	16.35		10:00	160.82	1.43	162.24	0.09	14.60
	11:00	160.17	0.00	160.17	0.09	14.42		11:00	163.94	0.48	164.42	0.09	14.80
	12:00	143.01	6.17	149.18	0.09	13.43		12:00	162.68	0.00	162.68	0.09	14.64
	13:00	139.43	53.20	192.63	0.09	17.34		13:00	159.29	1.90	161.19	0.09	14.51
	14:00	115.80	22.80	138.60	0.09	12.47		14:00	153.51	0.00	153.51	0.09	13.82
	15:00	103.78	0.00	103.78	0.09	9.34		15:00	155.10	0.95	156.05	0.09	14.04
	16:00	118.98	0.00	118.98	0.09	10.71		16:00	152.69	0.00	152.69	0.09	13.74
	17:00	116.03	0.00	116.03	0.09	10.44		17:00	129.04	0.00	129.04	0.09	11.61
	18:00	94.70	0.00	94.70	0.09	8.52		18:00	144.46	0.00	144.46	0.09	13.00
	19:00	59.22	0.00	59.22	0.03	1.78		19:00	151.98	0.00	151.98	0.03	4.56
	20:00	58.69	0.00	58.69	0.03	1.76		20:00	157.05	0.48	157.53	0.03	4.73
	21:00	42.70	0.00	42.70	0.03	1.28		21:00	154.50	0.48	154.97	0.03	4.65
	22:00	38.19	0.00	38.19	0.03	1.15		22:00	164.65	0.00	164.65	0.03	4.94
	23:00	34.47	39.43	73.89	0.03	2.22		23:00	168.07	0.00	168.07	0.03	5.04
	Total			3996.50		195.24		Total			3820.78		197.80

Table 37 and Table 38 present an hourly analysis of the energy consumption and operating cost of the cooling plant for the base case and optimal case scenarios. The comparison of daily average value is summarized in Table 39.

Table 39: Comparison of the average value of base case and optimal case

Scenario	Date	Energy Consumption [kWh]	Cost [$]
Base Case	7/11/2005	5940.47	319.56
	7/12/2005	6040.42	307.04
	7/13/2005	5115.69	303.63
	7/14/2005	4391.83	223.78
	7/15/2005	4004.60	190.05
	Average	**5098.60**	**268.81**
Optimal Case	7/25/2005	5508.02	282.77
	7/26/2005	3996.50	195.24
	7/27/2005	4922.87	214.30
	7/28/2005	3820.78	197.80
	Average	**4562.04**	**222.53**
	Savings	**10.5%**	**17.2%**

It can be seen from Table 39 that the optimal control case provides savings in energy consumption of about 10%, and about 17% savings in operating costs based on the average daily value. These savings figures are very encouraging but should be treated with caution for the following reasons: There is only limited data available for analysis, fan and pump power consumption have not been included, variation in weather and building use have not been accounted for. Nevertheless, the available experimental data support the further development and refinement of the control strategy.

6.7 Summary

This final chapter presents an analysis of the measured data of the real-time optimal control test conducted at the Energy Plaza facility in Omaha, Nebraska for a very short time period. Energy consumption was reduced by about 10% and costs were reduced by about 17% for the test period. The developed weather predictor and predictive control program had been running smoothly during the test period, but there was a problem in the process of transmitting the optimal results into the BAS system. As mentioned earlier, our server that is in charge of the optimal control program was not allowed to be connected directly with the local network of the building, but could only read and write the information by using a virtual private network (VPN) connection. Another reason for the instable operation is that the BAS server itself in the investigated building is relatively old, and not capable of handling many processes at the same time. After observing the server crash for several times, our program was viewed as being the last piece pushing the stone off the edge. The limited data confirms that our optimal value had been successfully transmitted into the BAS system provided each program is running, and the analysis of cooling load profiles during the test days in Figure 77 reveals the effect of load shifting as expected, but it is not sufficient data for us to draw meaningful conclusions about the performance of the program. Regardless of the poor condition of the existing BAS server, which is believed to be the major reason causing the failure of field implementation, will need to find a new way to implement the optimal results into the BAS system. DDE had been very effective, but it is not very reliable, especially the NDDE (Network DDE) implementation. Future efforts to bring this novel idea into reality should focus on developing a methodology including hardware and software to transmit the optimal results into conventional and possibly aged BAS systems.